

**Journal of Quantitative Spectroscopy and Radiative Transfer**  
**A practical guide to coding line-by-line trace gas absorption in Earth's atmosphere**  
--Manuscript Draft--

<b>Manuscript Number:</b>	
<b>Article Type:</b>	VSI: Goody 2023
<b>Keywords:</b>	Atmosphere absorption spectroscopy; line-by-line; open-source; code development; radiative transfer (RT); Earth science.
<b>Corresponding Author:</b>	Sergey Korkin University of Maryland Baltimore County Greenbelt, MD UNITED STATES
<b>First Author:</b>	Sergey Korkin
<b>Order of Authors:</b>	Sergey Korkin Andrew M. Sayer Amir Ibrahim Alexei Lyapustin
<b>Abstract:</b>	We present two new open-source codes, in C language, for simulation of the line-by-line molecular (gas) absorption in the “solar reflectance band”, with wavelengths up to ~2500 (nm). The first one, gcell, simulates absorption spectroscopy in a gas cell for a given length of the cell, temperature, and pressure. The second one, aspect, is for spectroscopy in Earth’s atmosphere - a common need for remote sensing applications. Both use the HITRAN database for the line shape (Voigt) modeling. Aspect adapts the height variations of the thermodynamic parameters (profiles) from MODTRAN. Separate discussion of the gas cell and the atmospheric modes simplifies software development, documentation, and support, and ultimately the transfer of knowledge between generations of scientists. These are the main goals of the current paper. Despite the existence of numerous computer programs for absorption spectroscopy, the code development process is poorly covered in literature. As a result, it is difficult for a non-developer to confidently modify an existing code or create a new tool within a reasonable amount of time. This paper supplements “A practical guide to writing a radiative transfer code” which we have published in 2022.
<b>Suggested Reviewers:</b>	Masahiro Momoi masahiro.momoi@grasp-earth.com  Pengwang Zhai pwzhai@umbc.edu  Vijay Natraj vijay.natraj@jpl.nasa.gov  Feng Xu fengxu@ou.edu  Dmitry Efremenko efremenkods@gmail.com  Souichiro Hioki souichiro.hioki@univ-lille.fr

**To:** Editorial Board of Journal of Quantitative Spectroscopy and Radiative Transfer (JQSRT)  
**Attn:** Editors of the Special JQSRT Issue on Richard M. Goody Award

**Cover Letter**

Dear Editors,

First and foremost, I would like to express my heartfelt gratitude to the Selection Committee for their decision and to those anonymous Colleagues who nominated me for the Goody Award in 2016. It's crucial to acknowledge that this recognition is not solely mine but is the result of a collaborative effort involving my Co-authors – only a few of whom are listed below.

In support of the JQSRT Special Issue, we are submitting a manuscript titled "*A Practical Guide to Coding Line-by-line Trace Gas Absorption in Earth's Atmosphere*" authored by S. Korkin, A. M. Sayer, A. Ibrahim, and A. Lyapustin. We hope this contribution will be considered for publication in the collection.

The manuscript complements our paper "*A Practical Guide to Writing a Radiative Transfer Code*", which focused on the numerical simulation of multiple scattering of solar light. It was published as a Feature article in Elsevier's Computer Physics Communications in 2022<sup>1</sup>. Understanding the theory and numerical simulation of the two fundamental physical phenomena – scattering and absorption, collectively referred to as Radiative Transfer (RT) – poses challenges, particularly for those new to the field or under time constraints.

Through our own careers in Earth Science, we have seen a gradual loss of RT expertise as many of those who have pioneered this research and development of codes have retired or passed away. Newer generations of scientists still often rely on codes developed decades before, increasingly becoming poorly-understood "black-boxes" in need of refactoring and enhancement for new features. We feel there's a gap in institutional support for RT code development (and fundamental training).

As a result, the objective of our "*Practical Guide*" series is to simplify RT software development, documentation, and support, with the ultimate goal of facilitating knowledge transfer across generations of scientists. To achieve this goal, our papers integrate essential theoretical concepts with corresponding code snippets, organized in a manner conducive to code development, which often contrasts with the typical presentation of theoretical foundations. This pairing feels to us like JQSRT is a natural home. While this approach is not novel in essence, its significance within the domain of RT studies may have been overlooked. It's also important to note that neither of our "*Practical Guides*" reports novel scientific findings. Both serve as academic demonstrations.

One drawback of our paper-and-code bundle strategy is its length: the manuscript spans 85 pages, excluding the list of 185 references. However, we believe that the scholarly efficiency of this approach, our emphasis on addressing a broad audience, the provision of a new publicly available open-source code explained within the paper, and, most importantly, the reproducibility of all reported results, outweigh this drawback.

On behalf of all co-authors,

Sincerely yours

*Sergey Korkin*

---

<sup>1</sup> <https://doi.org/10.1016/j.cpc.2021.108198>

## Highlights

- Despite the existence of numerous computer programs for absorption spectroscopy, the code development process is poorly covered in literature.
- Our paper shows how to create a code for line-by-line molecular absorption spectroscopy from scratch.
- We explain the process in three steps: a) simulation of absorption by a molecule using HITRAN database; b) simulation of absorption in a gas cell by a group of molecules; c) simulation of absorption in Earth atmosphere using MODTRAN profiles.
- The goals of the paper are the simplification of software development, documentation, and support, and ultimately the transfer of knowledge between generations of scientists.
- Our paper comes with an open-source code, in C-language, and numerical data for unit testing, thus insuring independent reproducibility of our results.

# A practical guide to coding line-by-line trace gas absorption in Earth's atmosphere

*Sergey Korkin*<sup>1,2,\*</sup>, *Andrew M. Sayer*<sup>1,2</sup>, *Amir Ibrahim*<sup>2</sup>, and *Alexei Lyapustin*<sup>2</sup>

<sup>4</sup> <sup>1</sup>University of Maryland Baltimore County, Baltimore, MD, USA

<sup>5</sup> <sup>2</sup>NASA Goddard Space Flight Center, Greenbelt, MD, USA

<sup>6</sup> \*Corresponding author: [sergey.v.korkin@nasa.gov](mailto:sergey.v.korkin@nasa.gov)

7

8 “Talk is cheap. Show me the code.”

– Linus Torvalds<sup>1</sup>

10 Abstract

We present two new open-source codes, in C language, for simulation of the line-by-line molecular (gas) absorption in the “solar reflectance band”, with wavelengths up to  $\sim 2500$  (nm). The first one, `gcell`, simulates absorption spectroscopy in a gas cell for a given length of the cell, temperature, and pressure. The second one, `aspect`, is for spectroscopy in Earth’s atmosphere - a common need for remote sensing applications. Both use the HITRAN database for the line shape (Voigt) modeling. `Aspect` adapts the height variations of the thermodynamic parameters (profiles) from MODTRAN. Separate discussion of the gas cell and the atmospheric modes simplifies software development, documentation, and support, and ultimately the transfer of knowledge between generations of scientists. These are the main goals of the current paper. Despite the existence of numerous computer programs for absorption spectroscopy, the code development process is poorly covered in literature. As a result, it is difficult for a non-developer to confidently modify an existing code or create a new tool within a reasonable amount of time. This paper supplements “A practical guide to writing a radiative transfer code” which we have published in 2022.

<sup>1</sup> [https://en.wikiquote.org/wiki/Linus\\_Torvalds](https://en.wikiquote.org/wiki/Linus_Torvalds) (see Sec. 2000-s: 2000-04)

25	<a href="#">Keywords</a>	
26	Atmosphere absorption spectroscopy, line-by-line, open-source, code development, radiative	
27	transfer (RT), Earth science.	
28	<a href="#">Contents</a>	
29	Abstract .....	1
30	Keywords .....	2
31	1. Introduction.....	3
32	2. Many tools for atmospheric spectroscopy: why publish one more?.....	9
33	3. Code structure and usage .....	14
34	3.1 Header files .....	15
35	3.2 Installation, input, and output parameters.....	16
36	3.2.1 Gas cell mode.....	16
37	3.2.2 Atmospheric mode .....	20
38	4. Calculation of absorption by a single HITRAN line .....	27
39	4.1 Reading one record form the HITRAN *.par file .....	28
40	4.2 Molparam.txt and TIPS q-files. ....	30
41	4.3 Basic code for a single line .....	33
42	4.4 Convolution – Voigt spectrum.....	36
43	4.5 Beyond Voigt: a few legacy and recent references.....	40
44	4.6 A few numbers for validation of code for an isolated line .....	42
45	5. Calculation of absorption in a gas cell .....	44
46	5.1 Picking necessary lines from the HITRAN *.par files .....	45
47	5.2 The line-mixing effect, which we also neglect .....	46
48	5.3 Simulation of LBL absorption .....	47
49	5.4 Gas cell validation.....	50

50	5.3.1 Oxygen A-band at 0.764 ( $\mu\text{m}$ ) .....	51
51	5.3.2 Methane band at 2.3 ( $\mu\text{m}$ ) .....	53
52	6. Absorption in the Earth atmosphere .....	55
53	6.1 Elements of MODTRAN .....	55
54	6.2 Column amount of gas in atmosphere .....	60
55	6.3 The mysterious <i>atm-cm/km</i> .....	64
56	6.4 Profile of optical thickness.....	68
57	6.5 Practical units for water vapor .....	70
58	6.6 Aspect validation .....	71
59	6.6.1 Literature references .....	71
60	6.6.2 Numerical example for PACE OCI .....	77
61	7. Conclusion .....	82
62	Acknowledgements.....	85
63	Authors contribution .....	85
64	Funding information .....	86
65	References.....	86
66		

## 67 1. Introduction

68 Absorption of radiation as a function of wavelength  $\lambda$  (widely used in the solar reflectance band)  
69 or wavenumber  $v \sim 1/\lambda$  (more common in spectroscopy) by the atmosphere-surface system is a  
70 fundamental physical process that influences the Earth's radiation budget and through that drives  
71 its climate (Luther et al., 1988; Kochanov et al., 2019; Pincus et al., 2020). Molecules absorb  
72 radiation at only specific wavelengths corresponding to differences in energy between different  
73 possible quantum excitation states – that is, different rotational, vibrational, and electronic  
74 configurations. For an isolated molecule, these lines are pure and monochromatic, though in  
75 practice (whether in a gas cell or Earth's atmosphere) the fact that molecules exist in groups,

76 interacting with one another, and with different populations of excitation states, greatly  
77 complicates matters and leads to broadening and shifting of lines (*Elsasser*, 1942; *Goody &*  
78 *Yung*, 1989; *Liou*, 2002).

79 The gas spectroscopy started to systematically attract the attention of scientists in as early as  
80 XIX-th century. *Pouillet* (1838) and *Tyndall* (1859) reported on the influence of gaseous on  
81 transfer of solar radiation through the atmosphere. *Foote* (1856) arguably was the first scientist  
82 to link the atmospheric heating rate (global warming) with CO<sub>2</sub> concentration. Later, *Arrhenius*  
83 (1896, 1897) continued this research. In the modern era, these pioneering works are continued by  
84 the Orbiting Carbon Observatory (OCO<sup>2</sup>), the Scanning Imaging Absorption Spectrometer for  
85 Atmospheric Chartography (SCIAMACHY<sup>3</sup>), the Greenhouse Gases Observing Satellite  
86 (GOSAT<sup>4</sup>), and other missions. Thus, the importance of the effect of atmospheric absorption was  
87 recognized about two centuries ago and since then has remained a focus of the atmospheric  
88 community.

89 Besides climate and weather, accurate simulation of absorption is necessary for satellite remote  
90 sensing. Optical (solar and thermal) and radio instruments, both passive (radiometers) and active  
91 (lidars, radars), detect signal in “atmospheric windows”. The atmospheric windows are range of  
92 wavelengths (spectral bands) where absorption is low, but still not negligible. In these spectral  
93 bands the atmospheric absorption is not an object of study, but an obstacle. Accurate retrieval  
94 algorithms must take this absorption into account.

95 In the Earth atmosphere, the radiation is absorbed by particles (aerosols) and molecules of trace  
96 gases. Gas absorption is usually divided into two components. First, is the absorption in spectral  
97 lines of the molecules, which has a pronounced spectral pattern – the absorption power may vary  
98 by orders of magnitude even within a narrow spectral band – due to the aforementioned  
99 dependence on specific permitted rotational, vibrational, and electronic structure transitions.  
100 Second is the continuum absorption, which is smoother and often attributed to water vapor  
101 (*Clough* et al., 1989; *Shine* et al., 2012; *Mlawer* et al., 2012 & 2023). In practice parameters to fit  
102 observed gas absorption lines are determined empirically from measurements on a line-by-line

---

<sup>2</sup> <https://ocov2.jpl.nasa.gov/>

<sup>3</sup> <https://www.sciamachy.org/>

<sup>4</sup> <https://www.gosat.nies.go.jp/en/>

103 (LBL) basis assuming some basic line absorption shape, and then the continuum is calculated as  
104 the difference between these measurements and LBL calculations. Then one fits this residual  
105 absorption – arising due to the complex interplay between molecules that is intractable to model  
106 purely theoretically - with models that are largely empirical. Further in this paper, we focus only  
107 on the first component – absorption by spectral lines – of atmospheric spectroscopy.

108 Apart from the water vapor continuum, mostly affecting wavelengths in the red and longer  
109 wavelengths, there are other gases manifesting spectrally smooth variations in the UV-Vis part.  
110 Ozone,  $O_3$ , is the most important absorber in this spectral range. The presence of this gas causes  
111 a drop in the atmospheric transmittance towards shorter wavelengths (e.g., see the second chart  
112 from the top of Fig. 2.13 in *Bohren & Clothiaux*, 2006), causing the need for atmospheric  
113 correction. Fortunately, *a*) the ozone is located high in the Earth atmosphere, and the ozone  
114 correction theoretical background is simply a direct transmittance, exponential w.r.t. absorption  
115 optical thickness, frequently noted in RT as  $\tau$ , along the solar and view directions; *b*) the  
116 transmittance depends on the ozone absorption cross-sections, which possess moderate  
117 temperature and pressure dependence, measured in a laboratory at different concentrations, a  
118 limited set of thermodynamical conditions, and reported as look-up tables (*Hearn*, 1961; *Orphal*  
119 et al., 2016). Besides ozone, these smooth components of spectral absorption are measured for  
120 other important atmospheric trace gases (*Bogumil* et al., 2003). We do not include this  
121 “continuum-type” absorption in our paper.

122 Since the mentioned pioneering works in Earth science, as well as in astrophysics, the field of  
123 absorption in planetary atmospheres has been growing. Results of these studies are published in  
124 dedicated journals (e.g., *Journal of Molecular Spectroscopy* and *Journal of Quantitative*  
125 *Spectroscopy and Radiative Transfer*), monographs, chapters in books, and papers in journals not  
126 specialized in spectroscopy. Spaceborne spectrometers studying Earth and other planets, and  
127 countless laboratory measurements generate an avalanche of experimental data. Numerous  
128 datasets combine the data in a raw and processed format (e.g., after parametrization). Some of  
129 the datasets, like the widely used high-resolution transmission molecular absorption database  
130 (HITRAN<sup>5</sup>), have become standards in science and industry (*McClatchey* et al. 1973; *Rothman*  
131 et al., 1978, 2005, 2010, 2021). Examples of other spectral databases include GEISA (*Delahaye*

---

<sup>5</sup> <https://hitran.org/>

132 et al., 2020), which has been developed since 1980-s, CDMS (*Müller* et al., 2005), ASTER  
133 (*Baldridge* et al., 2009), to name a few. In this paper we use that part of the HITRAN database  
134 that models lines with the Voigt shape profile. We refer the reader to Sec. 4.4 below for  
135 references on the Voigt spectrum and to Sec. 4.5 for some legacy and recent references on the  
136 non-Voigt line shape.

137 In this paper we also do not include one type of absorption with a smooth spectral dependence,  
138 which is included in HITRAN to a certain degree. This phenomenon is (inelastic) collision induced  
139 absorption – CIA (*Goody & Yung*, 1989: Sec.5.3.4 for O<sub>2</sub> and 5.5.3 for CO<sub>2</sub>; *Richard* et al., 2012;  
140 *Karman* et al., 2019). This is not to be confused with (elastic) collisional broadening. During  
141 collision of molecules, some energy transitions forbidden for molecules at steady state may  
142 become possible, which leads to absorption of radiation at corresponding wavelengths. CIA is  
143 most important for O<sub>2</sub> and N<sub>2</sub> (*Karman* et al., 2018). The phenomenon manifests itself at high  
144 concentrations. It is parametrized in HITRAN as scaling factors (binary coefficients) and molecule  
145 concentrations, e.g.  $K_{ab}(v) = k(v)/(n_a \cdot n_b)$ . Here ‘a’ and ‘b’ denote two colliding molecules, ‘n’ is  
146 concentration, ‘k(v)’ is the absorption cross-section at a given wavenumber v. The dependence of  
147 n on temperature T and pressure p leads to the same in the CIA coefficients.

148 Analysis and application of the collected data relies on numerical modeling. The models are  
149 basically computer programs. Once developed, they may be used for decades, which assures  
150 reliability (*Korkin* et al., 2022: see references in Sec.1). But over time they are left as black  
151 boxes. Contrary to the scientific background (theory), and documenting of the measurement  
152 process (technique), codes do not get enough attention. They either start as or often become  
153 poorly written software: obscure coding practices (as these evolve over time), unclear structure,  
154 lack of documentation and unit testing. Input/output formats, runtime, or accuracy may no longer  
155 meet the requirements of new missions. New tools are needed to improve reprocessing of  
156 heritage missions, and to get the most out of upcoming Earth science missions such as NASA’s  
157 Plankton, Aerosol, Cloud, ocean Ecosystem (PACE<sup>6</sup>: *Werdell* et al., 2019). The PACE Ocean  
158 Color Instrument (OCI) has a finer wavelength resolution than heritage NASA imagers, which

---

<sup>6</sup> <https://pace.gsfc.nasa.gov/>

159 demands flexible (for simulation of different and variable atmospheric constituents) and accurate  
160 (to avoid bias in retrievals) software tool for atmospheric spectroscopy.

161 As a result of the neglect of software it is hard or impossible, to confidently support (apply minor  
162 changes) or modify (significantly change) a “black box”<sup>7</sup> and/or a “spaghetti code”<sup>8</sup> within a  
163 reasonable amount of time - especially when the need is pressing. This problem has been  
164 recognized not only in planetary spectroscopy but in science in general (*Kendall et al., 2008;*  
165 *Sanders & Kelly, 2008; Segal & Morris, 2008; Easterbrook & Johns, 2009; LeVeque et al., 2012;*  
166 *Pipitone & Easterbrook, 2012; Kanewala & Bieman, 2014; Wilson et al., 2014; Heaton &*  
167 *Carver, 2015; Storer, 2017; Adorf et al., 2018; Hinsen, 2019, Dubey, 2022*). In Earth science,  
168 legacy tools currently used at many institutions are largely limited to heritage sensors (e.g.  
169 MODIS) and no longer supported as the developers have retired or passed away. Other tools  
170 exist (see Sec.2), but access or support are often unavailable. Lack of support makes it difficult  
171 to confidently change the code. The need to change the code arises from needs to: **a)** update  
172 atmospheric spectroscopy database as new information becomes available, e.g. new HITRAN  
173 release (*Zhu et al., 2019*); **b)** add new atmospheric profile, or add absorption by a new molecule  
174 or its isotopes; **c)** update with improved models of the spectral line shape, such as speed-  
175 dependent Voigt profile (see Sec.4.5).

176 Code is therefore the main topic of the paper. We use and refer to known equations, but only to  
177 support code documentation. We do not get into details of spectroscopy (although the reader is  
178 referred to various books and papers) and refer to equations and relevant parameters as they  
179 appear in the code. However, in the paper we do not discuss those “technical” parts relevant to  
180 the code only: declaration of variables, memory allocation/deallocation, printouts. The reader  
181 will see all that in the source that comes with the paper. In the text we focus on the tight coupling  
182 between an equation and its representation as an element of code. Thus, at any moment, the  
183 developer is focused on what is needed now.

184 For simplicity of coding, the paper introduces the process of development sequentially from  
185 simple to complicated. Sec.4 shows how to read the HITRAN database, briefly explains  
186 necessary parameters, and shows relevant code for calculation of the relative (per molecule)

---

<sup>7</sup> [https://en.wikipedia.org/wiki/Black\\_box](https://en.wikipedia.org/wiki/Black_box)

<sup>8</sup> [https://en.wikipedia.org/wiki/Spaghetti\\_code](https://en.wikipedia.org/wiki/Spaghetti_code)

absorption cross-section by a single line. We calculate the Voigt line shape in Sec.4.4 and list a few references for “beyond Voigt” models of spectral line shape in Sec.4.5. Sec.4.6 gives a few numbers to test calculation by a single line – unit testing. In Sec.5 we combine absorption from many spectral lines assumed independent. The line mixing effect (e.g., interference of broad lines) is ignored, however we provide references for further reading in Sec.5.2. For a given temperature, pressure, and length of the cell we calculate the absorption optical thickness of the gas. Such gas cells are used in laboratories and field measurements. Our C-code `gcell` aims to support measurements that use gas cells. Sec.5.3 gives some independently created data to test code `gcell`.

An atmosphere is basically a vertical stack of gas cells, each with some given temperature, pressure, and particle species number concentrations varying with height – profiles. In Sec.6 we combine the gas cell calculation with MODTRAN (*Berk et al.*, 2014 & 2017) atmospheric profiles, described briefly in Sec.6.1. Later in Sec.6 we integrate the profiles over high in order to calculate  $\tau$  between top-of-the-atmosphere (TOA) and user-defined level of height, paying particular attention to units of the amount of gas in the atmospheric column. An open-source C code for LBL simulation of the atmospheric spectroscopy, `aspect`, is the main product presented in the paper. Note that `aspect` is a revised and updated version of the LBL solver of the Spherical Harmonics Interpolation and Profile Correction (SHARM-IPC) tool (*Lyapustin, 2003*) for broad band RT. We show how to test `aspect` in Sec.6.6.

We endeavor to give the interested reader a chance to start using our codes as soon as possible. For that, Sec. 3 is devoted to software. It explains how to install `gcell` and `aspect`, helps understand input, output, content of the header files, lists all files that come with the package and explains the purpose of each. The section shows structure of both codes (call graphs). As both codes overlap significantly in terms of source files used, we recommend readers understand `gcell` even if one needs to simulate absorption in the atmosphere. Information from Sec. 3 is sufficient to start using our codes.

One more topic that should be clarified from the very beginning is terminology. In what follows, the word “*line*” will refer to a spectral line of a molecule, while a line with ASCII symbols in the HITRAN database file will be called “*record*”. We use the word “*profile*” when we talk about the change of atmospheric parameters with height. For the dependence of absorption by a single

217 line vs. wavenumber, which is often called “*line profile*”, we use the word “*line shape*”. We do  
218 not deal with scattering in this paper. As a result, we often drop the word “*absorption*” for  $\tau$ . For  
219 the same reason, “*extinction*” and “*absorption*” are used synonymously here. “*Spectral*  
220 *dependence*” refers to variation of some parameter over wavenumber or wavelength, depending  
221 on the context. Speaking about software, we say “C-code” for simplicity. However, we use some  
222 features from C++, e.g. we allocate and deallocate memory using `new` and `delete` functions,  
223 hence one must use a compiler with C++ support.

224 In this project, we use C for the reasons of numerical efficiency, standardization, long-lasting  
225 history, and wide usage in science and engineering (Press et al., 1992 & 2007; Oliveira &  
226 Stewart, 2006; Gottschling, 2021). C can be easily wrapped in Python and the two follow the  
227 same column-major rule for allocation of matrices in memory; the original SHARM-IPC LBL  
228 tool, which we have refactored, was also developed in C. However, we do not expect much  
229 knowledge of C/C++ from the reader. Basically, our codes use 1D arrays, nested loops, and  
230 functions that may take scalars and arrays as input and output arguments. Tools like ChatGPT<sup>9</sup>  
231 quickly provide small, clear, compliable examples for all that.

232 In the following Sec.2, which we have not yet mentioned, we provide references to some already  
233 existing tools for gas spectroscopy. The list is long and by far not complete. However, we argue  
234 in that section that our tools `gcell` and `aspect` may also find their place among the existing  
235 ones and be useful for the community.

## 236 2. Many tools for atmospheric spectroscopy: why publish one more?

237 An enormous number of tools for numerical simulation of abortion spectroscopy has been  
238 created within the past ~50 years in order to meet a huge variety of practical needs. This is  
239 caused by different physical environments (Earth, stars, planets), observation geometries  
240 (laboratory, open air horizontal path, plane-parallel or spherical atmosphere), spectral resolutions  
241 (broad band, LBL), numerical techniques (real-time calculations, lookup tables - LUTs, principal  
242 component analysis - PCA, neural network – NN approaches), physical effects (spectral line  
243 absorption, continuum absorption, scattering by molecules and/or aerosols and clouds), desired  
244 input (spectral database and atmospheric profiles) and output parameters (transmittance,

---

<sup>9</sup> <https://chat.openai.com/>

245 radiance, flux, derivatives), target instrument design (air- vs. spaceborne, field of view, spectral  
246 response functions), and, last but not least, forms of software product (stand-alone tool, linked  
247 library, language, open-source or proprietary).

248 These and other needs are satisfied by the following RT tools<sup>10</sup>, a complete list of which is likely  
249 impossible to compile<sup>11</sup>: 4A (*Scott & Chedin*, 1981), AER<sup>12</sup> set of RT models (e.g., LBLRTM in  
250 *Clough et al.*, 2005), AMSUTRAN (*Turner et al.*, 2019), ATREM (*Gao et al.*, 1993; *Thompson*  
251 et al., 2015), BTRAM<sup>13</sup> (*Chapman et al.*, 2010), FARMS (*Xie et al.*, 2016), FASCODE (*Clough*  
252 et al., 1981), GENLN2 (*Edwards et al.*, 1992), LINEPAK<sup>14</sup> (*Gordley et al.*, 1994), KOPRA  
253 (*Stiller et al.*, 2001), LOWTRAN (*Kneizys et al.*, 1988), MCARaTS<sup>15</sup> (*Iwabuchi & Okamura*,  
254 2017), MODTRAN (*Berk et al.*, 2014 & 2017), MolecFit<sup>16</sup> (*Smette et al.*, 2015), MOLIERE  
255 (*Urban et al.*, 2004), MOSART (*Cornette et al.*, 1994), PSG<sup>17</sup> (*Villanueva et al.*, 2018), RADIS  
256 (*Pannier & Laux*, 2019), RFM (*Dudhia*, 2017), RRTM (*Mlawer et al.*, 1997), RTTOV (*Saunders*  
257 et al., 1999), SpectraPlot<sup>18</sup> (*Goldenstein et al.*, 2017), STREAMER & FLUXNET<sup>19</sup> (*Key &*  
258 *Schweiger*, 1998), TAPAS<sup>20</sup> (*Bertaux et al.*, 2017), TAU<sup>21</sup> (*Hollis et al.*, 2013 & 2014), VSTAR  
259 (*Bailey & Kedziora-Chudczer*, 2012 ),  $\sigma$ -IASI (*Amato et al.*, 2002; *Carissimo et al.*, 2005).  
260 Source code and user's guide, in addition to publication(s), are available from corresponding  
261 websites (see footnotes). Some websites provide an online interface to run calculations (see, in  
262 particular, NASA GSFC's PSG – Planetary Spectrum Generator). Graphics processing units  
263 (GPUs) are used for LBL calculations in (*Collange et al.*, 2008) – an example of modern  
264 hardware usage for known theory. This GPU paper explains the implementation at a high level,  
265 however, no details about the code itself are given.

---

<sup>10</sup> [https://en.wikipedia.org/wiki/Atmospheric\\_radiative\\_transfer\\_codes](https://en.wikipedia.org/wiki/Atmospheric_radiative_transfer_codes)

<sup>11</sup> We refer the reader to respective papers for definition of the acronyms.

<sup>12</sup> <http://rtweb.aer.com/lblrmt.html>

<sup>13</sup> <https://blueskyspectroscopy.com/>

<sup>14</sup> <https://www.spectralcalc.com>

<sup>15</sup> <https://sites.google.com/site/mcarats/monte-carlo-atmospheric-radiative-transfer-simulator-mcarats>

<sup>16</sup> <https://www.uibk.ac.at/eso/software/molecfit.html.en>

<sup>17</sup> <https://psg.gsfc.nasa.gov/>

<sup>18</sup> <https://spectraplot.com/>

<sup>19</sup> <https://stratus.ssec.wisc.edu/fluxnet/>

<sup>20</sup> <http://cds-espri.ipsl.fr/tapas/>

<sup>21</sup> <http://www.ucl.ac.uk/exoplanets/>

266 In order to account for absorption in atmospheric windows, comprehensive RT packages that  
267 focus on scattering of radiation, like ARTS<sup>22</sup> (Buehler et al., 2018), SASKTRAN<sup>23</sup> (Bourassa et  
268 al., 2008), SCIATRAN<sup>24</sup> (Rozanov et al., 2014), SHARM-IPC (Lyapustin et al., 2010), or  
269 libRadtran<sup>25</sup> (Emde et al., 2016) come with built-in and/or stand-alone tools for simulation of  
270 molecular absorption. PCA (Liu et al., 2016; Yang et al., 2016; Havemann et al., 2018) and  
271 AI/ML/NN techniques are also used, e.g. to reduce computational burden in broadband  
272 calculations and for other purposes (Zhou et al., 2021; Kistenev et al., 2022; Prischepa et al.,  
273 2023; Chen et al., 2024).

274 Input for LBL computations come from datasets containing spectral optical properties of  
275 molecules and defining models that describe how these optical properties change with  
276 temperature and pressure. HITRAN, updated roughly every four years, is arguably the oldest and  
277 most used spectroscopic database (Rothman et al., 1978 – earliest report in the HITRAN format,  
278 1987 – the name HITRAN is introduced, 2005 & 2010 & 2021 – reviews of HITRAN). GEISA<sup>26</sup>  
279 (Delahaye et al., 2021), ABSKO (Payne et al., 2020), and SCIAMACHY molecular absorption  
280 spectra<sup>27</sup> (Bogumil et al., 2003) are other examples of databases for atmospheric applications;  
281 some references to IR, far IR, microwave, and submillimeter databases are listed in (Gordon et  
282 al., 2016). Appendix A in (Rothman et al., 2008) explains how to convert the line intensities  
283 from the Jet Propulsion Laboratory (JPL, Pickett et al., 1998) and Cologne Database for  
284 Molecular Spectroscopy (CDMS: Müller et al., 2005) catalogs to that of HITRAN.

285 Our paper focuses on the terrestrial atmosphere and solar reflectance band, up to the wavelength  
286  $\lambda \sim 2500$  (nm). For typical atmospheric conditions further in the paper we also rely on HITRAN  
287 for simulation of absorption by a spectral single line. The HITRAN Application Programming  
288 Interface (HAPI<sup>28</sup>: Kochanov et al., 2016) is an open-source Python package that can download  
289 LBL data from the HITRAN online database, HITRANonline (Hill et al., 2013 & 2016). The  
290 package is well documented in the above-mentioned papers, manual, and in a carefully written

---

<sup>22</sup> <https://www.radiativetransfer.org/>

<sup>23</sup> <https://usask-arg.github.io/sasktran/>

<sup>24</sup> <https://www.iup.uni-bremen.de/sciatran>

<sup>25</sup> [www.libradtran.org](http://www.libradtran.org)

<sup>26</sup> <https://geisa.aeris-data.fr/>

<sup>27</sup> <https://www.iup.uni-bremen.de/gruppen/molspec/>

<sup>28</sup> <https://hitran.org/hapi>

291 code. HAPI contains functions for calculation of absorption spectrum for a given temperature  
292 and pressure. Different line shape models are available, but height dependence of temperature  
293 and pressure are not built in. Therefore, HAPI is not convenient for atmospheric calculations on  
294 a large scale but can be used for validation of the gas cell calculations and absorption coefficient  
295 at a given height in atmosphere.

296 The mentioned non-exhaustive list of codes shows that some spectroscopic tools are new (use  
297 modern language, GPU, provide interface for online calculations), some are old, some are  
298 publicly available, but some are not. Corresponding papers and user guides describe theory  
299 behind the tools, input, and output, which is convenient for an end user. But as a drawback, such  
300 tools are often used as a “*black box*” which does not allow “*to better understand the physics of*  
301 *radiative transfer*”, complicates research by obscuring “*intermediate variables*”, and imperfect  
302 for “*pedagogical purposes*” (Schreier et al., 2019: pp.2-3). A paper or a manual about a package  
303 does not necessarily mean a paper or a manual explaining how to create – hence confidently  
304 modify – the package. Further, a full radiative transfer package, like the one simulating spectral  
305 radiance in an atmosphere, is too powerful for a simple problem, like light absorption by a gas in  
306 a cell or along a horizontal path, and too complicated to learn how to use and develop from  
307 scratch. Big codes are not always a good fit for small needs. The user runs onto a bigger problem  
308 if there is a need to replace an absorption database in a third party developed code that supports,  
309 say, only HITRAN.

310 The “*black box*” software model prevents debugging, refactoring, long-lasting support, and  
311 transition of knowledge with the workforce – be those new hires, or experts coming from other  
312 fields. An example of the need for relatively simple refactoring is the update of the HITRAN  
313 database file format. In 2004, the file format changed from 100 characters per record (line in  
314 ASCII file) to 160 (Rothman et al., 2005: p.142). Sec.4.1 below shows that a knowledgeable user  
315 would spend a few minutes to make and test the necessary change. But even for the developer,  
316 the update of theoretical foundation for absorption by a single line (Sec.4.3) will require more  
317 time. The latter task is barely manageable by someone who does not understand the insights of  
318 the code. In addition to lack of time for in-depth studying of the existing code, the gap in  
319 knowledge may be caused by the way the existing open-source code is written.

320 The need for publication of codes was recognized in spectrometry in the 1960's (*Armstrong*,  
321 1967). Despite that, our abovementioned literature analysis revealed a gap in discussing the  
322 software development of the spectroscopic codes, as opposed to theoretical background. A rare  
323 example is the Generic Atmospheric Radiation LBL Infrared Code (GARLIC: *Schreier* et al.,  
324 2014), which is a Fortran 90/2008 re-implementation (refactoring) and extension of the Modular  
325 InfraRed Atmospheric Radiative Transfer (MIRART) Fortran 77/90 code (*Schreier & Boettger*,  
326 2003). MIRART and GARLIC are programs for infrared-microwave atmospheric RT forward  
327 modeling and retrievals. GARLIC offers limb and nadir observation geometry, user-defined  
328 instrumental field-of-view and spectral response function, Jacobians, different spectral line  
329 shapes, optimized algorithms for LBL calculations of molecular cross sections, and other  
330 features useful for applications. Noteworthy, the developers paid attention to software side of the  
331 scientific code (see Sec. 3: "Implementation - GARLIC" in their paper). They did not simply add  
332 new features into the previous version, MIRART, but invested time in refactoring: translation  
333 from Fortran 77/90 to Fortran 90/2008, with emphasis on modular structure, and validation of  
334 intermediate results (unit testing).

335 Overall, the MIRART-GARLIC family is an example of caring about software in addition to  
336 science: MIRART was first announced in 2000 (*Schreier & Schimpf*, 2001), this "transition  
337 phase" from MIRART to GARLIC took place in 2007, the GARLIC paper was published in  
338 2014. In 2019, GARLIC was reimplemented again – this time as PYthon scripts for  
339 Computational Atmospheric Spectroscopy (Py4CAtS) in order to use numeric and scientific  
340 Python modules for computationally-intensive code sections (*Schreier* et al., 2019). Py4CAtS  
341 inherits and further extends the GARLIC capabilities, and it is publicly available<sup>29</sup>.

342 Now we come to answer the question from the title of this section. Despite an avalanche of tools  
343 for atmospheric spectroscopy has already been reported in countless papers, and many of the  
344 tools offer publicly available codes, the process of development of a spectroscopic tool is poorly  
345 covered. In our paper, we discuss the development of a simple, compared to many others, code.  
346 But we show the process of the development from the very beginning in three modes: absorption  
347 by a single line ("basic"), absorption in a gas cell by a group of lines ("moderate"), and  
348 absorption in atmosphere that involves atmospheric profiles ("hard"). If the user needs to

---

<sup>29</sup> <https://atmos.eoc.dlr.de/tools/Py4CAtS/>

349 simulate absorption in a gas cell or along a horizontal path (no profiles), the “hard” part can be  
350 dropped. Through that, we wish not to overload the reader with unnecessary details. We used a  
351 similar approach in our previous paper on how to understand and write from scratch a program  
352 for numerical simulation of multiple scattering of sunlight in a plane-parallel atmosphere,  
353 commonly referred to as radiative transfer code (*Korkin et al., 2022*).

354 In a short, our goal is a simple tool explained at the code level. To meet the goal, we target  
355 developers first and users next. However, before one starts digging through the code  
356 development process, it is a good idea to prove that the offered code works. It is also practical to  
357 immediately show the complexity of the code, so that a potential developer would estimate the  
358 time needed for the job. Our next section explains the code structure and shows how to install  
359 and use it.

### 360 3. Code structure and usage

361 This section serves as a quick start guide. It explains a simple installation process, input, output,  
362 and structure of the code – see **Fig.1(a, b)**. After reading this section, the reader will be able to  
363 confidently use our codes for calculating of the LBL absorption optical thickness  $\tau(v)$  at the  
364 desired wavenumbers,  $v (cm^{-1})$ , in a gas cell or in the atmosphere. The wavenumber is literally  
365 the number of wavelengths fitting 1 (cm):  $v (cm^{-1}) = 10^4 / \lambda (\mu m) = 10^7 / \lambda (nm)$ .

366 In this section and onwards, we use the following notation. The *Courier* font is used for the  
367 software relevant text: elements of code, commands, file names, paths, input and output data. We  
368 use **bold** symbols for arrays, and *italic* for parameters (mostly defined in headers). Hence  
369 the **bold\_italic** refers to an array defined in a header file. We use the C-notation to refer to  
370 an element *i* of an array: **A[i]**. As the reader will see, `gcell` and `aspect` uses 1D arrays  
371 only. We type the unit conversion constants in `grey`. In naming convention, we prefer  
372 `under_score` over `CamelCase`, despite the latter was found preferable for speed and  
373 accuracy of manipulating programs (*Binkley et al., 2009*).

374 The code has no preferences regarding the C-compiler and has been tested using GCC under  
375 Linux, and Intel C compiler integrated into Microsoft Visual Studio via oneAPI toolbox. Before  
376 compilation, it is necessary to check paths to the HITRAN database in the header  
377 `./src/paths.h` and update, if necessary, as explained in the next section. We also

378 recommend the reader to get acquainted with the content of the headers before using, not to  
379 mention changing, the code.

380 [3.1 Header files](#)

381 Code `aspect` uses three primary header files, `paths.h`, `const_param.h` and  
382 `hprofiles.h`, and one auxiliary header `cmplx.h`. The goal of the three is to localize all  
383 parameters, including paths to files with the HITRAN data, in just a few files. Using these files,  
384 updating or adding a new molecule, isotope, or changing the profile (in `aspect`) is  
385 straightforward. The first header is short. It contains paths to the HITRAN database, `*.par` and  
386 TIPS (Sec.4.2) files. The user must check these paths before compilation and update as needed.

387 The next header, `const_param.h`, contains values of physical constants (e.g., speed of light,  
388 standard temperature and pressure, the Planck constant, etc.), precomputed mathematical  
389 constants (e.g.,  $\pi$ , square root of  $\pi$ , natural logarithm of 2, etc.), scale factors to convert units  
390 (e.g., `mbar_to_atm = 1.0/1013.25` converts pressure from millibars to atmospheres),  
391 file names (e.g., HITRAN `*.par` files with the line parameters, “q”-files for isotopes),  
392 parameters of isotopes for each molecule (e.g., number of isotopes per each molecule,  
393 abundance, molar mass, etc.), some accuracy parameters, e.g., `tau_min` is the smallest value  
394 of the total  $\tau$  to be saved in the binary file - all smaller  $\tau$  are ignored; `delta_nu = 25.0`  
395 means that contribution from all HITRAN lines within  $\Delta\nu = 25 \text{ (cm}^{-1}\text{)}$  from the given frequency  
396 is significant. This  $25 \text{ (cm}^{-1}\text{)}$  is a standard cutoff in line shape models in the solar reflectance  
397 band (*Clough et al., 1981: p.152; Lyapustin, 2003: p.870; Shine et al, 2012: p.542*). Beyond that,  
398 one should check appropriate literature and update the parameter as necessary.

399 A peculiar parameter is `water_mass_density = 1.0` ( $\text{g/cm}^3$ ) which is used to convert  
400 the water vapor columnar amount in *atm-cm* (Sec. 6.3) to the precipitated (liquid) water  
401 equivalent in *cm* and at standard temperature. Of course, this scale factor of 1.0 could be  
402 dropped in calculations, however, at the expense of code readability.

403 The last header, `hprofiles.h`, contains extracts from MODTRAN: temperature, pressure, air  
404 density, and molecular concentration height profiles, for six standard atmospheric profiles and  
405 eight molecules. It also defines grid of heights, `zkm[ ]`. In Sec.6, we talk more about its  
406 content.

407 As a first step, the user is supposed to download the package `aspect_gcell` from the  
 408 journal website<sup>30</sup> or from our GitHub repository<sup>31</sup>; unzip if necessary. Note that GitHub has a  
 409 25Mb limitation on file size. Because of that, we have zipped `./hitran/01_hitdb.par`  
 410 and `./hitran/06_hitdb.par` (HITRAN data for H<sub>2</sub>O and CH<sub>4</sub>, respectively) before  
 411 uploading. These must be unzipped into the same directory before use. We uploaded other  
 412 HITRAN \*.par files, including the one for a single O<sub>2</sub>-record, without compression. We assume  
 413 in subsequent that all files and folders are in `aspect_gcell` folder; all paths are defined  
 414 relevant to it – see our GitHub repository for structure of folders and files. Once all paths have  
 415 been confirmed, both programs are ready for compilation.

416 [3.2 Installation, input, and output parameters](#)

417 [3.2.1 Gas cell mode](#)

418 As software goes, `gcell` is a relatively simple, small code. **Table 1** shows files necessary to  
 419 run the code; **Fig.1(a)** shows its structure. The HITRAN database and TIPS files for molecules  
 420 #1-7 and 10 (HITRAN molecular numbering is discussed shortly in Sec. 4.1) come with the code  
 421 in `./hitran/` and `./hitran/TIPS/`, respectively, but are not shown in the table and on  
 422 the chart.

423 **Table 1:** Description of files for `gcell`. The build file and the `main(...)` program file come first in  
 424 the list, followed by other source files, headers, input and output ASCII files. Location of each file in the  
 425 distributive is shown assuming `./` is the directory where the package was extracted. Files used only for  
 426 the gas cell code (and not `aspect`) are highlighted in gray.

File name and location	File purpose
<b>General files</b>	
<code>./gcell.bld</code>	File with GCC commands to compile all sources and create an executable.
<b>C source files</b>	
<code>./src/main_gcell.cpp</code>	Main program file. Calculates LUT with $\tau(v)$ for a gas cell and saves the LUT into a file.

---

<sup>30</sup> In this case, all source files are in the same directory; `make_directories.py` creates proper subdirectories.

<sup>31</sup> [https://github.com/korkins/aspect\\_gcell/](https://github.com/korkins/aspect_gcell/)

<code>./src/count_lines.cpp</code>	Counts the number of records (lines in HITRAN file) within an interval [ $v_{\min} : v_{\max}$ ] in the HITRAN *.par file and returns the index for the first line, if found.
<code>./src/isotops.cpp</code>	Calculates TIPS ratio for the given temperature and returns parameters of all isotopes of the given molecule
<code>./src/ix1ix2.cpp</code>	For a given interval, it returns the first $ix1$ and last $ix2$ indices of array elements belonging to the interval; zero-offset for $ix$ is assumed.
<code>./src/read_hitran160.cpp</code>	Reads the HITRAN data from a *.par file assuming 160-symbols long format
<code>./src/voigt/humlicek.cpp</code>	Calculation of the Voigt spectrum using Humlicek algorithm; borrowed from SHARM-IPC ( <i>Lyapustin, 2003</i> )
<code>./src/voigt/cmplx.cpp</code>	Defines complex arithmetic operations for humlicek.cpp; borrowed from SHARM-IPC ( <i>Lyapustin, 2003</i> )
<b>Headers</b>	
<code>./src/paths.h</code>	Defines paths to HITRAN database and TIPS files
<code>./src/const_param.h</code>	Defines physical and mathematical constants, HITRAN and TIPS file names.
<code>./src/voigt/cmplx.h</code>	Header for humlicek.cpp and cmplx.cpp files; borrowed from SHARM-IPC ( <i>Lyapustin, 2003</i> )
<b>Input and output ASCII files</b>	
<code>./gcell-ao2.inp</code>	Test input for oxygen A-band scenario (Sec. 5.3.1).
<code>./gcell-ch4.inp</code>	Test input for methane scenario (Sec. 5.3.2).
<code>./check/gcell_check_O2.txt</code>	Output for gcell-ao2.inp for checking purpose
<code>./check/gcell_check_CH4.txt</code>	Output for gcell-ch4.inp for checking purpose
<code>./check/gcell_check_noinp.txt</code>	Output for gcell when run without input file

427

428 The `gcell.bld` file contains GCC commands, with flags, to compile all sources under Unix  
 429 and link these into an executable. Under Windows, the user simply creates a Visual Studio  
 430 project, damps the source files in it, and compiles in Debug or Release mode.

431 Once compiled, `gcell` can be checked by running this command without arguments (we  
 432 assume a Unix environment hereafter)

```

 433 $ ./gcell
 434 In this case, gcell tells the user that no input file is provided and the AO2-band case will run.  

 435 In ~0.1sec a file named O2.txt will appear in the gcell directory, containing two columns:  

 436 left is the wavenumber,  $v (cm^{-1})$ ; right is the absorption cross-section per molecule,  $k(v)$   

 437 ( $cm^2/molec$ ). This mode quickly tests the package – see gcell_check_noinp.txt for  

 438 numbers.
  
```

439 A user defined input comes from a text file with a fixed (in terms of sequence of input  
 440 parameters) format:

```

 441 molec_id  nu_usr_min  nu_usr_max  dnu  lcm  T_kelv  p_atm  fmt
 442 Parameters in the line (with data types), left to right are:
  
```

443 `molec_id` (integer) defines a molecule of gas following the HITRAN notation: 1 (H2O) –  
 444 water vapor; 2 (CO2) – carbon dioxide; 3 (O3) – ozone; 4 (N2O) – nitrous oxide; 5 (CO) –  
 445 carbon monoxide; 6 (CH4) – methane; 7 (O2) – molecular oxygen; 10 (NO2) – nitrogen  
 446 dioxide. These are some species typically used for passive remote sensing of Earth's  
 447 atmosphere and surface from satellites in the visible and near-infrared portions of the solar  
 448 spectral range. However, the user should check for the importance of absorption by other  
 449 species in their spectral region of interest.

450 `nu_usr_min`, `nu_usr_max`, `dnu` (double) define grid of wavenumbers,  $v (cm^{-1})$ . The  
 451 minimum (left) and maximum (right) points in the grid are `nu_usr_min` and  
 452 `nu_usr_max`, respectively.

453 `lcm` (double) length of the gas cell in  $cm$ .

454 `T_kelv` (double) temperature in the gas cell in Kelvins ( $K$ ).

455 `p_atm` (double) pressure in the gas cell in atmospheres (*atm*).

456 `fmt` (char) defines output quantity:  $\tau$  (or  $\tau\alpha$ ) – calculate  $\tau$ , otherwise calculate absorption  
 457 cross-section  $k (cm^2/molec)$ . In the latter case, `lcm` is not relevant.

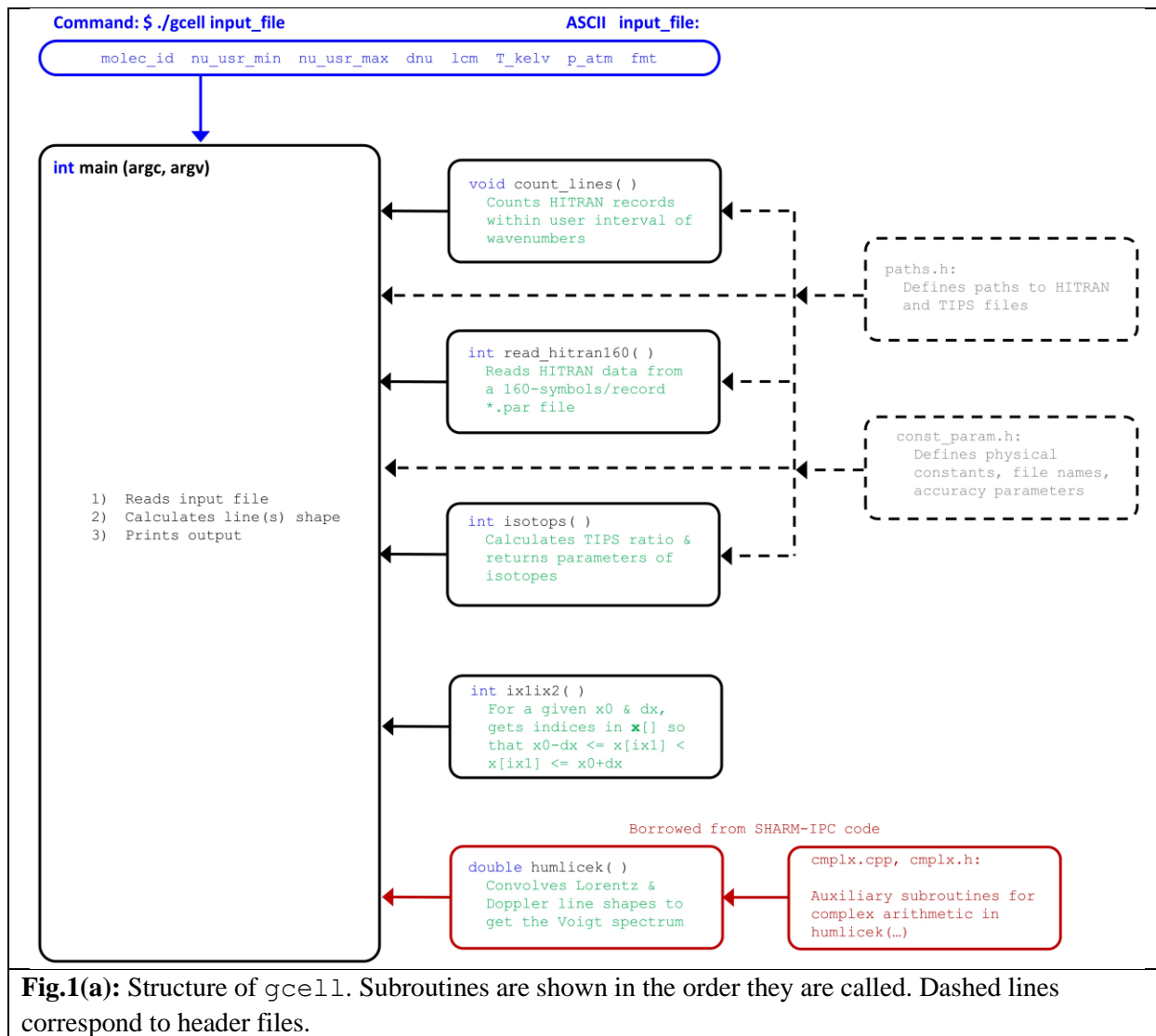
458 Consider gcell.inp with the following content:

459 6 4081.901 4505.699 0.002 8.0 296.0 1.0 k

460 One runs this case by typing<sup>32</sup>

461 \$ ./gcell gcell.inp

462



463

464 It corresponds to simulation of methane, CH<sub>4</sub>, which is HITRAN's molecule #6, across the  
465 [4081.901, 4505.699] (cm<sup>-1</sup>) spectral band with step 0.002 (cm<sup>-1</sup>) in an 8 (cm) long gas cell at

<sup>32</sup> In MS Visual Studio, add the file via Configuration Properties\Debugging\Command Arguments

466 temperature 296 (*K*) and pressure 1 (*atm*). According to the last character *k*, the output file  
467 CH4.txt will contain absorption cross-section (2<sup>nd</sup> column) as a function of wavenumber (1<sup>st</sup>  
468 column); the wavenumber goes in increasing order. If the input and the executable files are not in  
469 the same directory, a full path must be specified. As defined in paths.h, the full path length  
470 must not exceed 256 characters: path\_len\_max = 256.

471 A similar input gcell-ch4.inp will result in CH4.txt, but containing  $\tau$  because of the last  
472 input parameter tau ( $\tau$  is also acceptable because gcell decides based on the first  
473 character). We also provide an input file gcell-ao2.inp. The content of this input matches  
474 the no-input run of the gcell code, except this explicit input will return  $\tau$ .

475 Spaces and tabs in the input files are ignored. However, due to fixed format of the input, lcm is  
476 not optional even if the user calculates the absorption cross-sections. In the gas cell mode, we  
477 assume natural atmospheric abundances for isotopes (which HITRAN parameters already  
478 account for). Otherwise, one must rescale the abundances from HITRAN's default to those used  
479 *de facto*.

480 The gas cell assumes a single type of molecule. By changing one line of code, see Eq.(8) below,  
481 it is easy to account for a gas-air mixture. Thus, the gas cell mode can be used for simulation of  
482 absorption of molecules of the gas on a horizontal path in the air. In this case, the temperature  
483 and pressure remain constant, but one must modify input to account for the mixing ratio, and the  
484 "gas cell" will be long, e.g., lcm = 100000.0 for a 1 (km)-long trace. With these few last  
485 comments made, we continue to the atmospheric mode – code aspect.

486 3.2.2 Atmospheric mode

487 The codes aspect and gcell share some source files. In addition to those from **Table 1**  
488 without grey highlighting, **Table 2** shows files that pertain exclusively to aspect. For example,  
489 aspect uses all the same headers as gcell, and one more, hprofiles.h – the only one  
490 listed in Table 2. **Fig. 2(b)** shows structure of aspect.

491 **Table 2:** Description of files for aspect. The content is like in Table 1, which non-highlighted files are  
492 also dependencies of aspect.

File name and location	File purpose
------------------------	--------------

<b>General files</b>	
<code>./aspect.bld</code>	File with GCC commands to compile all sources and create an executable.
<b>C source files</b>	
<code>./src/main_aspect.cpp</code>	Calculates LUT with spectral and height dependence of $\tau(v)$ and saves the LUT into a file.
<code>./src/hisotops.cpp</code>	For each isotope of a given molecule, calculates the TIPS ratio as a function of height, and returns the molar mass, abundance, and the number of isotopes.
<code>./src/intparab.cpp</code>	Approximates 3 points with a parabola and integrates it for a given interval, covered by the parabola.
<code>./src/kabs.cpp</code>	Calculates the spectral absorption cross-section per molecule.
<code>./src/simpson.cpp</code>	Numerically integrates a function using Simpson's rule <sup>33</sup> .
<code>./src/tauabs25.cpp</code>	Integrates the extinction profile over height from TOA to a set of user-defined heights not exceeding $z = 25$ (km). For any altitude above this point, the function returns integral from TOA to 25 (km)
<b>Headers</b>	
<code>./src/hprofiles.h</code>	Contains MODTRAN profiles for temperature, pressure, air number density, relative concentration of the gas species, and grid of heights.
<b>Input and output ASCII data files</b>	
<code>./aspect-ch4.inp</code>	Test input for a methane scenario; runtime ~1800 seconds (45823 relevant HITRAN-2020 lines).
<code>./aspect-ao2.inp</code>	Test input for the oxygen A-band scenario; runtime ~2 seconds (345 relevant HITRAN-2020 lines)
<code>./check/aspect_check_noinp.txt</code>	Output for aspect called without input file.
<code>./check/aspect_check_CH4.txt</code>	Output for aspect-ch4.inp for checking purpose
<code>./check/aspect_check_O2_dat.txt</code>	Output for aspect-ao2.inp containing metadata: initial point of the wavenumber interval $v_0$ , step $dv$ , number of points over $v$ , number of altitude points.

<sup>33</sup> [https://en.wikipedia.org/wiki/Simpson%27s\\_rule](https://en.wikipedia.org/wiki/Simpson%27s_rule)

	This file also shows 2 Python commands for reading the binary files (see below).
<b>Output binary data files</b>	
./check/aspect_check_O2.bin	Output for aspect-ao2.inp with $\tau(v)$ as 32-bit floating point numbers as a function of height (lead dimension) and wavenumber.
./check/aspect_check_O2_inu.bin	Output for aspect-ao2.inp with the wavenumber grid expressed as a 32-bit integer index.

493

494 Once compiled, the following command is used to run aspect from the command line (like for  
 495 gcell, we assume commands are typed in Unix environment)

496 \$ ./aspect filename

497 The filename is an ASCII file with input parameters in the following format:

498 molec\_id iatm column\_amount nu\_usr\_min nu\_usr\_max dnu nzkm **zkm[]** fmt

499 Parameters, left to right are:

500 molec\_id (integer) defines a molecule of gas following the HITRAN notation (see  
 501 gcell discussion above)

502 iatm (integer) – defines atmospheric profile of temperature and pressure following  
 503 MODTRAN: 1 – Tropical, 2 – Midlatitude Summer, 3 – Midlatitude Winter, 4 – Subarctic  
 504 Summer, 5 – Subarctic Winter 6 – Standard US 1976 atmosphere (see Sec. 6.1);

505 column\_amount (float) defines the atmospheric total column amount of the selected gas.  
 506 For the water vapor, molec\_id = 1, the column amount indicates centimeters of  
 507 precipitated water (see Sec. 6.5). For all other molecules, the column amount is defined in  
 508 parts per million in a volume (*ppmv*). Negative value, e.g. -1.0, instructs aspect to borrow  
 509 the column amount from MODTRAN (see Sec. 6.2).

510 nu\_usr\_min, nu\_usr\_max, dnu (double) define a grid of wavenumbers,  $v(cm^{-1})$ . The  
 511 minimum (left) and maximum (right) points in the grid are nu\_usr\_min and  
 512 nu\_usr\_max, respectively. To include the maximum point, aspect calculates the

513     number of points in the grid, `nnu`, by rounding the number of intervals towards the nearest  
514     greater integer using `ceil`

515     `nnu = int(ceil((nu_usr_max - nu_usr_min)/dnu))+1`

516     Note, higher `nnu` impose higher requirements on memory.

517     `nzkm` (integer) defines the number of heights at which the absorption optical depth will be  
518     calculated. The amount of memory required for calculations and the size of the output file  
519     depend on `nnu*nzkm`.

520     `zkm[nzkm]` (float, array of `nzkm` elements) – defines array of heights, in kilometers (*km*),  
521     from the lowest to the highest one, w.r.t. the ground level,  $z = 0.0$  (*km*). The output value at  
522     the requested height `zkm[i z]` corresponds to  $\tau$  from the MODTRAN’s TOA level,  $z = 120$   
523     (*km*), to the given height.

524     `fmt` (string of 3 characters) defines format of output: `txt` – ASCII (1 file will be returned), `bin`  
525     – binary (3 files will be returned: `2 * .bin` and `1 * .txt`).

526     Tab(s) or more than one space are allowed as delimiters in the input file. We assume it is the  
527     user’s responsibility to provide meaningful input. Neither `aspect` nor `gcell` check the input  
528     file for correctness. The only exception is to check if the given `imolec` is included. It is  
529     convenient to keep the input file(s) in the same folder with the `aspect` executable. Otherwise,  
530     the user is expected to provide a full path to the input file. If the input file is missing at the  
531     specified location, `aspect` will notify the user and stop execution. If the input file is not  
532     specified at all, `aspect` will run a default scenario for the oxygen A-band,  $\text{AO}_2$ , defined as  
533     follows:

534     7   6   -1.0   13050.0   13160.0   0.01   3   0.0 2.5 5.0   txt

535     This default option is good for a quick check. As explained above, this input is for oxygen  $\text{O}_2$   
536     (`molec_id = 7`), standard US 1976 MODTRAN profile (`iatm = 6`, see Sec.6.1) and the  
537     total amount of gas from the same (`column_amount = -1.0`, see **Table 6** below), for the  
538     wavenumber grid ranging from  $13050$  ( $\text{cm}^{-1}$ ) to  $13160$  ( $\text{cm}^{-1}$ ) with step  $0.01$  ( $\text{cm}^{-1}$ ), and for  
539     `nzkm = 3` heights located at BOA,  $0.0$  (*km*),  $2.5$  (*km*), and  $5.0$  (*km*). The last parameter,  
540     `txt`, tells `aspect` to save output as an ASCII file. Note, again, that `aspect` returns partial

- 541 column optical thicknesses (from TOA to the given altitudes), not the layer one calculated as  
542 difference between partial column optical thicknesses.

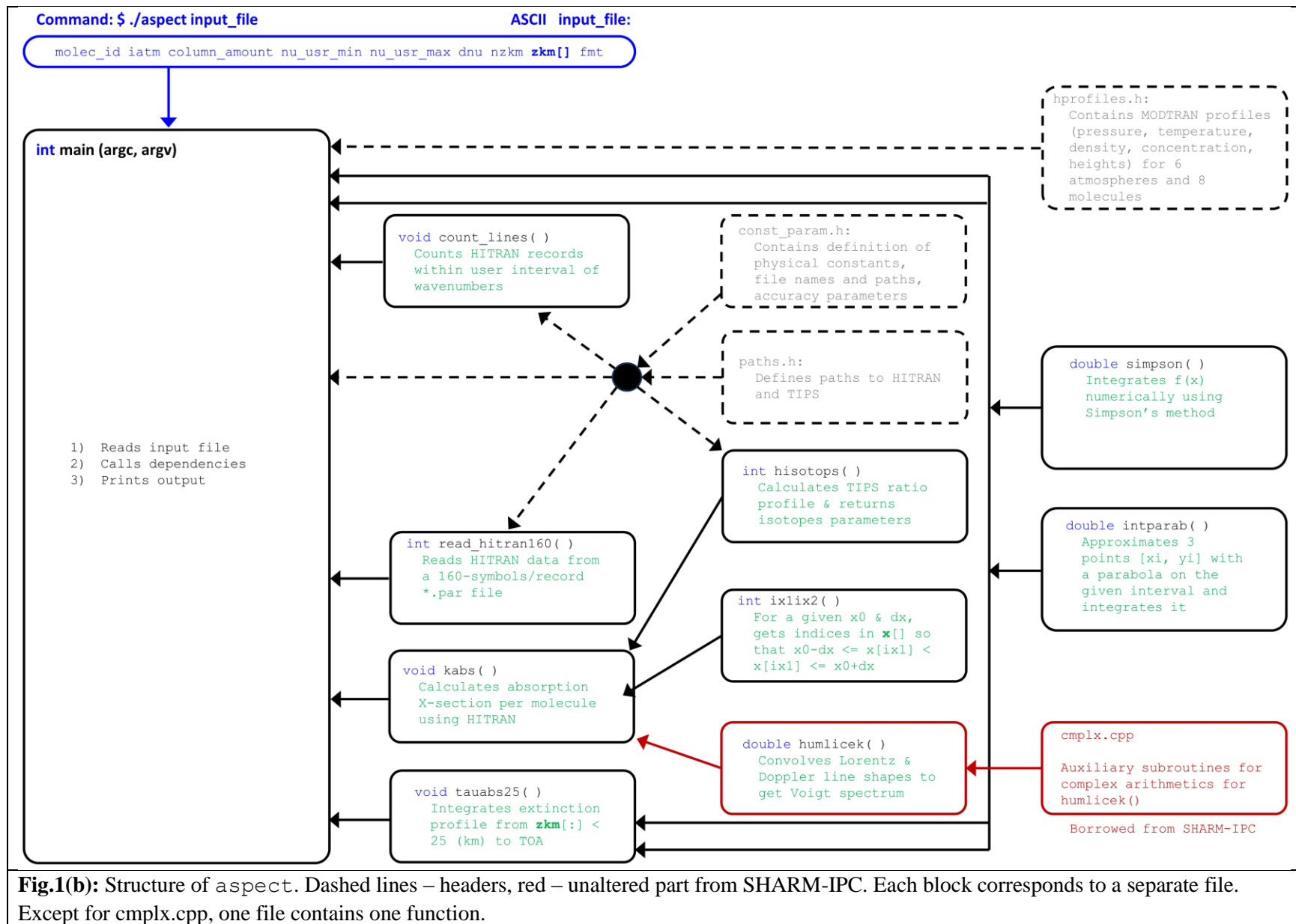


**Fig.1(b):** Structure of aspect. Dashed lines – headers, red – unaltered part from SHARM-IPC. Each block corresponds to a separate file. Except for cmplx.cpp, one file contains one function.

544 The output file `O2.txt` (note that the name is assigned automatically based on the `molec_id`  
545 value) for the default case looks as follows (the first 4 and last 3 lines are shown; the result may  
546 look slightly different if the HITRAN database has changed, these correspond to HITRAN 2020)

```
547 # nu, zkm = 0.000 2.500 5.000
548 0 13050.0000 2.782330e-01 1.396493e-01 6.701932e-02
549 1 13050.0100 2.897391e-01 1.454148e-01 6.978132e-02
550 2 13050.0200 3.020048e-01 1.515606e-01 7.272536e-02
551 ...
552 10998 13159.9800 4.861486e-01 2.428781e-01 1.161131e-01
553 10999 13159.9900 4.984823e-01 2.486472e-01 1.186825e-01
554 11000 13160.0000 5.125586e-01 2.553003e-01 1.216783e-01
```

555 Starting from the second line onwards, the left column indicates an integer wavenumber index,  
556 `inu`, and the corresponding wavenumber `nu[inu]`, calculated as follows

```
557 nu[inu] = nu_usr_min + inu*dnu;
```

558 Next comes  $\tau$  as integrated from TOA to 0.0, 2.5, and rightmost column 5.0 ( $km$ ). Excluding the  
559 header line (#), the file contains 11001 records:

```
560 nnu = (13160 - 13050)/0.01 + 1 = 11001.
```

561 Based on the user-defined threshold for  $\tau$  at the lowest height (usually, at BOA), aspect may  
562 skip insignificant values to reduce the size of the output file. In this case, the number of records  
563 will not match the number of grid points. The threshold  $\tau$  is defined in `const_param.h`; the  
564 current setting is `tau_min = 1.0e-4`, which corresponds to a one-way vertical transmittance  
565 in atmosphere  $T(v, \mu = 1) = 0.9999$  (see Eq.(24) below).

566 The ASCII file is convenient for visual inspection, e.g. at debugging stage. For a smaller size of  
567 the output file and faster reading of the data into memory, the binary format is preferable: `fmt`  
568 = `bin`. In this case, aspect generates three files on output. The first one, `O2_dat.txt`,  
569 contains information necessary to read in the binary files: the number of the spectral and height  
570 grid points. It also tells that floating-point numbers are stored in the single precision 32-bit  
571 format. The other two, `O2_inu.bin`, and `O2.bin`, contain 32-bit integer indices `inu` for the  
572 corresponding wavenumbers. In `O2.bin`, the height grid is the lead dimension; for each given  
573 wavenumber index, optical thicknesses at different heights are stored consecutively.

574 The following Python script reads  $\tau$  from the binary file and converts the 1D array into a 2D  
575 array with heights changing column wise and wavenumbers – row wise:

```
576 import numpy as np
577 data = np.fromfile('O2.bin', dtype=np.float32)
578 tau[0:nnu, 0:nzkm] = np.reshape(data, (nnu, nzkm))
579 # O2_dat.txt contains nnu & nzkm
```

580 For the default AO2 case, `O2.bin` is about 5.5 times smaller than `O2.txt`: 709Kb/129Kb.  
581 Also, when saving and reading the binary files on different machines, the user must care for  
582 endianness<sup>34</sup>.

583 At this point, the reader is familiar with two modes of the code, and input and output format.  
584 This is the basic user level. An extension to the user level is understanding of the code structure:  
585 C-functions and their purpose, as charted in **Fig.1 (a, b)**. Now we proceed to the level of  
586 development. The first step is calculation of the absorption coefficient  $k$  ( $cm^2/molec$ ) by a single  
587 line as parameterized by a corresponding HITRAN record. Since `gcell` does not consider  
588 height profiles, we recommend following our discussion with that code.

#### 589 4. Calculation of absorption by a single HITRAN line

590 This section shows how to calculate the absorption cross-section  $k$  ( $cm^2/molec$ ) for a single line  
591 using HITRAN parameters. As the units of  $k$  indicate, the cross-section is defined per one  
592 molecule of gas present. This standard practice will be assumed hereafter and the words “per  
593 molecule” will be dropped. As a prerequisite, we assume the user has downloaded the HITRAN  
594 database for molecules 1 through 7 and 10. The HITRAN ASCII `*.par` files with the line  
595 shape parameters come in the current 160-symbols-long format. The user should get acquainted  
596 with the HITRAN theoretical background using, e.g., online HITRAN manuals<sup>35, 36</sup> or papers  
597 (Rothman, 1998: p.708; Pliutau & Roslyakov, 2017 – note, the latter describes an educational  
598 software). Since typos are always possible, we recommend checking references from different

---

<sup>34</sup> <https://en.wikipedia.org/wiki/Endianness>

<sup>35</sup> <https://hitran.org/docs/definitions-and-units/>

<sup>36</sup> <http://www.bytran.org/howtolbl.htm>

599 authors, or different years from the same authors. All numerical results that we show in this  
600 paper correspond to HITRAN 2020 downloaded from the HITRANonline website<sup>37</sup>.

601 [4.1 Reading one record form the HITRAN \\*.par file](#)

602 It is instructive to create and read a HITRAN file with only one record. As an example, we pick  
603 one O<sub>2</sub> line at  $v = 13000.816219$  ( $cm^{-1}$ ) and read it using the `read_hitran160(...)` function.  
604 For reproducibility and simplicity of debugging, our `./hitran/` folder contains a file in the  
605 HITRAN 160-symbols-long format with only the named line `07_hitdb_one_line.par`.  
606 The main command executed in `read_hitran160(...)` is

```
607     fscanf(fin, "%2c%1c%12c%10c%10c%5c%5c%10c%4c%8c%93c%c",
608             str_molec_id, // molecule ID
609             str_isotop_id, // isotope ID
610             str_nuij, // transition wavenumber in vacuum
611             str_Sij, // line intensity at T=296K scaled by isotope abundance
612             str_Aij, // Einstein coefficient (not used in the paper)
613             str_gamma_air, // air-broadened Lorentzian HWHM
614             str_gamma_self, // self-broaden HWHM at T = 296 (K) and P = 1 (atm)
615             str_Elower, // Lower state energy, E'
616             str_n_air, // temperature exponent for the air-broadened HWHM
617             str_delta_air // air induced pressure shift referred to P = 1 (atm)
618             str_tail, // the rest of the line is not used
619             chr_end_of_line);
```

620 It explicitly shows the structure of the HITRAN \*.par file. Note that the total number of  
621 characters being read is 160 as the function name says. However, it is easy to adapt this  
622 command for reading an old 100-characters long \*.par file used until HITRAN 2004 edition  
623 (Rothman, 2005: Table 1). All these parameters, except for `str_molec_id` (known at input)  
624 and the Einstein coefficient (not used in our calculations), are converted from the character data  
625 type either to integer (using `atoi`) or the floating point number (`atof`), as appropriate.

626

627 **Table 3:** Output of the `read_hitran160(...)` function; the function `count_lines(...)` from  
628 Table 1 defines the number of lines `nlines` to be read and the first line `iline0` to start reading. The  
629 reference temperature and pressure are  $T_{ref} = 296^{\circ}(K)$  and  $p_{ref} = 1.0(atm) = 1013.25(Pa) = 760(torr)$ ,

---

<sup>37</sup> <https://hitran.org/lbl/>

630 respectively. For list of all HITRAN parameters with units see (*Rothman*, 1986: p.4060) and (*Gordon*,  
 631 2017: p.5).

Name	type[size]	Notation	Units	Explanation
<b>isotop_id</b>	int[nlines]	-	none	Isotope ID, as in HITRAN, to get proper isotope properties (e.g., molar mass): 1 = most abundant, 2 = second, etc.
<b>nuij</b>	double[nlines]	$v_{ij}$	$cm^{-1}$	Transition wavenumber between levels $i$ and $j$ (also called frequency)
<b>sij</b>	double[nlines]	$S_{ij}$	$\frac{cm^{-1}}{molec \cdot cm^{-2}}$	Line intensity weighted with isotope abundance, $I_a$ , at $T_{ref}$ .
<b>gamma_air</b>	double[nlines]	$\gamma_{air}$	$\frac{1}{atm \cdot cm}$	Air-broadened Lorentzian HWHM at $p = 1$ (atm) and $T = 296$ (K) for Voight line shape.
<b>gamma_self</b>	double[nlines]	$\gamma_{air}$	$\frac{1}{atm \cdot cm}$	Self-broadened Lorentzian HWHM at $p = 1$ (atm) and $T = 296$ (K) for Voight line shape
<b>Elower, Epp</b>	double[nlines]	$E''$	$cm^{-1}$	Lower state energy
<b>n_air</b>	double[nlines]	$n_{air}$	none	Temperature-dependence exponent for the air-broadened HWHM, $\gamma_{air}$
<b>delta_air</b>	double[nlines]	$\delta_{air}$	$\frac{1}{atm \cdot cm}$	Pressure shift induced by air, referred to $p = 1$ (atm)

632

633 Historically, the HITRAN database convention used one symbol for the isotope number thus  
 634 assuming up to 9 isotopes (1 = most abundant, 2 = second...) per molecule at most. However, for  
 635 some molecules more isotopes have been introduced over time. E.g., for CO<sub>2</sub> (`molec_id` =  
 636 2), HITRAN defines 12 isotopes using ID-s 0, A, and B for isotopes 10, 11, and 12, respectively,  
 637 which must be checked before converting the isotope ID from character to integer. Note also that  
 638 the line intensity,  $S_{ij}$ , is already scaled by the isotope abundance (*De Biévre* et al., 1984;  
 639 *Böhlke* et al., 2005) as found in the terrestrial atmosphere, so for such applications no further  
 640 scaling is necessary.

641 Other than these two peculiarities, reading the standard HITRAN database in ASCII format is  
 642 not a problem. For our example of the single O<sub>2</sub> line, we have `nline` = 1 (total number of

643 lines), `iLine0 = 0` (zero-offset index of the first line in the HITRAN file) and the line  
644 parameters are

```
645     isotop_id = 1
646     nuij = 13000.816219 (cm-1)
647     Sij = 2.708e-27 (cm-1/(molec cm-2))
648     gamma_air = 0.04580 (cm-1 atm-1)
649     gamma_self = 0.047 (cm-1 atm-1)
650     Epp = 1814.01040 (cm-1)
651     n_air = 0.67 (unitless)
652     delta_air = -0.007400 (cm-1 atm-1)
```

653 Negative `delta_air` means the center of the line is shifted towards the lower wavenumber  $\nu$   
654 (“left”) in air w.r.t. its position in vacuum. Despite the simplicity, it is recommended to plot, e.g.,  
655 line intensity and check the plots vs. HITRAN online tool (*Hill*, 2016) or figures reported in  
656 literature (*Rothman*, 2003: Fig.2; 2013: Fig.5; *Gordon*, 2017: Figs. 5, 6, 8; 2022: Fig. 5). The  
657 latter references also compare molecules from different HITRAN versions.

658 [4.2 Molparam.txt and TIPS q-files.](#)

659 The other two HITRAN files are `molparams.txt` and `TIPS.txt`. For all HITRAN  
660 molecules, `molparam.txt` contains a global ID molecule code (not used in this paper), the  
661 isotope abundance for the Earth environment (note again,  $S_{ij}$  is already scaled by this), the total  
662 internal partition sum (TIPS)  $Q(296)$  (explained later) at the reference temperature  $T = 296^\circ (K)$ ,  
663 the statistical weight  $g_j$  (not used in this paper), and the molar mass (in grams). In our codes, we  
664 moved all necessary information from `molparam.txt` file to the header `const_param.h`.  
665 Considering O<sub>2</sub> as an example, the content of the `molparam.txt` file<sup>38</sup>

Molecule #	Iso Abundance	$Q(296K)$	$g_j$	Molar Mass (g)
O2 (7)				
66	9.95262E-01	2.1573E+02	1	31.989830
68	3.99141E-03	4.5523E+02	1	33.994076
67	7.42235E-04	2.6581E+03	6	32.994045

671 corresponds to the following in `const_param.h`:

672     // (7) O2:

---

<sup>38</sup> To be exact, we used information from this page <https://hitran.org/docs/iso-meta/>, instead of the `.txt` file.

```

673     int const niso_o2 = 3;
674     char const fname_iso_o2[niso_o2][fname_len_max] =
675         {"q36.txt", "q37.txt", "q38.txt"};
676     double const
677         Qref_o2[niso_o2] = {215.73450400, 455.22995200, 2658.12071500},
678         molar_mass_o2[niso_o2] = {31.989830, 33.994076, 32.994045},
679         Ia_iso_o2[niso_o2] = {9.95262e-1, 3.99141e-3, 7.42235e-4};

680 Here niso_o2 is the number of isotopes, Qref_o2 are the TIPS at the reference temperature
681  $T_{ref} = 296^{\circ}(K)$ , molar_mass_o2 are the isotope molar masses, and the isotope abundances are
682 Ia_iso_o2. Note that the isotope ID number, isotope_id, which one reads from the
683 HITRAN *.par file, is used in our codes as an index to get the appropriate isotope parameters
684 from the mentioned arrays. It is therefore easy to add a new isotope by adjusting the total number
685 of isotopes and updating the arrays with new parameters. One must keep in mind that the
686 HITRAN isotope number is a unit offset integer, contrary to the C-array zero offset indexing.

687 The array fname_iso_o2, contains the file names with TIPS precomputed in a wide range of
688 temperatures  $T$  from a few degrees to a few thousand (Laraia, 2011; Gamache 2017, 2021). The
689 TIPS describes statistical properties of gas in thermodynamic equilibrium. In particular, the
690 number of molecules (population) at different energy states  $E_i$  which in its turn determines the
691 transition intensity of a line,  $S_{ij}$ . Since the dependence of the line intensity on TIPS is linear, the
692 TIPS ratio is used to scale the intensity from the value at the reference temperature,  $T_{ref} = 296^{\circ}$ 
693 ( $K$ ) to an arbitrary one.

694 Each q-file contains only two columns: left is temperature  $T (K)$  in increasing order with equal
695 step  $\Delta T = 1^{\circ} (K)$ , right is the TIPS value  $Q(T)$ . This is convenient for reading and interpolation.
696 Each q-file name is based on the global isotope ID. For example, for the oxygen, isotope_id
697 = 1, the corresponding TIPS file q36.txt in line 296 reads 215.73450400, which is the TIPS
698 value at the reference temperature Q(296°K).

699 Aspect and gcell, use special functions for the isotope data. In gcell it is

700     niso = isotops(molec_id, T_kelvin, Qratio, mmass_iso, Ia_iso);

701 Using molec_id, and a given temperature T_kelvin, the function returns the total number
702 of isotopes niso for the given molecule, ratio of TIPS  $Q(T_{ref})/Q(T)$ , the molar mass and

```

703 abundances for all niso isotopes (hence all these output parameters are arrays). In aspect,  
704 this function is slightly different because of the variation of temperature with height –  
705 hisotops (...) .

706 Specifically, based on `molec_id`, the `isotops` (...) function decides what isotopes to read  
707 from `const_param.h`

```
708     switch (molec_id)
709     {
710         ...
711         case 7: // O2
712             niso = niso_o2;
713             for (iso = 0; iso < niso; iso++)
714             {
715                 Qref[iso] = Qref_o2[iso];
716                 mmass_iso[iso] = molar_mass_o2[iso];
717                 Ia_iso[iso] = Ia_iso_o2[iso];
718                 strcpy(fname_iso[iso], fname_iso_o2[iso]);
719             } // for iso
720             break;
721         ...
722     } // switch (molec_id)
```

723 Then, for each isotope, the function opens an appropriate `qXY.txt` TIPS file, reads it  
724 consecutively until the range of temperatures for `T_kelvin` is found, interpolates TIPS linearly  
725 and calculates the TIPS ratio

```
726     for (iso = 0; iso < niso; iso++)
727     {
728         strcpy(fpath, path_TIPS);
729         strcat(fpath, fname_iso[iso]);
730         fin = fopen(fpath, "r");
731         fscanf(fin, "%lf %lf", &T2, &Q2);
732         while (T2 < T_kelvin)
733         {
734             T1 = T2;
735             Q1 = Q2;
736             fscanf(fin, "%lf %lf", &T2, &Q2);
737         } // while T2 < T_kelvin
738         Q = Q1 + (T_kelvin - T1)*(Q2 - Q1)/(T2 - T1);
```

```

739         Qratio[iso] = Qref[iso]/Q;
740         fclose(fin);
741     } // for iso

742 This straightforward, but not the most efficient way, could be improved by: (a) reducing the
743 range of  $T$  ( $K$ ) in the qXY.txt files to that typically found in the Earth atmosphere; (b)
744 converting the qXY.txt files from ASCII to an array in header (e.g., in const_param.h) –
745 this will allow to immediately find indices of the interval containing T_kelvin; (c) avoid files
746 by coding an explicit expression for  $Q(T)$  (Rothman, 1998: p.695), or by using these Fortran or
747 Python programs39. As we will see later, the performance of this subroutine is not a bottleneck.
748 Because of that, and to avoid unnecessary alteration of the default HITRAN qXY.txt file, we
749 use this simple LUT-based solution with consecutive search for the gas cell calculations.

```

#### 750 4.3 Basic code for a single line

751 Now we are ready for calculation of the absorption cross section,  $k$  ( $cm^2/molec$ ), in a gas cell. So  
752 far, we keep the abovementioned `*.par` file with one oxygen record. All commands in this  
753 section are operators of the `main(...)` function located in the `main_gcell.cpp` file.

754 For numerical calculations the user defines the following parameters:

755       nu – wavenumber to compute the absorption coefficient ( $cm^{-1}$ );

756       T\_kelvin – gas temperature ( $K$ );

757       p\_atm – gas pressure ( $atm$ ).

758 The first step is to compute the center of the spectra line  $\nu_{ij}^{pshift}$  as it shifts w.r.t. its position in  
759 vacuum  $\nu_{ij}$  due to user specified pressure  $P$  ( $atm$ ) assumed constant – like in a gas cell or at a  
760 given level in the atmosphere (same for temperature and gas concentrations)

$$761 \quad \nu_{ij}^{pshift} = \nu_{ij}(P) = \nu_{ij} + \delta_{air} P \quad (1)$$

762       nuij\_pshift = nuij + delta\_air\*p\_atm;  
763       13000.808819 = 13000.816219 + (-0.007400)\*1

---

<sup>39</sup> <https://hitran.org/suppl/TIPS/TIPS2021/>

764  $cm^{-1} = cm^{-1} + cm^{-1}/atm \cdot atm$ . Next, the intensity of the spectral line is scaled from the reference  
 765 temperature  $T_{ref} = 296^\circ (K)$  to the user-defined one. This step requires calculation of several  
 766 exponential functions which can be combined to reduce the number of calls to a computationally  
 767 expensive function `exp()`. However, it would make the code less readable and does not provide  
 768 much gain in performance.

$$769 \quad e_{11} = \exp(-c_2 E''/T) \quad (2)$$

```

770   e11 = exp(-c2_rad*Epp/T_kelvin);
771   0.00016661 ≈ exp(-1.438777*1814.01040/300.0);
772

```

$$773 \quad e_{21} = \exp\left(-c_2 E''/T_{ref}\right) \quad (3)$$

```

774 e21 = exp(-c2_rad*Epp/T_ref);
775 0.00014813 ≈ exp(-1.438777*1814.01040/296.0);
776

```

$$777 \quad e_{12} = 1 - \exp(-c_2 v_{ij}^{pshift}/T) \quad (4)$$

```

778 e12 = 1.0 - exp(-c2_rad*nuij_pshift/T_kelvin);
779 1.0 ≈ 1.0 - exp(-1.438777*13000.808819/300.0);
780

```

$$781 \quad e_{22} = 1 - \exp\left(-c_2 v_{ij}^{pshift} / T_{ref}\right) \quad (5)$$

```

782 e22 = 1.0 - exp(-c2_rad*nuij_pshift/T_ref);
783 1.0 ≈ 1.0 - exp(-1.438777*13000.808819/296.0).

```

In Eqs.(2)-(5),  $c_2 = hc / k \approx 1.44 \text{ (cm}\cdot\text{K)}$  is the second black body radiation constant. Given its value, the spectral boundary for atmospheric remote sensing in the solar region,  $\lambda_{\max} \sim 2.5 \text{ (\mu m)}$  or  $\nu_{\min} \sim 4000 \text{ (cm}^{-1}\text{)}$ , and the highest value temperature within  $z = 0 \dots 120 \text{ (km)}$   $T_{\max} \sim 350^\circ \text{ (K)}$ , both exponents in Eqs.(4) and (5) vanish. We preserve these terms for a tutorial, rather than numerical reason, but note that they can be safely dropped for the Earth atmosphere remote sensing leveraging scattered sunlight. Also we note, that the two equations rely on Eq.(1). Apparently, similar equations in the HITRAN and BYTRAN manuals contain a typo: unshifted  $\nu$  is used in both.

792 With Eqs.(2) - (5), one calculates the temperature-affected intensity of the spectral line as

793 
$$S_{ij}(T) = S_{ij}Q_{ratio}(T) \frac{e_{11}}{e_{21}} \frac{e_{12}}{e_{22}}$$
 (6)

794  $S_{ijT} = S_{ij} * Q_{ratio} * e_{11} * e_{12} / e_{21} * e_{22}$

795  $3.005168e-27 \approx 2.708e-27 * 0.98664770 * 0.00016661 * 1.0 / 0.00014813 / 1.0$

796  $[S_{ijT}] = [S_{ij}]$

797 In Eq.(6),  $Q_{ratio}(T)$  is the ratio of total internal partition functions  $Q$  at the reference and user-defined temperatures  $Q(T_{ref})/Q(T)$  (note  $T_{ref}$  is in the numerator). As stated previously, by default the HITRAN line intensity  $S_{ij}$  is already scaled by the isotope abundance typical for the Earth environment, so users need make no changes.

801 In addition to the intensity, the line width is also affected by temperature and pressure. It is common to account for two effects contributing to the line broadening: the Doppler component and the Lorentzian component. The Doppler thermal (Brownian) motion broadening is caused by the Doppler effect of change of frequency of wave when the source of light (an emitting molecule) moves w.r.t. the observer. The Kirchhoff's law requires the same change to happen for an absorbing molecule. The Doppler line shape is modeled by the Gaussian distribution with the following half-width-half-maximum (HWHM) parameter

808 
$$\alpha_D = \frac{v_{ij}^{pshift}}{c} \sqrt{\frac{2N_A k T \ln(2)}{m_{iso}}}$$
 (7)

809  $\text{alf\_doppler} = \text{nuij\_pshift} *$   
810  $\text{sqrt}(2.0 * n\_avogadro * k\_boltzman * T\_kelvin * \ln(2) / mmass\_iso) / c\_light;$   
811  $0.014257689 \approx 13000.808819 *$   
812  $\text{sqrt}(2.0 * 6.02214129e+23 * 1.3806488e-16 * 300.0 * \ln(2) /$   
813  $31.98983) / 29979245800.0$

814 The Lorentzian-broadening accounts for the natural broadening (finite radiative lifetime makes an excited atom eventually emit radiation) and collision/pressure broadening (emission of radiation by an excited atom when colliding against another atom of the same – self component – or another – foreign component – type). Again, Kirchhoff's law requires the same energy transition to happen during absorption. The HWHM parameter for Lorentzian effects is

819 
$$\gamma_L = \left( \frac{T_{296}}{T} \right)^{n_{air}} \left( \gamma_{air} (P_{total} - P_{self}) + \gamma_{self} P_{self} \right) \quad (8)$$

```
820 gam_lorentz = pow(T_ref/T_kelvin, n_air)*
821     (gamma_air*(p_tot - p_atm) + gamma_self*p_atm);
822 0.046579204 ~
823 (296.0/300.0)^0.670* ( 0.04580*(1.0 - 1.0) + 0.047*1.0 )
```

824 In Eq.(8),  $P_{self}$  is the partial pressure of the gas. In the case of the gas cell, it coincides with the  
 825 total pressure and only self-broadening takes place:  $P_{total} = P_{self}$  and the parameter  $\gamma_{air}$  becomes  
 826 irrelevant. However, if the user slightly modifies input to provide the total and the partial  
 827 pressures, the `gcell` code can be used for simulation of absorption along horizontal path in  
 828 atmosphere that contains mixture of gases or in gas cell containing the same.

829 The Doppler and Lorentzian broadenings take place together and their combined effect is  
 830 expressed as a convolution of the respective line shapes, resulting in the Voigt line shape model.  
 831 This is an important step for modeling of the physics of the absorption process. Also, calculation  
 832 of the Voigt contour is the most time-consuming step in both our codes. For these reasons, we  
 833 consider details of the Voigt spectrum in a separate section.

#### 834 4.4 Convolution – Voigt spectrum

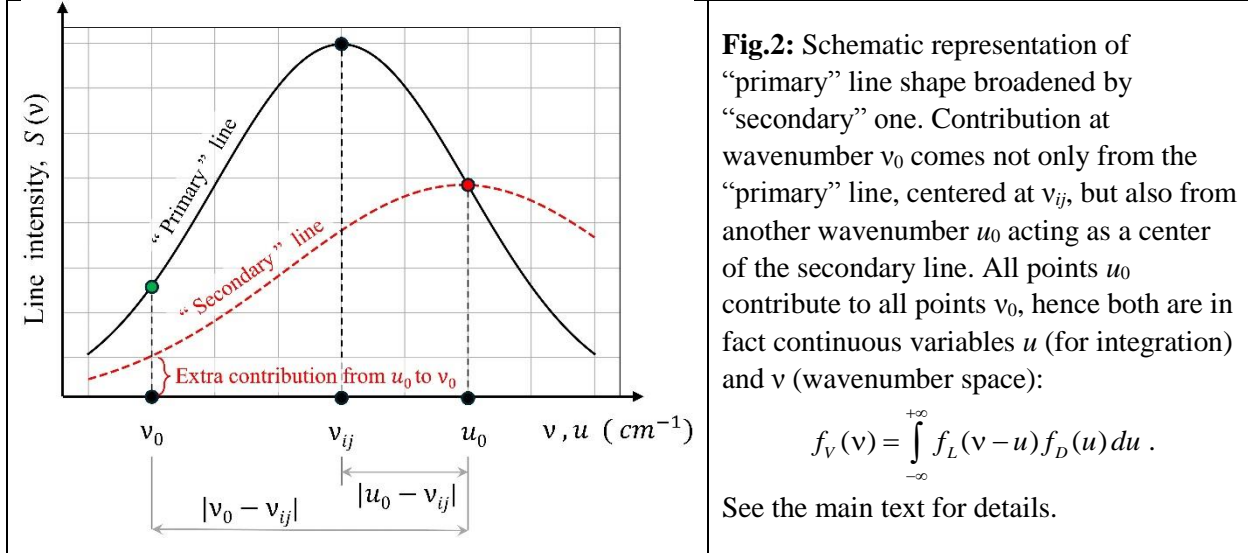
835 The Voigt spectrum model is a result of the Lorentzian or pressure-broadening, that dominates in  
 836 the lower atmosphere, and speed-dependent Doppler-broadening that dominates at higher  
 837 temperatures and lower pressure (*van de Hulst & Reesinck*, 1947). Both are simulated by the  
 838 normalized (unit integral over the wavenumber,  $v$ ) line shape functions. Like in Eqs. (7) - (8), we  
 839 use subscripts  $L$  and  $D$  for the Lorentz and Doppler functions, respectively:

840 
$$f_L(v - v_{ij}^*) = \frac{1}{\pi} \frac{\gamma_L}{\gamma_L^2 - (v - v_{ij}^*)^2}, \quad (9)$$

841 
$$f_D(v - v_{ij}^*) = \sqrt{\frac{\ln 2}{\pi \alpha_D^2}} \exp\left(-\frac{(v - v_{ij}^*)^2 \ln 2}{\alpha_D^2}\right). \quad (10)$$

842 For simplicity, Eqs. (9) - (10) do not show  $T$  and  $p$  as arguments and indicate that the line shapes  
 843 depend on distance between a given wavenumber  $v$  and the line center  $v_{ij}^*$  pressure-shifted

844 according to Eq. (1). **Figure 2** schematically shows mutual broadening of the lines when the two  
 845 effects take place at the same time.



846

847 Suppose we wish to calculate the line shape at a wavenumber  $v$  considering the fact that  
 848 wavenumbers  $u$  also contribute to  $v$  due to broadening. Assuming the Doppler line as the primary  
 849 one, we calculate the line intensity at  $u$  exactly as Eq.(10) shows

$$850 \quad f_D(u) = \sqrt{\frac{\ln 2}{\pi \alpha_D^2}} \exp\left(-\frac{(u - v_{ij}^*)^2 \ln 2}{\alpha_D^2}\right). \quad (11)$$

851 Eq.(11) is for the black solid line (Fig.2) centered at the HITRAN’s pressure-shifted  $v_{ij}^*$ . It is not  
 852 indicated as the function argument because it is a constant parameter. Now, this line intensity  
 853  $f_D(u)$  acts as a “secondary” line contributing to  $v$  via Lorentzian broadening,

$$854 \quad f_L(v-u) = \frac{1}{\pi} \frac{\gamma_L}{\gamma_L^2 - (v-u)^2} . \quad (12)$$

855 In Eq.(12), we note a new line center,  $u$ . One accumulates the contribution from all points  $u$  to  $v$   
 856 by integration:

$$857 \quad f_v(v) = (f_L * f_D)(v) = \int_{-\infty}^{+\infty} f_L(v-u) f_D(u) du . \quad (13)$$

858 Eq.(13) is a convolution (\*) of two functions, which commutativity tells that it is not important  
 859 what line is called “primary”. Also, negative wavenumbers are unphysical. However, we are far  
 860 from wavenumbers close to zero and the line shapes attenuate quickly, within  $\sim 20\text{-}25$  ( $cm^{-1}$ ) in  
 861 the band of our interest. For mathematical reasons, which we consider shortly, it is beneficial to  
 862 use the limits as in Eq.(13).

863 Eqs.(11) - (13) and an appropriate linear scaling of the integration variable  $u$  yields

$$864 \quad f_v(v) = \sqrt{\frac{\ln 2}{\pi \alpha_D^2}} \frac{\gamma_L}{\pi} \int_{-\infty}^{+\infty} \frac{1}{\gamma_L^2 - (v-u)^2} \exp\left(-\frac{(u-v_{ij}^*)^2 \ln 2}{\alpha_D^2}\right) du = \sqrt{\frac{\ln 2}{\pi \alpha_D^2}} K(x, y), \quad (14)$$

865 where

$$866 \quad K(x, y) = \frac{y}{\pi} \int_{-\infty}^{+\infty} \frac{\exp(-t^2)}{y + (x-t)^2} dt, \quad x = \frac{\sqrt{\ln 2}}{\alpha_D} (v - v_{ij}^*), \quad y = \frac{\sqrt{\ln 2}}{\alpha_D} \gamma_L. \quad (15)$$

867 Code `gce11` implements calculation of the Voigt line shape, Eq.(15), in a straightforward  
 868 manner, i.e. making commands look similar to what is published in literature. In the code snippet  
 869 below we deliberately hide operators explained earlier and show only those corresponding to  
 870 Eqs.(14)-(15).

```
871     nuij_pshift = ...; // Eq. (1)
872     alf_doppler = ...; // Eq. (7)
873     gam_lorentz = ...; // Eq. (8)
874     y = sqrt_ln2 * gam_lorentz / alf_doppler; // Eq. (15)
875     e11 = ...; // Eq. (2)
876     e21 = ...; // Eq. (3)
877     e12 = ...; // Eq. (4)
878     e22 = ...; // Eq. (5)
879     SijT = ...; // Eq. (6)
880     for (inu = inu1; inu < inu2+1; inu++)
881     {
882         x = sqrt_ln2 * fabs(nu[inu] - nuij_pshift) / alf_doppler; // Eq. (15)
883         k_abs[inu] = SijT * (sqrt_ln2 / sqrt_pi) *
884                         humlicek(x, y) / alf_doppler; // Eqs. (14) - (16)
885     } // inu = inu1 : inu2
```

886 We use the loop over `inu` to calculate absorption cross-section on the user’s grid of the  
 887 wavenumbers `nu[inu]`

$$888 \quad k_{ij}(v, T, p) = S_{ij}(T) f_V(v, v_{ij}, T, p). \quad (16)$$

889 Note that absolute value `fabs(nu[inu] - nuij_pshift)` enforces symmetry of the line  
 890 shape. However, the symmetry may be violated (see Sec.4.5 below).

Humlek (1982) developed an algorithm for calculation of  $K(x, y)$ , Eq.(15), with reported relative error not exceeding  $10^{-4}$  and published a corresponding FORTRAN function. Despite using complex arithmetic, the function contains only 30 lines, including 7 comments and 7 non-executable lines: FUNCTION, 4 RETURN-s, END statements and one line with definition of 3 local variables and the function output. Another 7 lines are mostly filled with precomputed values for 3 different “regions” of input parameters, accurate numerical evaluation of which is the main topic of that paper. A vectorized version of this subroutine (Schreier, 1992: Appendix 2) was translated into C (Lyapustin, 2002: function humlicek (...)), which we borrow for use in gcell and aspect.

900 Strictly speaking, calculation of  $K(x, y)$  is of general mathematical nature, rather than  
 901 spectroscopy (like calculation of weights for Gaussian quadrature or Legendre polynomials for  
 902 use in multiple scattering of light). Therefore, for confident use of the `humlicek(...)` function it  
 903 is sufficient to understand its input,  $x$  and  $y$ , Eq.(15). Here we only note that (a) *Humlíček* (1982:  
 904 Eq.(1)) considered the entire complex probability function from which the Voigt line shape  
 905 needs only the real part; and (b) calculation of the Voigt line shape is the slowest part of our code  
 906 (takes ~ 90% of the runtime). *Schreier* (1992) compared accuracy and runtime for several  
 907 techniques for computation of the Voigt function. It was found that depending on the method, the  
 908 computational speed for the Voigt function varies by 2 orders of magnitude, even after the code  
 909 optimization. The *Humlíček* (1982) algorithm was found as overall best based on accuracy,  
 910 speed, and flexibility (*Schreier*, 1992: p.760). We have used it for decades (*Lyapustin*, 2002) and  
 911 stick to it in this paper.

However, “*accurate yet efficient computation of the Voigt ... function is a challenge*” (Schreier, 2018(a): Abstract). Kuntz (1997), with corrections by Ruyten (2004), offered a new numerical implementation of the Humlíček algorithm. Depending on a computer architecture, a factor of 1.2 – 3.3 in acceleration was reported. Apart from computational efficiency, Mohankumar & Sen (2019) evaluated the Voight function with a 30-digit accuracy for reference purposes using

917 trapezoidal integration, residue correction, and quadruple precision. Corresponding FORTRAN  
918 code and coefficients are reported in their paper.

919 Depending on application, it could be possible to use either Eq.(11) or Eq.(12) and avoid the  
920 time-consuming Voigt convolution, Eq.(13). Alternatively, the Voigt effect can be simulated  
921 approximately by a rectangular core (central) part and v<sup>-2</sup>- shaped wings (*Fels*, 1979), or using  
922 analytical, hence fast, approximations, e.g., as a sum of the Lorentzian profiles (*McLean et al.*,  
923 1994: see Appendix for codes in C that approximately calculate the Voigt function and parameter  
924 derivatives). However, one must follow the analytical path with caution (*Schreier*, 2018b). *Wells*  
925 (1999) discuss an approximate algorithm tailored for atmospheric line-by-line calculations,  
926 which is efficient “*if the maximum relative error criteria can be relaxed*” (Abstract). It was  
927 suggested to express the algorithm in real arithmetic, use a simple analytical expression for a  
928 new “region” far from the line center, redefine boundaries of the regions (*Wells*, 1999: p.33). In  
929 the Appendix to *Wells* (1999), one finds codes in FORTRAN77 for calculation of the Voigt  
930 spectrum in SUBROUTINE HUMLIK (...), and derivatives  $\partial K(x, y)/\partial x$  and  $\partial K(x, y)/\partial y$  in  
931 SUBROUTINE HUMDEV (...). The Voigt code is longer compared to that in *Humlíček* (1982),  
932 also based on many precalculated numerical parameters, and yields a user-controlled accuracy.  
933 *Abrarov & Quine* (2015) approximate the Voigt function as an analytical – hence fast – series  
934 expansion (see their Eq.(17)). Their MATLAB code (in Appendix) also relies on a set of  
935 precomputed coefficients. For broadband atmospheric radiative transfer, *Nordebo* (2021)  
936 suggested replacing the Voigt with the Lorentzian calculation, but on the bounds altered as  
937 described in the paper, and based on the dominating role of the far wings of spectral lines in  
938 calculation of atmospheric transmittance.

939 This sparse literature review indicates that calculation of the Voigt function, despite decades of  
940 use, may be problematic. On top of that comes the fact that under some conditions the Voigt line  
941 shape model may not be physically correct. Despite our paper does not go “beyond Voigt”, we  
942 feel obligated to say a few words supported by references.

#### 943 4.5 Beyond Voigt: a few legacy and recent references

944 The Voigt line shape as convolution of the Doppler and Lorentzian contours, is only a model. Its  
945 limitations come, e.g., from the assumption of ideal gas to simulate elastic molecular collisions.  
946 In fact, the speed of molecules decreases at collision, so does the Doppler effect, causing

947 “collision narrowing” of spectral lines and increasing absorption at the line centers – the *Dicke*  
948 (1953) effect<sup>40</sup>. Back in 1960’s *Galatry* (1961) and *Rautian & Sobel’man* (1967) gave a non-  
949 Voigt expression for a spectral line accounting for the effect of change of speed on the line  
950 shape. This effect is most important for simulation of laser light absorption by narrow lines.  
  
951 Likewise, the Lorentzian model works well near the center of spectral lines, where absorption is  
952 high, but less accurate at the line wings. Lower absorption in the wings is important for remote  
953 sensing in atmospheric windows. This effect is often accounted for as continuum (see references  
954 in the Introduction), based on measurements, and most important for broad lines in the  
955 microwave region. Like for the Doppler model, “generalized” Lorentzian contours exist. Two  
956 examples are the *van Vleck – Weisskopf* line shape and the *Benedict* scaling of the wings that  
957 reduces absorption (*Goody & Yung*, 1989: p.110, Eqs.(3.52) and (3.75), respectively).  
  
958 HITRANonline<sup>41</sup> notes that “*the line shape function for many applications is much more*  
959 *complex*”. The new line shape functions with better simulation of molecular collision are being  
960 applied, while the Voigt model for computation of radiative parameters pertains today to a “*not-*  
961 *so-distant past*”. Indeed, literature has used the term “beyond Voigt” (*Ngo et al.*, 2013, 2014;  
962 *Wcisło et al.*, 2021) for cases where the Voight model is not satisfactory.  
  
963 *Spänkuch* (1989) reviewed methods compensating deviations from the Lorentzian line shape.  
964 *Boone et al.* (2007) claims that “*the Voigt profile does not provide a sufficiently accurate*  
965 *representation of the line shape for air-broadened H<sub>2</sub>O vapor over a significant range of*  
966 *conditions commonly encountered in atmospheric remote sensing*” – although “sufficiently  
967 accurate” depends on the end user’s individual application. They offer a speed-dependent Voigt  
968 profile for analysis of infrared measurements collected by the Atmospheric Chemistry  
969 Experiment (ACE) mission. A FORTRAN code for their line mixing approach, used in ACE, is  
970 publicly available from the journal website (*Boone et al.*, 2011).  
  
971 The need for accurate modeling of the high-resolution spectral measurements spawned general  
972 terms like non-Voigt, beyond Voigt, speed-dependent Voigt, line-mixing, and Rautian profiles  
973 (*Ngo et al.*, 2013; *Schreier & Hochstafel*, 2021; *Tran et al.*, 2013). Relevant, but more specific

---

<sup>40</sup> [https://en.wikipedia.org/wiki/Dicke\\_effect](https://en.wikipedia.org/wiki/Dicke_effect)

<sup>41</sup> <https://hitran.org/docs/definitions-and-units/> (see between Eqs. (9) and (10))

974 terms, found in literature are “partially-correlated quadratic-speed-dependent hard-collision  
975 profile (pCqSD-HCP)” and “quadratic speed dependent Voigt profile (qSDV)” (*Tran et al.*,  
976 2013). An open-source FORTRAN code is available for (*Tran et al.*, 2013) from the journal  
977 website. A typo in theoretical evaluations in (*Ngo et al.*, 2013 and *Tran et al.*, 2013) was  
978 corrected in (*Tran et al.*, 2014). In order to accurately capture the influence of pressure on the  
979 line shape in high-resolution spectra (of water), the IUPAC Task Group recommends replacing  
980 the Voigt profile with use the pCqSD-HCP and call it the Hartmann-Tran profile for simplicity  
981 (*Tennyson et al.*, 2014). *Domysławska et al.* (2016) presented laboratory measurements of the  
982 oxygen B-band at low pressure (to make lines narrow). They used the qSDV-profile to simulate  
983 the speed-dependence of collisional broadening and shifting of the Voigt shape. *Schreier* (2017)  
984 analyzed different numerical approaches to calculation of the speed-dependent Voight profile  
985 and suggested his own technique.

986 As a result of these studies, the “beyond-Voigt” line shape parameters have been introduced into  
987 the HITRAN database (*Wcislo et al.*, 2021) for certain molecules and lines. However, for most  
988 molecules in atmospheric applications, the Voigt line shape model simulated using HITRAN  
989 parameters is still the baseline<sup>42</sup>. Determining the need to go beyond-Voigt in remote sensing of  
990 the atmosphere is a separate problem. How important is it for the UV-Vis-NIR bands? What  
991 molecules are affected? For what temperature and pressure? We consider this beyond the scope  
992 of the present study but mention all that to prepare the reader for potential changes in standard  
993 practice soon. At present, we limited ourselves with a well-tested *Humlíček* algorithm explained  
994 in the relevant open source codes, and provided reference for further reading.

995 [4.6 A few numbers for validation of code for an isolated line](#)

996 In Sec.2 we noted that finding reliable (accurate and reproducible) numerical results to test the  
997 final output, not to mention unit testing, was not easy. It is, of course, possible to use tools like  
998 HAPI. But if results do not match, the developer is left with a question: “does my software have  
999 an error, or have I misunderstood the benchmark tool?”. It is therefore desirable to tabulate some  
1000 numbers, like we did in Sec. 3.2.2 above and earlier in Sec. 4, for a clearly defined input.

---

<sup>42</sup> <https://hitran.org/docs/definitions-and-units/>

1001 For checking purposes, here we plot the oxygen isotope #1 for 3 temperatures,  $T = 270, 300, 330$   
 1002 ( $^{\circ}\text{K}$ ) at fixed pressure  $p = 1$  (*atm*) and, vice versa, for 3 pressures  $p = 0.9, 1, 1.1$  (*atm*) at a fixed  $T$   
 1003 =  $300^{\circ} (\text{K})$ .

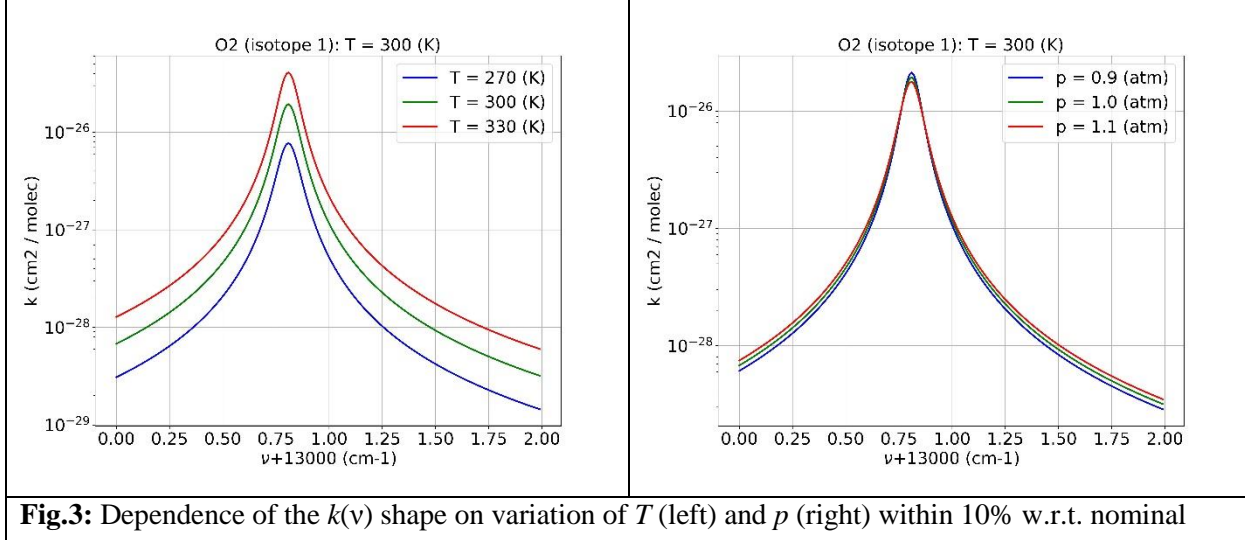


**Fig.3:** Dependence of the  $k(v)$  shape on variation of  $T$  (left) and  $p$  (right) within 10% w.r.t. nominal values  $T = 300^{\circ} (\text{K})$ ,  $p = 1$  (*atm*). See **Table 4** for a few benchmark numbers at the peak.

1004

1005 Despite the equations and the code described so far are simple, this intermediate benchmark  
 1006 helps catch typos, e.g. the commonly encountered wrong order of magnitude caused by wrong  
 1007 units. It also leads to a better understanding of the physical background. For example, higher  
 1008 temperature causes higher absorption, and the dependence is strong. But for pressure, the  
 1009 dependence at the peak is the opposite and overall it is much weaker. **Table 4** shows some  
 1010 reference numbers for the absorption cross-section,  $k$  ( $\text{cm}^2/\text{molec}$ ), and for input defined in  
 1011 Sec.4.1.

1012

1013 **Table 4:** The peak values for 6 curves shown in Fig.3. Because of the wavenumber grid step  $\Delta v = 0.01$   
 1014 ( $\text{cm}^{-1}$ ), the shown peak values are at  $v = 13000.81$  ( $\text{cm}^{-1}$ ), which may not precisely coincide with the actual  
 1015 maximum value of the spectral line. Columns, left to right, indicate pressure  $p$  (*atm*), location of the  
 1016 maximum value of the line, Eq.(1), and three temperatures  $T$  ( $\text{K}$ ).

$p$ ( <i>atm</i> )	$v(p)$ ( $\text{cm}^{-1}$ )	$T = 270$ ( $\text{K}$ )	$T = 300$ ( $\text{K}$ )	$T = 330$ ( $\text{K}$ )
0.9	13000.809559	-	2.125930E-26	-
1.0	13000.808819	7.711446E-27	1.935411E-26	4.082727E-26
1.1	13000.808079	-	1.774578E-26	-

1017

1018 Calculation of the optical thickness and transmittance requires scaling of the cross-section by  
1019 number of particles placed in the gas cell. In the next chapter, we calculate absorption cross-  
1020 section by multiple lines of the same gas, O<sub>2</sub> and separately CH<sub>4</sub> (all isotopes), compute spectral  
1021 dependence of  $\tau(\lambda)$ , spectral transmittance  $T(\lambda) = \exp(-\tau(\lambda))$ , and compare our numerical results  
1022 with a few published experiments.

1023 [5. Calculation of absorption in a gas cell](#)

1024 This section shows how to calculate the absorption cross-section  $k$  ( $cm^2/molec$ ), optical thickness  
1025  $\tau$ , and transmittance  $T(v)$  for a group of spectral lines at a given temperature and pressure.  
1026 Practically this scenario corresponds to simulation of absorption of light in a gas cell in  
1027 laboratories and remote sensing systems. As a prerequisite, we assume the user has downloaded  
1028 the HITRAN database files in the current 160-character ASCII format and compiled the package  
1029 in the `gcell` mode (see Sec.3.2.1 and Fig.1a).

1030 For the gas cell scenario, the user's input is

1031       `molec_id` – molecule as numbered in HITRAN: 1-7 and 10 in the current version.

1032       `T_kelvin` – gas temperature in Kelvins ( $K$ );

1033       `p_atm` – gas pressure in atmospheres (*atm*);

1034       `l_cm` – length of the gas cell in centimeters (*cm*);

1035       `nu_usr_min` – lower boundary for the desired wavenumber spectral range ( $cm^{-1}$ );

1036       `nu_usr_max` – upper boundary for the same ( $cm^{-1}$ );

1037       `dnu` – wavenumber spectral resolution ( $cm^{-1}$ ).

1038 Using these parameters, in the next 3 parts, we begin by reading the HITRAN database, then we  
1039 accumulate absorption from a group of spectral lines, and finally we test the result. Some steps  
1040 are the same for the atmospheric and the gas cell computations. We refer to these as  
1041 `aspect/gcell`; otherwise, we use `gcell`. Sec.5.1 and 5.2 show commands from the  
1042 `main(...)` functions located in the `main_gcell.cpp` and `main_aspect.cpp` respectively  
1043 for the `gcell` and `aspect` modes.

1044     5.1 Picking necessary lines from the HITRAN \*.par files

1045     After reading the input data with `read_hitran160(...)` in Sec. 4.1 above, `aspect/gcell`  
 1046     determines boundaries of the HITRAN spectral interval which lines contribute to the user  
 1047     defined interval either directly (the HITRAN line center belongs to the user interval) or via line  
 1048     wings – an “extended” spectral interval:

```
1049         nu_hit_min = nu_usr_min - delta_nu;
1050         nu_hit_max = nu_usr_max + delta_nu;
```

1051     Following the common practice, we use  $\Delta\nu = 25$  ( $cm^{-1}$ ) for `delta_nu` (see Introduction).

1052     Next, using these extended interval boundaries, `aspect/gcell` computes the number of the  
 1053     pertaining HITRAN records, `nlines`, and location of the first contributing line in the HITRAN  
 1054     \*.par file `iline0` - both are output parameters of this function:

```
1055         count_lines(molec_id, nu_hit_min, nu_hit_max, iline0, nlines);
```

1056     Based on the value of `molec_id`, the function reads an appropriate \*.par file sequentially  
 1057     from the beginning (lowest wavenumber). The number of the very first detected line that belongs  
 1058     to the extended spectral interval is saved in `iline0`; the total number of lines is counted and  
 1059     saved in `nlines`.

1060     To comply with C’s array indexing, we define `iline0` with zero offset: `iline0 = 0`  
 1061     corresponds to the first record in the HITRAN database that contributes to the user spectral  
 1062     interval (i.e., belongs to the extended interval). If `count_lines()` finds no lines contributing  
 1063     to the extended interval, it returns `iline0 = nlines = 0`. The `nlines` parameter yields  
 1064     memory allocation for parameters of all spectral lines. E.g., for H<sub>2</sub>O in the interval  $\lambda = [0.25,$   
 1065      $2.5] (\mu m)$  or  $\nu = [4000, 40000] (cm^{-1})$ , `nlines = 205134` (in HITRAN 2020). That many  
 1066     double precision floating point numbers occupy ~1.6Mb of memory. Table 3 above shows that  
 1067     `aspect/gcell` store the HITRAN parameters in 7 arrays of the mentioned size and 1 integer  
 1068     32-bits array. Thus, storing all necessary HITRAN parameters in memory for intermediate  
 1069     calculations is not a problem even for a wide band. It is the output that consumes memory most.  
 1070     Especially if one needs wide band, and high resolution over both wavenumber and height grids.  
 1071     We return to that problem later in Sec. 6.4 for aspect mode.

1072 Allocation of 8 arrays to store parameters for each line and reading the HITRAN database has  
1073 already been discussed in Sec.3.1 and 3.2. After that, `gcell` reads information about isotopes  
1074 using the `isotops(...)` function, while `aspect` uses similar function `hisotops(...)` because  
1075 of dependence of the TIPS ratio on height via temperature. Once completed, `aspect/gcell`  
1076 proceed to the next step – simulation of a single line shape and accumulation of contribution  
1077 from different lines.

1078 [5.2 The line-mixing effect, which we also neglect](#)

1079 Quoting from *Tonkov et al.* (1996: Abstract) “*It is well known that, due to line mixing effects,  
1080 spectral regions with overlapping lines cannot be described by the sum of separate profiles*”.  
1081 Indeed, in general, the overlapping lines interfere with each other, changing the shape of the  
1082 Lorentz contour (*Goody & Yung*, 1989; *Liou*, 2002). This effect is important in some lines of  
1083 CO<sub>2</sub>, CH<sub>4</sub>, O<sub>2</sub> absorption in the microwave and in the A- bands, and O<sub>3</sub> in the IR, when the  
1084 HWHM is comparable or exceeds distance between them.

1085 *Tran et al.* (2006) considers the line mixing effect, combined with collision induced absorption  
1086 (CIA), in the AO<sub>2</sub> band at high pressure, 20-200 (*atm*), and temperature 200°-300° (*K*) for both  
1087 pure O<sub>2</sub> and O<sub>2</sub>-N<sub>2</sub> mixtures. They showed that neglecting the line mixing overestimates  
1088 absorption in the wings and underestimates absorption at the peaks. Smooth spectral dependence  
1089 of the effects allows treating them as “continuum” and model the difference between  
1090 measurements and LBL simulation using some convenient fitting function.

1091 *Tran et al.* (2006) used the resulting model and data to build a database and software suitable for  
1092 the calculation of oxygen atmospheric (hence, “regular” pressure) absorption and for inclusion in  
1093 RT codes. Then, they studied the influences of both line-mixing and collision-induced processes  
1094 on atmospheric photon path escape factors and on cloud-top altitude retrievals (*Sayer et al.*,  
1095 2023). They concluded that the mentioned effects “*make significant contributions and explain a  
1096 large part of the discrepancies between measured and calculated atmospheric absorption  
1097 observed recently*” (in particular, see their Fig.11 for numerical quantification of the effects). The  
1098 model was later improved by *Tran & Harmann* (2008: see Fig.1 for influence on transmission at  
1099 oblique traces) and applied to O<sub>2</sub>-CO<sub>2</sub> mixture by *Vangvichith et al.* (2009), also in the A-band.

1100 Nevertheless, in this paper, we neglect the effect of line coupling for simplicity, and because  
1101 HITRAN includes CIA as a separate dataset<sup>43</sup>. We simulate joint contribution of lines via simple  
1102 summation of the absorption cross-sections.

1103 [5.3 Simulation of LBL absorption](#)

1104 Using a loop over `nlines` HITRAN records it is easy to account for their joint contribution to  
1105 any user-defined wavenumber  $v$  by simple accumulation, if the line-mixing effect is ignored

1106 
$$k(v) = \sum_l^{nlines} k_l(v, v_l) w(v - v_l) . \quad (17)$$

1107 In Eq.(17),  $k(v)$  is the total (accumulated) absorption cross-section at the user defined wavenumber  
1108  $v$ ,  $k_l(v, v_l)$  is the cross-section at the user requested wavenumber  $v$  by a line centered at  $v_l$ , and the  
1109 weight

1110 
$$w(v - v_l) = \begin{cases} 1, & \text{if } |v - v_l| \leq 25 \text{ (cm}^{-1}\text{)} \\ 0, & \text{otherwise} \end{cases} \quad (18)$$

1111 instructs to account for contribution only from those HITRAN records located no further than 25  
1112 ( $\text{cm}^{-1}$ ) from the user's  $v$  (Schreier, 1992: p.760; Lyapustin, 2003: p. p.870). This is standard  
1113 practice when line parameters are derived and used to separate line and continuum absorption  
1114 (Clough et al. 1981; Burch, 1982; Mlawer et al., 2023). The function `ix1ix2(...)` in  
1115 `aspect/gcell` implements Eq.(18) with the following interface

1116 `code = ix1ix2(nuij, delta_nu, nu, nnu, inu1, inu2);`

1117 Namely, it returns indices `inu1` and `inu2` of elements of an array `nu[nnu]` falling within  
1118 `delta_nu` from `nuij` and `code = 1` in case of success. If `code = -1` is returned, it means  
1119 that all user-defined wavenumbers lie too far from the selected HITRAN record  $v_l$  to receive any  
1120 significant contribution. The corresponding pseudocode is (see Sec. 4.4 between Eqs.(15) - (16))

```
1121     for (inu = 0; inu < nnu; inu++)  
1122         kabs[inu] = 0.0  
1123     for (iline = 0; iline < nlines; iline++) {  
1124         if (ix1ix2(nuij, delta_nu, nu, nnu, inu1, inu2) > 0) {  
1125             Calculate nuij_pshift
```

---

<sup>43</sup> <https://hitran.org/cia/>

```

1126     Calculate Doppler and Lorentz HWHM
1127     Calculate e11, e12, e21, e22
1128     Calculate line intensity Sij
1129     for (inu = inu1; inu < inu2+1; inu++) {
1130         Calculate Voigt spectrum
1131         Accumulate absorption power:
1132             kabs[inu] += (line intensity) * (Voigt)
1133             } // for inu - all wavenumbers affected by iline
1134         } // if iline contributes to nu[]
1135     } // for iline - all HITRAN lines within extended interval

1136 This sequence of loops – over HITRAN lines first, over user’s wavenumbers next – allows to
1137 calculate the HITRAN parameters only once and reuse these for all v-s affected by the line
1138 wings. However, this option forces the user to keep the array kabs [nnu] in memory. This may
1139 cause memory issues if one needs a high spectral and altitude resolutions because the
1140 corresponding array has two dimension kabs [nnu*nkm] (recall, the codes unravel all arrays
1141 to 1D for efficient memory allocation). We briefly discuss this problem with regard to aspect
1142 further in Sec. 6.4.

1143 The monochromatic cross-section,  $k(v, T, p)$  ( $cm^2/molec$ ), is defined per unit column number
1144 density of molecules of the absorbing gas,  $n$  ( $molec/cm^2$ ), at a given temperature and pressure.
1145 The dimensionless absorption optical thickness is

1146  $\tau(v, T, p) = nk(v, T, p)$ . (19)

1147 Using the notation  $V$ ,  $S$ , and  $l$  respectively for the volume, square and length of the column,  $N$  for
1148 the total number of molecules in it,  $k_B$  for the Boltzmann constant, and an assumption of an ideal
1149 gas, one writes

1150  $p = N k_B T / V = n k_B T / l$ . (20)

1151 If the thermodynamic conditions do not change along the path, like in gas cell, the absorption
1152 optical thickness is

1153  $\tau(v, T, p) = \frac{pl}{k_B T} k(v, T, p)$  (21)

1154 // Note: a) n_column = l_cm * n_volume and b) units conversion

```

1155 `n_column = l_cm*atm_to_cm_g_s*p_atm/(k_boltzman*T_kelvin);`  
 1156 `tau[inu] = k_abs[inu]*n_column;`

1157 The absorption coefficient  $a$  ( $cm^{-1}$ ) is

1158 
$$a(v, T, p) = \tau(v, T, p) / l = \frac{p}{k_B T} k(v, T, p). \quad (22)$$

1159 If the thermodynamic conditions vary, e.g., with height  $h$ , the absorption optical thickness  
 1160 between two given heights would be (see Sec. 6.2 for relevant code)

1161 
$$\tau(v) = \int_{h_1}^{h_2} a(v, h) dh = \frac{1}{k_B} \int_{h_1}^{h_2} \frac{p(h) k(v, h)}{T(h)} dh. \quad (23)$$

1162 In Eq.(23), the absorption cross-section depends on  $h$  via  $T$  and  $p$ . The monochromatic  
 1163 transmittance along the path, inclined at zenith angle  $\theta = \arccos(\mu)$  w.r.t normal, is

1164 
$$T(v, \mu) = \exp(-\tau(v)/\mu). \quad (24)$$

1165 Finally, the spectrally integrated transmittance of the solar light  $S(v)$  through a gas cell to a  
 1166 system with spectral response function (filter)  $f(v)$  is

1167 
$$T(\mu) = \frac{\int_{\Delta v} T(v, \mu) S(v) f(v) dv}{\int_{\Delta v} S(v) f(v) dv}. \quad (25)$$

1168 Using Eqs.(24) and (25), it is possible to derive a spectrally integrated (efficient) absorption  
 1169 optical thickness

1170 
$$\tau(\Delta v) = -\mu \log(T(\mu)). \quad (26)$$

1171 Note that neither `gcell` nor `aspect` provide transmittance – the user is supposed to calculate  
 1172 it externally because Eq.(24) is trivial. Also integration in Eq.(25) often requires interpolation  
 1173 from the HITRAN grid of wavenumbers to that of the Sun or spectral response functions, often  
 1174 defined as functions of wavelength. In the last part of this section, we report a few benchmark  
 1175 results for checking purpose.

1176 5.4 Gas cell validation

1177 Spectral calculations often involve hundreds and thousands of numbers which are rarely  
1178 published making numerical comparisons difficult. In most cases, precise benchmark is possible  
1179 if one uses software developed by others (proper understanding of that software – not only input  
1180 - is therefore essential in this case) or ask the developer to generate numbers (which is not  
1181 always convenient). Contrary to numerical results, graphical plots for absorption cross-section  $k$   
1182 (usually in  $\text{cm}^2/\text{molec}$ ), absorption coefficient  $a$  ( $\text{cm}^{-1}$  or  $\text{km}^{-1}$ , depending on application),  
1183 absorption optical thickness  $\tau$ , or corresponding direct transmittance  $T$  (both dimensionless) have  
1184 been published widely - see, e.g., *Hearn* (1961: Fig.1) for ozone. This simple visual test allows  
1185 one to check magnitude (hence units conversion) and overall shape of the spectral dependence of  
1186 transmittance, optical thickness, or cross-section. Thus, the key requirement for the published  
1187 image is legibility.

1188 *Prischepa* et al. (2023: Fig. 1) shows spectral dependences of absorption coefficients of pure  $\text{N}_2$ ,  
1189  $\text{O}_2$ ,  $\text{H}_2\text{O}$  within 500 - 12000 ( $\text{cm}^{-1}$ ) at normal temperature and pressure. *Karlovets* et al. (2023:  
1190 Fig.2) shows absorption coefficient for nitrous oxide,  $\text{N}_2\text{O}$ , measured at pressure 10 (*Torr*), or  
1191 ~0.013 (*atm*), between 7250 and 7653 ( $\text{cm}^{-1}$ ) and details showing separate lines near 7577 ( $\text{cm}^{-1}$ )  
1192 at 2 different scales. Fig.3.21 in *Efremenko & Kokhanovsky* (2021) shows absorption cross-  
1193 section of water vapor in a relatively wide 900-1000 (*nm*) and narrow 934-926 (*nm*) bands. Figs.  
1194 3.22 and 3.23 in the same show, respectively, absorption cross-section for oxygen A, B, and C-  
1195 bands with 610-780 (*nm*), and  $\text{AO}_2$  band separately. *He* et al. (2019: Figs.1 & 6a) plot HITRAN-  
1196 2016 line intensities for  $\text{O}_2$  in 600-1300 (*nm*) – a simple but useful intermediate result for visual  
1197 unit testing of, e.g., HITRAN database reader. *Stamnes* et al. (2017: Fig.4.13) shows absorption  
1198 coefficient spectrum for the 1510 – 1520 ( $\text{cm}^{-1}$ ) part of the 6.3 ( $\mu\text{m}$ ) water vapor band at 10  
1199 (*mbar*) and 240 (*K*), and at 1 (*bar*) and 296 (*K*) using HITRAN 1982 (!). Transmittance through  
1200 1 (*m*) of air at a pressure 150 (*hPa*) and a temperature of 215 (*K*) near 15 ( $\mu\text{m}$ ), where  $\text{CO}_2$  is the  
1201 dominant absorber, is shown in *Coakley & Yang* (2014: Fig. 5.4). *Rothman* (2013: Fig.7) plots  
1202 absorption cross-section for  $\text{CH}_4$  at  $T = 296$  (*K*) with 0.05 ( $\text{cm}^{-1}$ ) resolution. *Bohren & Clothiaux*  
1203 (2006) show absorption cross-section of a water molecule for a temperature of 20° (*C*) and a total  
1204 pressure of 1 (*atm*) within 12-16 ( $\mu\text{m}$ ) or 625 - 825 ( $\text{cm}^{-1}$ ) (Fig.2.9); absorption cross-section for  
1205 most strongly absorbing atmospheric gases in a wide range 0.1 ( $\mu\text{m}$ ) - 0.1 (*m*) at 1013 (*mb*) and  
1206 294 (*°K*) (Fig.2.13); water vapor absorption at 1013 (*mbar*) and 10 (*mbar*) within 1084.7 -

1207  $1085.7\text{ (cm}^{-1}\text{)}$  with and without continuum absorption (Fig.2.19) and combination of the two  
1208 (Fig.2.20). *Rothman* (2005: Fig.2) simulates  $\text{CO}_2$  laboratory spectra in the  $2\text{-}\mu\text{m}$  region at  $p = 30$   
1209 (torr) and  $25\text{ (m)}$  path. *Liou* (2002: Fig. 4.5) shows absorption coefficient  $k\text{ (atm}\cdot\text{cm)}^{-1}$  within  
1210  $600 : 0.01 : 700\text{ (cm}^{-1}\text{)}$  at  $p = 600\text{ (mbar)}$  and  $T = 260\text{ (}^{\circ}\text{K)}$ . *Greenblatt* et al. (1990) plot results of  
1211 measurement of  $\text{O}_2$  absorption for  $330\text{--}1140\text{ (nm)}$  (Fig.1) and  $675\text{--}800\text{ (nm)}$  (Fig.2) at a high  
1212 pressure of  $55\text{ (atm)}$ ,  $196^{\circ}\text{ (K)}$ , and a path length of  $89.5\text{ (cm)}$ . This list, by no means exhaustive,  
1213 is intended to show that a wide range of reproducible “visual” tests have been published in the  
1214 literature.

1215 In this paper, we test `gcell` in two scenarios, one for the oxygen A-band and another one for  
1216 methane, described in separate sections below. We use two strategies to test our code. For the A-  
1217 band we reproduce published images and test `gcell` “visually”. For methane, we numerically  
1218 compare our result vs. independently calculated ones. Unlike broadly published pictures of  
1219 spectra and contrary to numerical benchmarks for multiple scattering of radiation, numerical  
1220 benchmarks for spectroscopy are rarely available from literature. A code developer has to either  
1221 set up and run another code, like HAPI, or extract data from huge database. Neither way is  
1222 convenient for quick testing. To help overcome this issue, we provide our numerical results for  
1223 both tests in ASCII files together with our source code and report a few more numbers in the  
1224 subsequent sections.

### 1225 5.3.1 Oxygen A-band at $0.764\text{ (\mu m)}$

1226 The oxygen A-band, commonly shortened as  $\text{AO}_2$ , is located around  $\lambda \approx 0.764\text{ (\mu m)}$ :  $\Delta\lambda \approx$   
1227  $0.760\text{...}0.768\text{ (\mu m)}$ ,  $\Delta\nu \approx 13000\text{...}13160\text{ (cm}^{-1}\text{)}$ . We use an  $\text{AO}_2$  scenario described in (*Predoi-*  
1228 *Cross* et al., 2008; we will refer to their paper as *P-C* within this section). The spectral  
1229 transmittance, Eq.(24), was recorded in a multiple path cell of the total pathlength  $l = 1633.6$   
1230 ( $\text{cm}$ ), at pressure of  $0.724\text{ (bar)} \approx 0.7145\text{ (atm)}$ , at the room temperature, with spectral resolution  
1231  $0.0222\text{ (cm}^{-1}\text{)}$  (*P-C: Sec.2*). The measurement error of the line intensity is claimed not to exceed  
1232  $\sim 1\%$  (*P-C: Abstratct*). The room temperature varied from  $\approx 294^{\circ}\text{ (K)}$  to  $\approx 298^{\circ}\text{ (K)}$  (*P-C: Table 1*).  
1233 In our test, we do not intend to simulate the experiment with high precision. So, we use  $T = 296^{\circ}$   
1234 ( $\text{K}$ ) for calculation. For the given temperature, pressure and path length, Eq.(20) gives  $n \approx$   
1235  $2.8921135\cdot 10^{22}\text{ (molec/cm}^2\text{)}$ .

1236 **Fig.4 (a)** shows the simulated transmittance vs. wavenumber  $\nu = [13006, 13166]$  ( $cm^{-1}$ ) and the  
 1237 optical thickness vs. corresponding wavelength. **Fig.4 (b)** reproduces the same but within a sub-  
 1238 band,  $\nu = [13159.6, 13165.6]$  ( $cm^{-1}$ ). These spectral intervals are borrowed from Fig.1 in (P-C).  
 1239 Images like that published in (P-C) and here help debug the program qualitatively by visually  
 1240 inspecting the picture for presence of lines and quantitatively by checking their order of  
 1241 magnitude.

1242

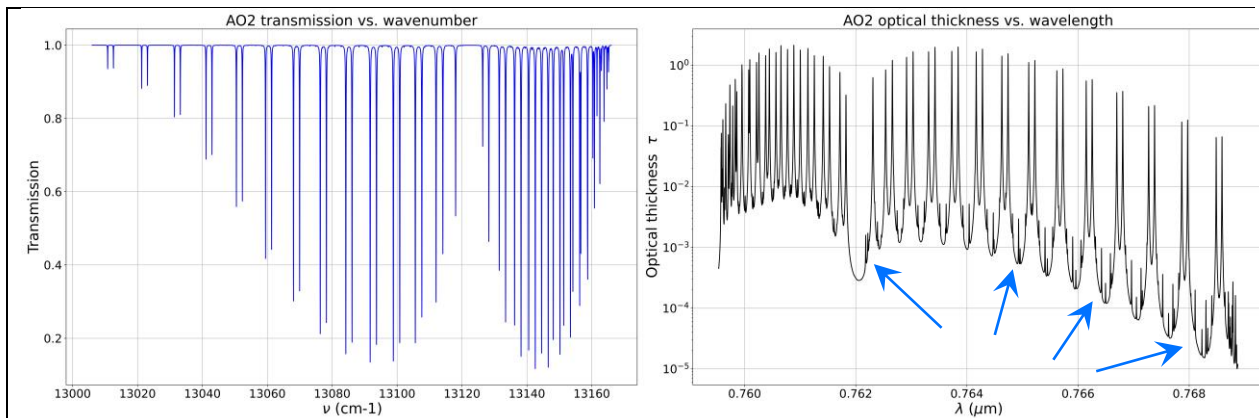


**Fig.4 (a):** Direct transmission (left) and corresponding optical thickness (right, log scale for y-axis) for the AO2 band. The left image reproduces Fig.1(A) from (Predoi-Cross *et al.*, 2008: p. 91). Visual comparison of the two serves as qualitative validation of code `gcell`. The arrows in the right image indicate some weak absorption lines caused by isotopes with low abundance.

1243

1244 Our experience shows that once possible problems at these two steps are resolved, the code  
 1245 should work without major problems.

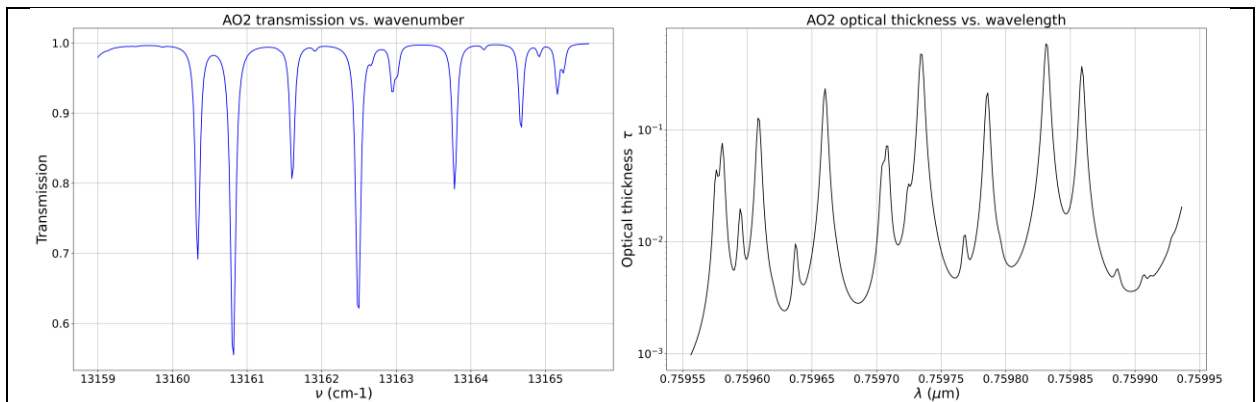


**Fig.4 (b):** Same as Fig.4 (a), except for narrow band. The left image reproduces Fig.1(B) from (Predoi-Cross *et al.*, 2008).

1246

1247 An ASCII file `./benchmarks/Sec5p3p1__test_gcell_ao2.txt` contains results  
1248 of our numerical simulation. The file contains 8000 rows, excluding a header one, and two  
1249 columns. The left column is the wavenumber  $v (cm^{-1})$  from 13006.00 to 13165.98 step 0.02. The  
1250 right one contains cross-section  $k (molec/cm^2)$ . Scaling  $k$  by the particles column number density  
1251  $n$  (indicated in the header), Eq.(19), yields  $\tau$  (right images in **Fig.4 (a-b)**). Plotting  $\exp(-\tau)$ ,  
1252 Eq.(24), shows left images.

### 1253 5.3.2 Methane band at 2.3 ( $\mu m$ )

1254 Our second benchmark scenario is for `imolec = 6`: methane, CH<sub>4</sub>, which is a greenhouse gas.  
1255 The gas is at the same room temperature,  $T = 296^\circ (K)$ , and slightly different pressure  $p = 1000.0$   
1256 ( $mbar$ )  $\approx 0.986923$  ( $atm$ ) compared to the previous scenario. Unlike for the published oxygen  
1257 scenario, we compare our numerical simulation vs. the one kindly provided by the GATS<sup>44</sup> Inc.  
1258 team. The GATS data contains the CH<sub>4</sub> spectral transmittance of an  $l = 8$  ( $cm$ ) gas cell, computed  
1259 using the SpectralCalc<sup>45</sup> tool (Gordley et al., 1994), convolved with a spectral filter for their  
1260 Digital-Array Gas-correlation Radiometer - DAGR<sup>46</sup>. The particles columnar number density,  
1261 Eq.(20), for this case is  $n \approx 1.9575594 \cdot 10^{20}$  ( $molec/cm^2$ ).

1262 The GATS data is based on HITRAN 2016 and defined within the inclusive interval  $v =$   
1263  $4081.901\dots 4505.699$  ( $cm^{-1}$ ), step  $dv = 0.002$  ( $cm^{-1}$ ). Considering their data as a benchmark, we  
1264 calculated spectra of optical thickness (**Fig.5 (a)** – top image), and corresponding direct one way  
1265 transmittance (**Fig.5 (b)** – second top), Eq.(24) with  $\mu = 1$ , and convolved the two. **Fig.5 (c)**  
1266 (second bottom image) shows the instrument filter (dash line), benchmark convolution (black  
1267 wiggling curve), and absolute difference between our and the benchmark data (red line – almost  
1268 at 0). The absolute difference, which is  $\sim 1000$  times smaller compared to the convolution, is  
1269 pictured separately in the **Fig.5 (d)** – bottom image.

---

<sup>44</sup> <https://www.gats-inc.com/>

<sup>45</sup> <https://www.spectralcalc.com/>

<sup>46</sup> [https://www.gats-inc.com/future\\_missions.html#DAGR](https://www.gats-inc.com/future_missions.html#DAGR)

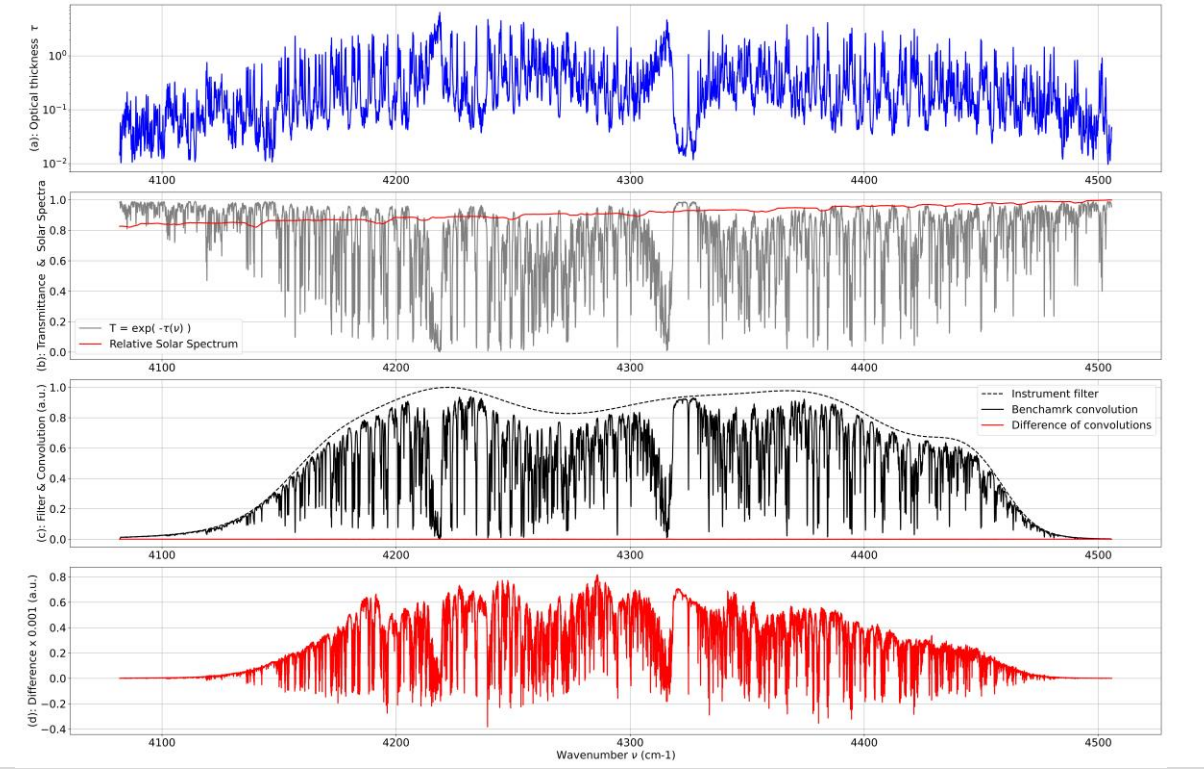


**Fig.5:** Graphical results for a methane gas cell test (see y-axis caption for letters (a-d) ). (a) Optical thickness  $\tau$  calculated using `gcell`; (b) Direct one-way transmittance,  $\exp(-\tau)$ , and solar irradiance relative to maximum within the band; (c) Instrument filter function (dash line), convolved with transmittance (solid line – benchmark result), and absolute difference between the benchmark result and that computed with `gcell` (red line – almost at 0). (d) The same difference pictured separately – note the scaling factor 0.001 on y-axis, i.e. the difference does not exceed 0.0008 (a.u.)

1270

1271 Next, we calculated an absolute signal transmitted through the methane gas cell. For that, we  
 1272 used the *Chance-Kurucz* extraterrestrial solar irradiance spectrum defined from 50 ( $cm^{-1}$ ) to  
 1273 50000 ( $cm^{-1}$ ) with 1 ( $cm^{-1}$ ) resolution (Kurucz, 1992 & 1997; *Chance & Kurucz*, 2010). **Fig.5 (b)**  
 1274 (second from top - red line) shows part of the solar spectrum relative to maximum value within  
 1275 the band and interpolated from 1 ( $cm^{-1}$ ) grid to 0.002 ( $cm^{-1}$ ) using Python’s cubic spline. We then  
 1276 calculated the transmitted signal

1277 
$$u = \int_{\Delta v} S_0(v) \exp(-\tau(v)) f(v) dv \quad (27)$$

1278 to obtain 187.03 ( $W/m^2$ ) using benchmark convolution and 187.14 ( $W/m^2$ ) using `gcell`.  
 1279 Switching between trapezoidal and Simpson integration in Eq.(27) did not change the numbers.  
 1280 For the spectrally integrated transmittances, Eq.(25), the values are 0.7007 (benchmark) and

1281 0.7011 (`gcell`) or +0.0004 vs. the benchmark in absolute units of transmittance. Corresponding  
1282 effective (spectrally integrated) absorption optical thicknesses, Eq.(26), are 0.3557 and 0.3552  
1283 (or -0.2% vs. the benchmark), respectively.

1284 We compiled an ASCII file, `./benchmarks/Sec5p3p2__test_gcell_ch4.txt`, for  
1285 accurate reproducibility of this numerical exercise. The file contains 211900 rows, excluding  
1286 header. Columns, left to right, contain wavenumber (floating point format with 3 digits after  
1287 decimal point), optical thickness calculated using our code `gcell` (scientific format, 7 digits  
1288 total), direct transmittance for the same (floating point format, 6 digits), filter function,  
1289 convolution of the `gcell` transmittance with the filter, benchmark convolution (all the three are  
1290 in scientific format with 6 digits total and provided by the GATS team), and difference of the last  
1291 two (scientific format, 2 digits). The header shows the total number of points and names of the  
1292 columns.

## 1293 6. Absorption in the Earth atmosphere

1294 In the previous section we explained in detail how to calculate absorption by gas in a cell, where  
1295 temperature, pressure, and the gas concentration are constant. In atmospheres, however, all these  
1296 parameters vary with height. Their profiles come from another established package,  
1297 MODTRAN, the elements of which we consider in the next section. After that, we integrate the  
1298 MODTRAN profiles over height to get column amount of each considered molecule in  
1299 atmosphere, discuss units expressing that amount, and calculate  $\tau$  profile – one topic per section.

### 1300 6.1 Elements of MODTRAN

1301 MODTRAN is a comprehensive RT code, in Fortran, for calculation of atmospheric radiances  
1302 and transmittance across the solar and thermal spectral region: from 100 to 50,000 ( $cm^{-1}$ ) or 0.2  
1303 to 100 ( $\mu m$ ). Multiple scattering is simulated using scalar RT code DISORT (Stamnes et al.,  
1304 1988; Laszlo et al., 2016). MODTRAN v.6.0 (Berk et al., 2014, 2017, 2019) is the current  
1305 release. It is not publicly available except for the online tool MODTRAN Demo<sup>47</sup>. However, the  
1306 atmospheric profiles for aspect are published in a manual for MODTRAN v.2 / LOWTRAN  
1307 v.7 (Kneizys et al., 1996), the latter being a precursor for MODTRAN.

---

<sup>47</sup> [http://modtran.spectral.com/modtran\\_home](http://modtran.spectral.com/modtran_home)

1308 The MODTRAN/LOWTRAN package defines 6 atmospheres. They are “Tropical (15N Annual  
 1309 Average)”, “Mid-Latitude Summer (45N July)”, “Mid-Latitude Winter (45N Jan)”, “Sub-Arctic  
 1310 Summer (60N July)”, “Sub-Arctic Winter (60N Jan)”, and “U. S. Standard (1976)”. Aspect  
 1311 calls them by an index `iatm` = 1 ... 6. The grid of heights, same for all profiles, consists of  
 1312 three parts (see **Fig.6 (a)**): lower - below 25 (km), middle – between 25 and 50 (km), and upper  
 1313 50-120 (km). The corresponding steps are 1, 2.5, and 5 (km). For reference, about 50%, 70% and  
 1314 95% of Rayleigh atmosphere are located below 5, 10, and 25 (km), respectively.

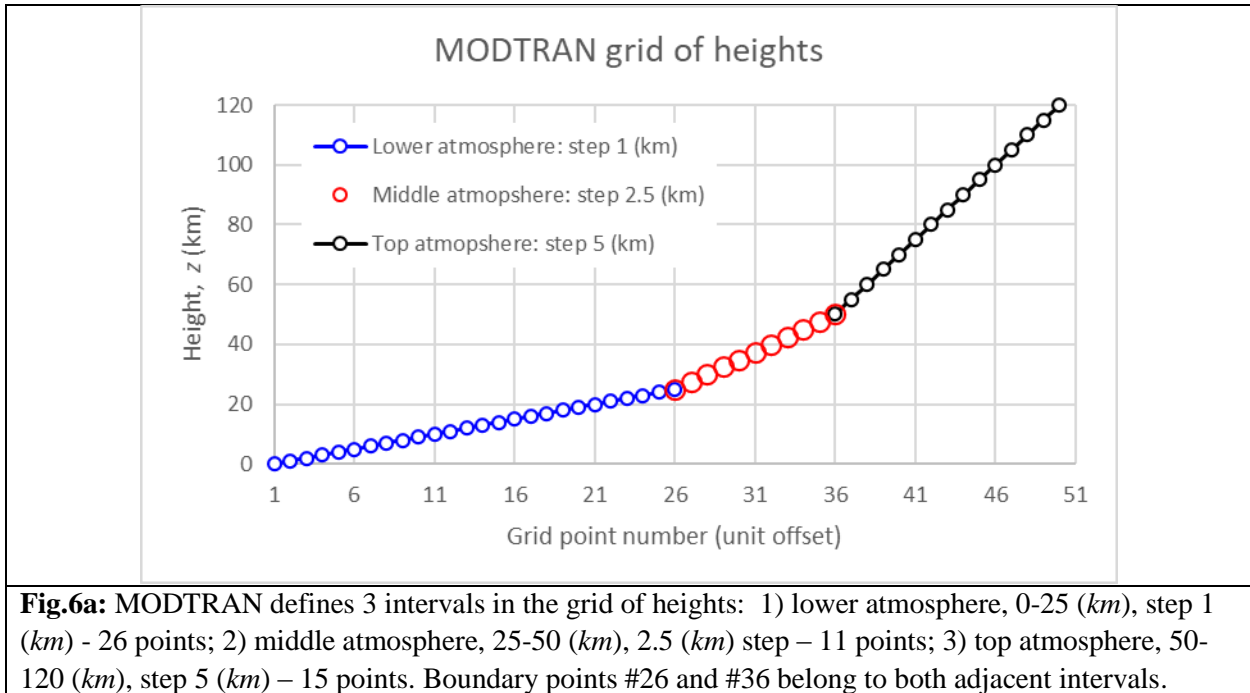


**Fig.6a:** MODTRAN defines 3 intervals in the grid of heights: 1) lower atmosphere, 0-25 (km), step 1 (km) - 26 points; 2) middle atmosphere, 25-50 (km), 2.5 (km) step – 11 points; 3) top atmosphere, 50-120 (km), step 5 (km) – 15 points. Boundary points #26 and #36 belong to both adjacent intervals.

1315  
 1316 For each of 6 atmospheres, MODTRAN/LOWTRAN provides LUTs with pressure  $p$  (mbar),  
 1317 temperature  $T$  (K), and molecular number density per unit volume (air density)  $D$  ( $\text{cm}^{-3}$ ) – **Fig.6**  
 1318 (**b**). The temperature profile shows the stronger variations, while the other two change little  
 1319 between 6 atmospheres. Lastly, for each of the 8 main atmospheric gases, the mixing ratio in  
 1320 parts-per-million in a volume ( $\text{ppmv}$ ) is defined. **Fig.6 (c-f)** illustrates the absolute number  
 1321 concentration in  $\text{cm}^{-3}$  for each molecule calculated as the product of the atmospheric air density  
 1322 and the volume mixing ratio (scaled by  $10^{-6}$  to account for “per million”). In each figure, left  
 1323 charts show the full range of the MODTRAN heights, 0-120 (km); right columns show lower  
 1324 atmosphere 0-25 (km) with 1 (km) step. For another reference, we note that NASA’s ER-2

1325 airplane carry airborne prototypes of satellite instruments at  $\sim 20$  (km) altitude (*Diner et al., 2013:*  
 1326 Sec.2.6; *Puthukkudy et al., 2020*: Sec.3.1).

1327

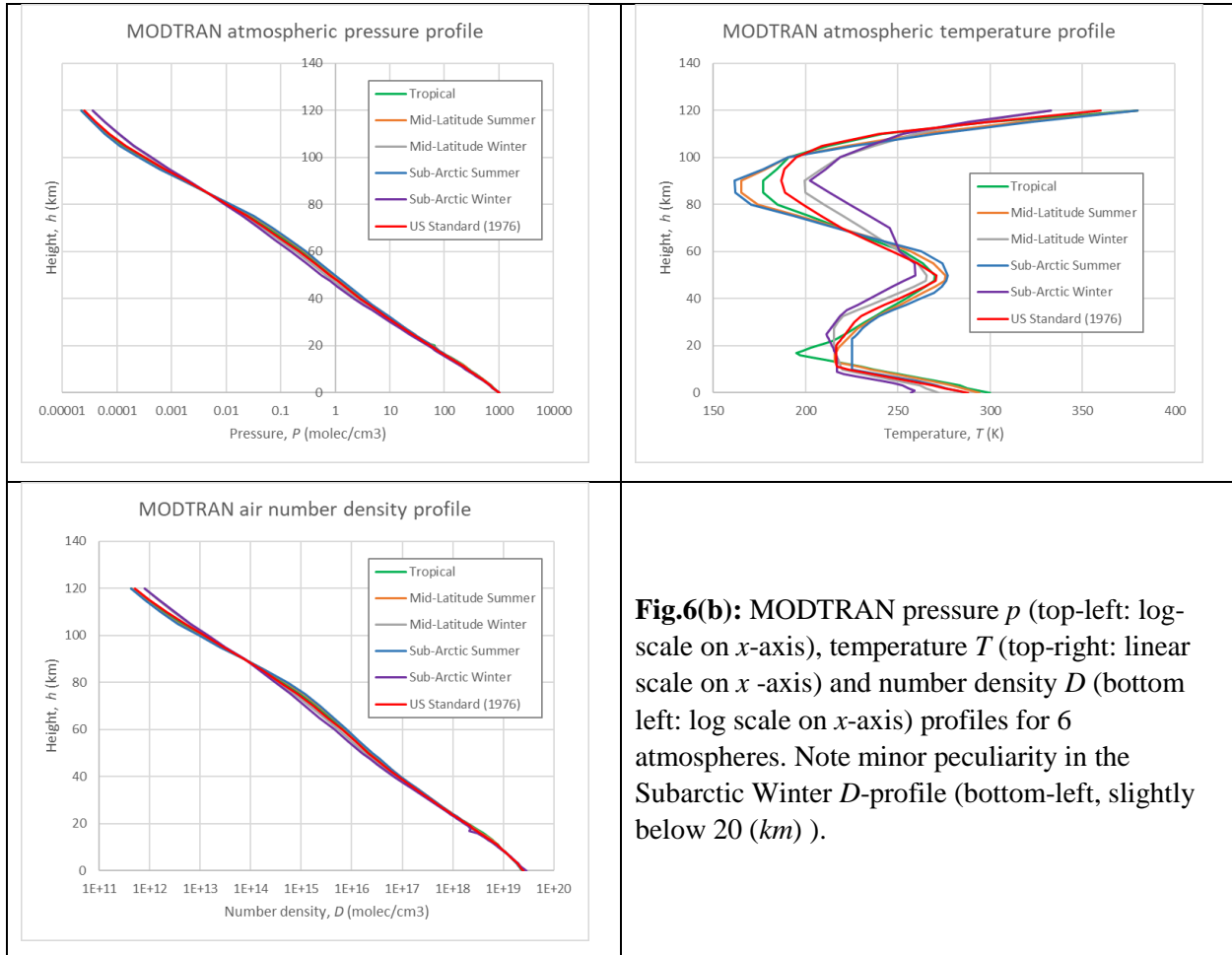
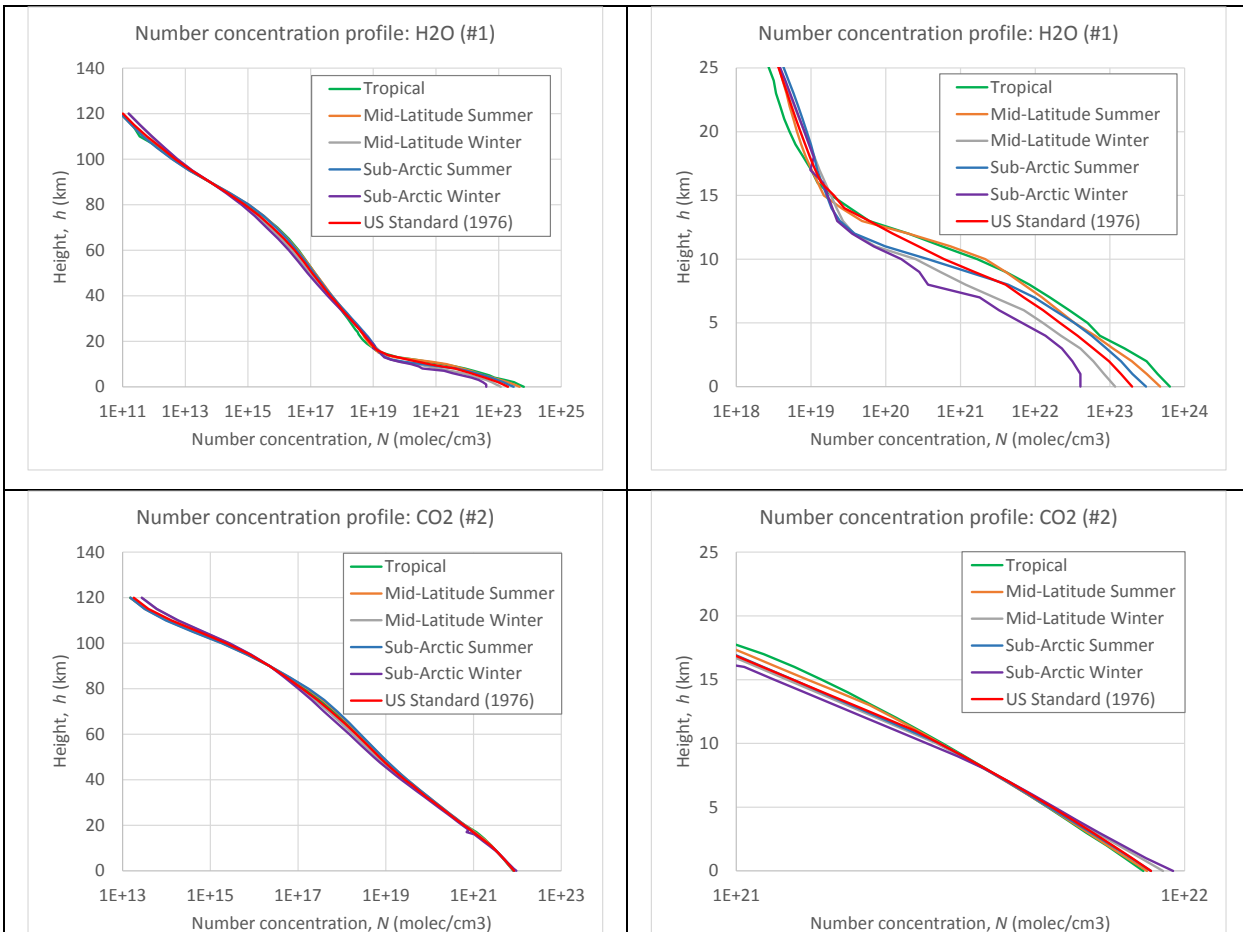


**Fig.6(b):** MODTRAN pressure  $p$  (top-left: log-scale on  $x$ -axis), temperature  $T$  (top-right: linear scale on  $x$ -axis) and number density  $D$  (bottom left: log scale on  $x$ -axis) profiles for 6 atmospheres. Note minor peculiarity in the Subarctic Winter  $D$ -profile (bottom-left, slightly below 20 (km)).

1328

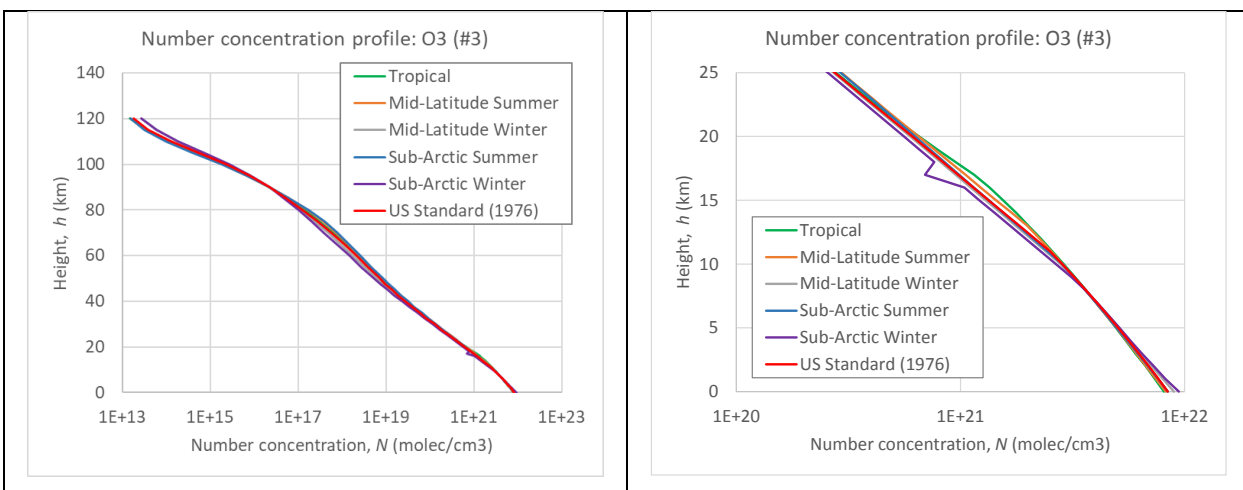
1329 Aspect defines all the mentioned parameters in `hprofiles.h`. This simplifies updating the  
 1330 existing parameters or adding a new one, if needed.

1331



**Fig.6(c):** Number concentration profiles for H<sub>2</sub>O (#1) and CO<sub>2</sub> (#2). The profiles are calculated based on the MODTRAN models for 6 atmospheric profiles. Left column: full range of the MODTRAN heights. Right column: lower atmosphere 0–25 (km) with 1 (km) step.

1332



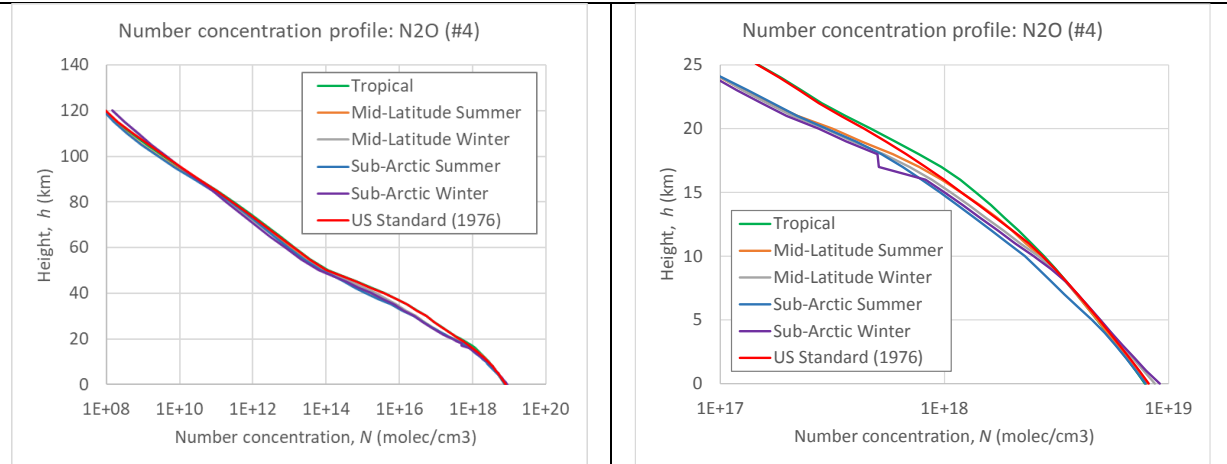


**Fig.6(d):** Same as Fig.6(c), except for O<sub>3</sub> (#3) and N<sub>2</sub>O (#4).

1333

1334

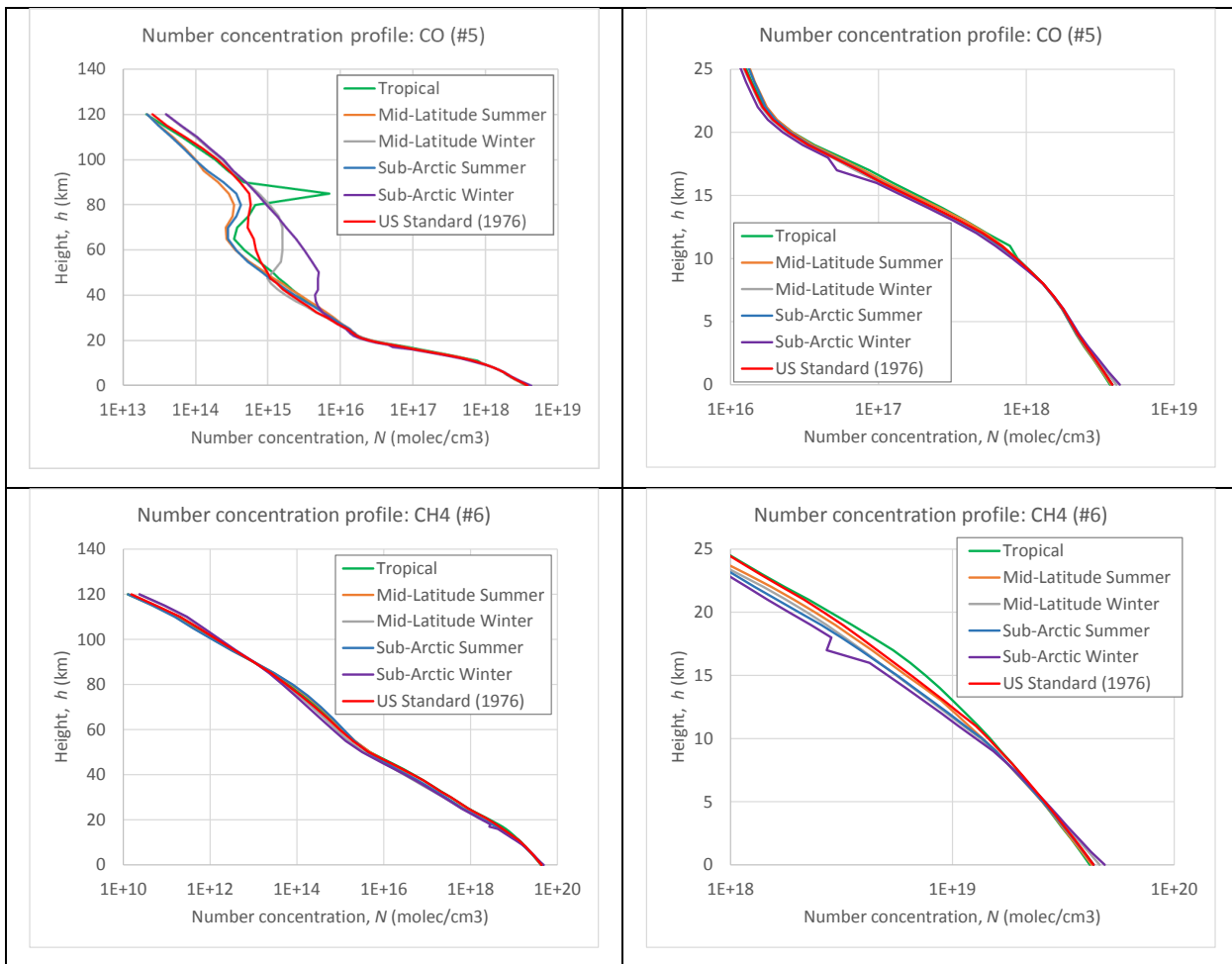


**Fig.6(e):** Same as Fig.6(c), except for CO (#5) and CH<sub>4</sub> (#6).

1335

1336

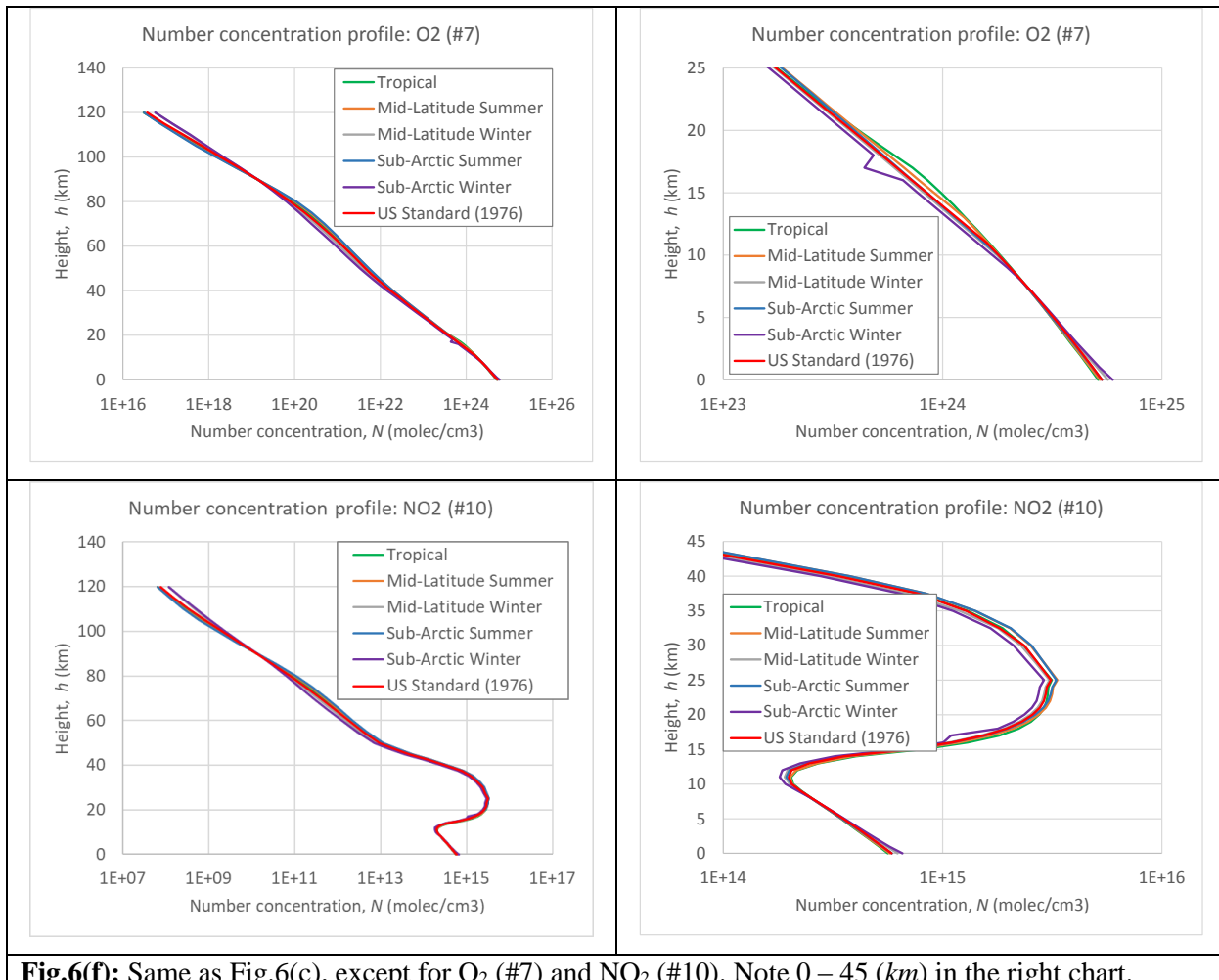


**Fig.6(f):** Same as Fig.6(c), except for O<sub>2</sub> (#7) and NO<sub>2</sub> (#10). Note 0 – 45 (km) in the right chart.

1337

## 1338 6.2 Column amount of gas in atmosphere

1339 Integration of the number concentration from BOA,  $z = 0$  (km), to TOA,  $z = 120$  (km), gives the  
 1340 columnar number density  $N_C$  ( $molec/cm^2$ )

$$1341 \quad N_C = \int_{0km}^{120km} D(z) dz . \quad (28)$$

1342 Eq.(28) uses, as an example, the MODTRAN's density of air  $D(z)$  ( $molec/cm^3$ ) and integrates  
 1343 over  $z$  (km) . To account for different units of length, a conversion scaling factor  $10^5$  ( $cm/km$ )  
 1344 pops up in subsequent calculations. Numerical integration as in Eq.(28) involves a certain error,  
 1345 which we quantify below.

1346 Absolute value of the optical thickness is directly proportional to the result of the integration.  
1347 Hence, relative error of the numerical integration is transported to the value of  $\tau$  as 1:1. We  
1348 quantify the error by comparing 3 methods of numerical integration: trapezoidal, Simpson, on  
1349 the native MODTRAN grid of heights, and Simpson on a fine grid using cubic spline  
1350 interpolation from the native grid to a finer one. We did the test in Python, hence it is not part of  
1351 our C-package, and picked one method to be coded in C-language.

1352 **Table 5** shows the result of the integration for all 6 atmospheric profiles and different methods of  
1353 integration. In each number, one space separates digits that are not in agreement with others in  
1354 the column. For the trapezoidal and Simpson integration we use Python's `numpy.trapz` and  
1355 `scipy.integrate.simpson`, respectively. To get the numbers in the "spline" row, we first  
1356 interpolated the MODTRAN profiles from the default grid (**Fig.6a**) to an equidistant fine grid  
1357 with step  $dz = 0.5$  (km) using Python's cubic spline. Then we integrated the interpolated profiles  
1358 on the fine grid using Simpson technique. The last line, `aspect`, shows respective results of our  
1359 implementation of the Simpson quadrature in C, which we picked based on the accuracy (better  
1360 than trapezoidal) vs. coding burden (no dependence on splines). Numerical results from **Table 5**  
1361 are suitable for intermediate validation of one's code (unit testing).

1362

1363 **Table 5:** Total atmosphere columnar number density  $N_C \cdot 10^{25}$  (molec/cm<sup>2</sup>), Eq.(28), for 6 model  
1364 atmospheres, and different techniques of integration. ML and SA correspond to Midlatitude and  
1365 Subarctic, respectively. The common scaling factor  $10^{25}$  is dropped. Space separates digits that are not in  
1366 agreement with others for the same atmosphere (same column).

Technique	Tropical	ML Summer	ML Winter	SA Summer	SA Winter	US 1976
Trapezoid	2.16 71	2.1 620	2.1 685	2.1 503	2.1 503	2.15 71
Simpson	2.164 6	2.159 3	2.165 5	2.147 7	2.146 6	2.154 5
Spline	2.164 5	2.159 3	2.165 3	2.147 6	2.146 1	2.154 4
aspect	2.164 2	2.159 5	2.165 1	2.147 4	<b>2.14 40</b>	2.154 6

1367

1368 Except for the Subarctic Winter model (see bold number in Table 5), `aspect` agrees with  
1369 Python's spline and Simpson methods within 4 digits. In `aspect`, we use our self-coded  
1370 Simpson's rule for the numerical integration over height. Simpson's rule approximates the

1371 function with a second-degree polynomial; hence the number of points must be odd. MODTRAN  
1372 uses 26 points in the lower atmosphere (**Fig.6a**). So, we use Simpson's rule for the first 25 points  
1373 - up to 24 (km)

1374     `hint0_24km = simpson(&conc_all, 25, 1.0);`

1375 Then we draw and integrate a separate parabola for the 24-25 (km) region using 23 (km) as a  
1376 third point (could be replaced just by trapezoidal integration)

1377     `hint24_25km = intparab(zkm_mod[24], zkm_mod[25], zkm_mod[23],`  
1378       `zkm_mod[24], zkm_mod[25], &conc_all[23], conc_all[24], conc_all[25]);`

1379 Afterwards, we use Simpson's rule again for the middle (11 points, 2.5 km step)

1380     `hint25_50km = simpson(&conc_all[25], 11, 2.5)`

1381 and upper (15 points, 5.0 km step)

1382     `hint50_120km = simpson(&conc_all[35], 15, 5.0)`

1383 parts of the atmosphere (note odd number of points for both). Adding all these gives one the  
1384 column number concentration `nmolec_all` (*molec/cm<sup>2</sup>*) in the whole atmosphere

1385     `nmolec_all = (hint0_24km + hint24_25km + hint25_50km +`  
1386       `hint50_120km) * km_to_cm;`

1387 where the scaling factor `km_to_cm = 1.0e5` relates kilometers in the grid of height and  
1388 centimeters in the volume number density, and `_all` refers to all molecules in the air mixture.

1389 Identically, by integrating a particular gas number concentration over height from BOA to TOA,  
1390 one gets the total columnar number concentration for that gas only. E.g., for methane (#6: CH<sub>4</sub>)  
1391 we first calculate the gas mixing ratio from the *ppmv*-value

1392     `case 6:`  
1393       `for (iz = 0; iz < nz_mod; iz++)`  
1394         `gas_ratio[iz] = CH4_ppmv[iatm-1][iz]/1.0e6;`  
1395       `break`

1396 and the height distribution of the volume number concentration `conc_cm3[]`

1397     `for (iz = 0; iz < nz_mod; iz++)`  
1398       `...`  
1399       `conc_cm3[iz] = Dcm3_mod[iatm-1][iz]*gas_ratio[iz];`

1400 ...  
 1401 The abovementioned numerical integration of the methane number concentration over height  
 1402 gives  $n_{molec} = 3.5523e+19$  ( $molec/cm^2$ ) or  $ppm\_ch4 = 1.6487$ , in terms of  $ppmv$   
 1403  $ppmv_{molec} = 10^6 n_{molec} / n_{all}$  (29)  
 1404  $column\_amount\_mod = nmolec * 1.0e6 / nmolec\_all;$   
 1405 for the US 1976 standard atmosphere. This is the “standard” MODTRAN value, which is used in  
 1406 calculations by default if the user provides negative gas concentration as input parameter (see  
 1407 Sec.3.2.2). For validation purposes, **Table 6** indicates the “standard” columnar amount of the  
 1408 considered gases, for all atmospheres, in absolute units and in  $ppmv$  – i.e., relative to the values  
 1409 from the bottom row aspect in **Table 5**.  
 1410  
 1411 **Table 6:** Absolute (top: in number of molecules) and relative (bottom: in  $ppmv$  w.r.t. Table 5: row =  
 1412 aspect) columnar amount of atmospheric gases, calculated by aspect.

#	Molec	Tropical	Mid Lat Sum	Mid Lat Win	Sub Arc Sum	Sub Arc Win	US 1976
1	H <sub>2</sub> O	1.3769E+23	9.8002E+22	2.8614E+22	6.9511E+22	1.4215E+22	4.7460E+22
		6362.24	4538.21	1321.60	3237.07	663.00	2202.72
2	CO <sub>2</sub>	7.1420E+21	7.1263E+21	7.1449E+21	7.0863E+21	7.0752E+21	7.1102E+21
		330.00	330.00	330.00	330.00	330.00	330.00
3	O <sub>3</sub>	7.6343E+18	8.9471E+18	1.0191E+19	9.3798E+18	9.9720E+18	9.2607E+18
		0.352747	0.414317	0.470691	0.436808	0.465114	0.429811
4	N <sub>2</sub> O	6.6300E+18	6.3862E+18	6.4632E+18	5.8955E+18	6.4306E+18	6.6159E+18
		0.306346	0.295727	0.298517	0.274547	0.299937	0.307058
5	CO	2.3730E+18	2.3608E+18	2.4218E+18	2.3688E+18	2.4433E+18	2.3879E+18
		0.109647	0.109322	0.111855	0.110314	0.113961	0.110828
6	CH <sub>4</sub>	3.5626E+19	3.4132E+19	3.4454E+19	3.3785E+19	3.4109E+19	3.5523E+19
		1.646144	1.580553	1.591323	1.573330	1.590893	1.648702
7	O <sub>2</sub>	4.5232E+24	4.5133E+24	4.5251E+24	4.4880E+24	4.4810E+24	4.5031E+24
		209000	209000	209000	209000	209000	209000
10	NO <sub>2</sub>	5.7520E+15	5.9628E+15	5.4231E+15	5.8875E+15	5.0470E+15	5.5625E+15

		0.000266	0.000276	0.000250	0.000274	0.000235	0.000258
--	--	----------	----------	----------	----------	----------	----------

1413

1414 To account for a different column amount of the gas, `column_amount_usr` (Sec.3.2.2) the  
 1415 user scales the vertical distribution of the number concentration and partial pressure, while the  
 1416 total pressure is not altered

```
1417     scalef = column_amount_usr/column_amount_mod;
1418     for (iz = 0; iz < nz_mod; iz++) {
1419         conc_cm3[iz] *= scalef;
1420         Pgas[iz] *= scalef;
1421     }
```

1422 After rescaling, we recommend integration over the column again, with the user-defined gas  
 1423 concentration, and checking the new `ppmv` value. It must match the input. `Aspect` does it by  
 1424 default and prints the user input on the screen. Regarding methane, we note that in recent years  
 1425 the amount of CH<sub>4</sub> in the atmosphere has grown to approximately 1.75 (*ppmv*) (Bernath et al.,  
 1426 2020: Fig.21). Thus, the default MODTRAN value ~1.6 (*ppmv*) may be significantly outdated.

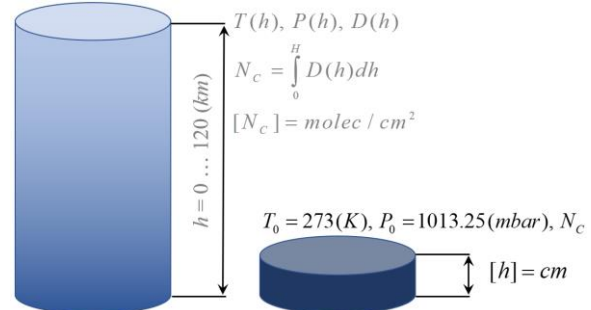
1427 The physically correct scaling of the partial pressure has non-linear effect on the resulting optical  
 1428 thickness. However, Fig.3 (right) shows that this effect may be overall insignificant. In this case,  
 1429 the resulting optical thickness would depend on the concentration linearly, which simplifies  
 1430 retrieval. For instance, one creates an optical thickness LUT for a unit amount of gas and scales  
 1431 it according to the change of concentration.

### 1432 6.3 The mysterious *atm-cm/km*

1433 In addition to *ppmv*, the atmosphere-centimeter per kilometer, *atm-cm/km*, is another way to  
 1434 define the relative (unitless) amount of gas in the atmosphere. It is widely used in practice by  
 1435 some atmospheric scientist but looks confusing to others. Finding the relation between the two  
 1436 units in literature is possible (see e.g., Berk et al., 1999: Sec. 3.4.1) but not always easy, which  
 1437 induced us to compile this section.

1438 The *atm-cm* in the numerator indicates height of the gas layer, in *cm*, if one would bring all  
 1439 molecules of the gas from the whole atmospheric column (which is measured in *km* -  
 1440 denominator) to standard conditions,  $T_0 = 273.15^\circ$  (*K*),  $p_0 = 1$  (*atm*), known as “standard  
 1441 (atmospheric) temperature and pressure” – SATP or STP, **Fig.7a**.

**Fig.7(a):** Definition of the units of  $atm\text{-}cm/km$ . The tall column on the left represents a realistic atmosphere with some temperature, pressure, and density profiles. The right column is at normal condition but holds the same number of the gas molecules  $N$  as the right one. Both columns stand on the unit area surface element  $S$ .



1442

1443 In order to convert the MODTRAN density profile in  $molec/cm^3$  into  $atm\text{-}cm/km$ , one uses

$$1444 \quad p = nk_B T = \frac{N}{Sh} k_B T, \quad (30)$$

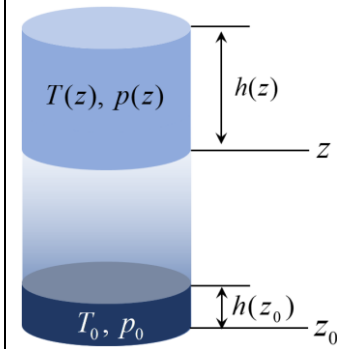
1445 where  $n$  ( $molec/cm^3$ ) is the volume number concentration. From this equation one gets the ratio  
1446 of two heights of gas in different thermodynamic conditions over the same (unit) area  $S$  of the  
1447 atmospheric column (**Fig.7b**)

$$1448 \quad \frac{h(z_0)}{h(z)} = \frac{T_0}{p_0} \frac{p(z)}{T(z)} = \frac{T_0}{p_0} nk_B \left( \frac{atm\text{-}cm}{cm} \right) = \frac{T_0}{p_0} nk_B 10^5 \left( \frac{atm\text{-}cm}{km} \right). \quad (31)$$

1449 In Eq.(31), the scaling factor  $10^5$  converts  $km$  to  $cm$ , and  $k_B$  and  $n$  are in SI units.

**Fig.7(b):** Graphical explanation for Eq.(31). Both heights  $h$ , measured at levels  $z$  and  $z_0$ , are small so that temperature and pressure are constant with the shown volumes; the number of molecules in both volumes is the same.

Any volume element  $h(z)$ , floating at level  $z$  in the atmosphere, can be reduced to the one at normal conditions,  $h(z_0)$ .



1450

1451 In terms of code, aspect would converts MODTRAN's number density profiles into  $atm\text{-}cm/km$   
1452 as follows

```
1453 c_stp = 1.0e5 * (k_boltzman * 1.0e-7) * To_stp / Po_stp * 1.0e6;
1454 atmcm_km = new double [nz_mod];
1455 for (iz = 0; iz < nz_mod; iz++) atmcm_km[iz] = c_stp*conc_cm3[iz];
```

1456 Note, the two factors  $1.0 \times 10^{-7}$  and  $1.0 \times 10^6$  bring the Boltzmann constant and the number density  
1457 to SI; `_stp` stands for “standard temperature and pressure”.

1458 In fact, `aspect` does not use the `atmcm_km` array in calculations. However, it can be used to  
1459 test numerical integration over height and to convert units from/to other data sources. For  
1460 example, the MODTRAN website<sup>48</sup> reports numerical results (5 significant digits) for the total  
1461 amount of species in *atm-cm* (integrated over height, hence no “per kilometer”). **Table 7**  
1462 replicates their results in our paper for convenience (only molecules #1-7 and #10), while **Table**  
1463 **8** compares numbers from **Table 7**, assumed baseline, vs. those for `aspect` and SHARM-IPC.  
1464 Negative sign in **Table 8** means our numerical result exceeds the one from **Table 7**.

1465

1466 **Table 7:** MODTRAN’s total vertical column amounts (*atm-cm*) listed in HITRAN order. CO<sub>2</sub> is indicated  
1467 for 380 (*ppmv*) as opposed to the default MODTRAN value of 330 (*ppmv*) – see Table 6 and 2\* below.

#	Molec	Tropical	Mid Lat Sum	Mid Lat Win	Sub Arc Sum	Sub Arc Win	US 1976
1	H <sub>2</sub> O	5.1194E+03	3.6359E+03	1.0597E+03	2.5894E+03	5.1773E+02	1.7623E+03
2*	CO <sub>2</sub>	3.0587E+02	3.0513E+02	3.0599E+02	3.0347E+02	3.0421E+02	3.0448E+02
3	O <sub>3</sub>	2.7727E-01	3.3176E-01	3.7681E-01	3.4492E-01	3.7550E-01	3.4356E-01
4	N <sub>2</sub> O	2.4649E-01	2.3743E-01	2.4037E-01	2.1920E-01	2.3993E-01	2.4593E-01
5	CO	3.0587E+02	3.0513E+02	3.0599E+02	3.0347E+02	3.0421E+02	3.0448E+02
6	CH <sub>4</sub>	1.3243E+00	1.2684E+00	1.2806E+00	1.2556E+00	1.2719E+00	1.3203E+00
7	O <sub>2</sub>	1.6823E+05	1.6782E+05	1.6829E+05	1.6691E+05	1.6732E+05	1.6746E+05
10	NO <sub>2</sub>	2.1091E-04	2.1814E-04	1.9842E-04	2.1543E-04	1.8654E-04	2.0418E-04

1468

1469 Regarding **Table 8**, we note that profiles and numerical integration technique used in SHARM-  
1470 IPC-LBL and `aspect` are not the same. First, in SHARM-IPC-LBL, the vertical distribution of  
1471 molecules is defined in (*atm-cm/km*), instead of the number density concentration (*molec/cm<sup>3</sup>*).

<sup>48</sup> [http://modtran.spectral.com/modtran\\_faq](http://modtran.spectral.com/modtran_faq), Table 1: Total vertical column amounts (atm·cm) for the 12 ambient band model species

1472 Next, the number of points over height is different. The middle atmospheres 25-50 (*km*) uses 5  
 1473 (*km*) step (6 points), and the upper atmosphere uses 25 (*km*) step. The TOA is assumed at 100  
 1474 (*km*), thus the upper part of atmosphere contains only 3 points. The total number of points in the  
 1475 height grid is 33 (compare with **Fig.6a**).

1476 SHARM-IPC-LBL uses the following algorithm for integration of its profiles. For the lower, 0:  
 1477 1:25 (*km*) the trapezoidal quadrature is used. For the middle atmosphere, 25:5:45 (*km*)  
 1478 atmosphere, the profile is first interpolated from 5 equidistant points, 5 (*km*) step, to 11  
 1479 equidistant points, 2 (*km*) step, using the quadratic spline interpolation. Then, Simpson's rule is  
 1480 used on these 11 interpolated points. The last four points, 45, 50, 75, and TOA at 100 (*km*), are  
 1481 interpolated with an exp-function

1482  $f(z) = f(45) \exp(-\alpha(z - 45)) .$  (32)

1483 In Eq.(32), the decay factor  $\alpha$  ( $km^{-1}$ ) is derived from the log-linear least squares fit at the last  
 1484 three points. We refer our reader back to Sec.6.2 for the vertical integration we use in aspect.

1485

1486 **Table 8:** Relative difference, in %, for MODTRAN (assumed as baseline, in Table 7) vs. aspect (left)  
 1487 and SHARM-IPC (right: gray). Negative values mean our result exceeds the one for MODTRAN.

#	Molec	Tropical		Mid Lat Sum		Mid Lat Win		Sub Arc Sum		Sub Arc Win		US 1976	
1	H <sub>2</sub> O	0.1	2.0	0.3	2.0	0.5	1.5	-0.1	1.5	2.2	1.2	0.2	1.4
2	CO <sub>2</sub>	0.1	0.0	0.1	0.0	0.1	0.1	0.1	0.0	-0.3	0.1	0.1	0.0
3	O <sub>3</sub>	2.5	2.6	0.4	1.6	0.7	0.5	1.2	0.4	-1.2	0.2	0.3	0.7
4	N <sub>2</sub> O	0.1	0.0	0.1	0.0	0.1	0.1	0.1	0.1	-0.2	0.1	0.1	0.0
5	CO	0.8	0.1	0.1	0.2	0.1	0.3	0.1	0.1	0.0	0.3	0.2	0.2
6	CH <sub>4</sub>	0.1	0.0	0.2	0.0	0.1	0.0	0.1	0.0	-0.2	0.0	0.1	0.1
7	O <sub>2</sub>	0.1	0.0	0.1	0.0	0.1	0.1	0.1	0.0	-0.3	0.1	0.1	0.1
10	NO <sub>2</sub>	1.5	2.5	1.7	2.6	1.7	2.6	1.7	2.8	0.7	2.8	1.4	2.7

1488

1489 Because of the difference in profiles and numerical integration technique, the overall maximum  
 1490 (and average) relative deviation of aspect and SHARM-IPC-LBL w.r.t. the MODTRAN

1491 values are 2.5% (0.5%) and 2.8% (0.8%), respectively. Table 8 shows that the Sharm-IPC  
1492 deviation is always higher, while that for aspect changes sign w.r.t to the MODTRAN values.  
1493 We ignored the change of sign in the overall errors mentioned. Also, based on our literature  
1494 search, we were unable to clarify MODTRAN’s technique for vertical integration.

1495 **6.4 Profile of optical thickness**

1496 Aspect uses three steps to calculate the absorption optical thickness profile. For one, profile of  
1497 the molecular absorption cross-section,  $k$  ( $cm^2/molec$ ), is calculated in `kabs(...)` for each  
1498 wavenumber  $v$  from the user’s grid [ $v_{min}, v_{max}$ ] with step  $\Delta v$ . This is like the one for the gas cell  
1499 (Sec.5): one picks all HITRAN line contributions to the user-defined band and accumulates  
1500 them. The only two differences from simulation of the gas cell are: (1) one deals with a mixture  
1501 of gases – hence Eq.(8) for the Lorentzian HWHM parameter uses both the total atmospheric and  
1502 partial gas pressures, and two HITRAN parameters:  $\gamma_{self}$  and  $\gamma_{air}$ ; and (2): the atmosphere is a  
1503 stack of “gas cells”, one on top of the other. Therefore, `kabs(...)` accepts as input the user’s  
1504 range of wavenumbers, parameters of the HITRAN lines (limited to those contributing to the  
1505 user interval – see Sec.5.1), and profiles of temperature and pressure. The output of `kabs(...)`  
1506 is the spectral and height dependence of the absorption cross-section,  $k(v, z)$  ( $cm^2/molec$ ), on the  
1507 user grids of  $v$  ( $cm^{-1}$ ) and heights,  $z$  ( $km$ ) – an array `knu[nz*nmu]`.

1508 A few comments must be made here regarding the array `knu[ ]`. First, in order to allocate the  
1509 elements of an array in memory consecutively, we prefer a 1D array over the 2D one (Oliveira &  
1510 Stewart, 2006: Sec.8.3). Second, the grid of heights  $z$  is the lead dimension of the array for  
1511 efficiency of the vertical integration performed independently for each  $v$ . Third, the MODTRAN  
1512 profiles are used. Before calling `kabs(...)`, the array `knu[nz_mod*nmu]` must be allocated  
1513 for the number of the MODTRAN points over height `nz_mod`. Fourth and the last one, at present  
1514  $nz\_mod = 53$  and the user must be careful with the number of the spectral nodes, `nmu`. A  
1515 wide spectral range combined with a very fine spectral resolution may lead to insufficient  
1516 memory. Aspect checks that and, if it happens, stops, and notifies the user. The easiest way to  
1517 deal with the problem is to split the wide band into a few smaller ones, generate corresponding  
1518 LUTs and, if needed, tailor them together into a single big file. Also, using single precision  
1519 instead of double saves memory.

1520 The next steps are trivial: for a given `v`, `aspect` calculates the extinction profile by multiplying  
1521 the cross-section and the number concentration profiles (the height grids must match); then it  
1522 integrates the extinction over height from TOA to a user-defined level to get the optical thickness  
1523 between TOA and the given level (i.e., optical depth). The corresponding element of code in  
1524 `aspect` is

```
1525     for (inu = 0; inu < nnu; inu++) {  
1526         for (iz = 0; iz < nz_mod; iz++)  
1527             ext_km[iz] = knu[inu*nz_mod+iz]*conc_cm3[iz]*1.0e5;  
1528         tauabs25(ext_km, zkm_mod, ztau, nzkm, tau_abs);  
1529     }
```

1530 The scaling factor `km_to_cm = 1.0e5` relates  $cm^{-1}$  (in  $k$ ) and  $km^{-1}$  (in the grid of heights).

1531 The subroutine `tauabs25` (...) integrates the extinction profile defined on the MODTRAN grid  
1532 of heights, `zkm_mod[nzkm_mod]`, using the two functions already explained in Sec.6.2:  
1533 `simpson` (...) and `intparab` (...). On output, this subroutine gives an array,  
1534 `tau_abs` [`nzkm`], of optical depths at every user requested height `ztau` [`nzkm`]. For the  
1535 code simplicity, we assume the user requests optical depths at levels not exceeding 25 ( $km$ ). As  
1536 Sec.6.1 shows, MODTRAN uses equidistant grid of heights with 1( $km$ ) step below the 25 ( $km$ )  
1537 threshold. Therefore, it is easy to quickly get the left and right indices of the interval of heights  
1538 containing the user requested altitude. Using these indices, one integrates from  $z = 25$  ( $km$ ) to the  
1539 user level by accumulating Simpson integral and, optionally, trapezoidal integral to include the  
1540 part not covered by Simpson's rule due to the odd vs. even number of points.

1541 At and above  $z = 25$  ( $km$ ), `tauabs25` (...) provides the vertical integral from 25 to 120 ( $km$ ) –  
1542 regardless the user requested level. The 25-120 ( $km$ ) value is calculated using only Simpson's  
1543 rule for the middle (11 points, 2.5 km step) and top (15 points, 5 km step) atmosphere which are  
1544 added to the final result.

1545 Also, for the code simplicity, `tauabs25` (...) loops through the user's heights independently. If  
1546 the user requests many levels, `nzkm >> 1`, this is inefficient: a lower level includes integral  
1547 from TOA to the level above it. However, our option *a*) helps keep the code simple; *b*) yields  
1548 flexibility: the order of the user's levels is not important; and *c*) is not a bottleneck for the  
1549 runtime – calculation of the Voigt line shape is.

1550 The output result, **`tau_abs`** [nzkm], is saved either to ASCII or to a binary file as explained in  
1551 Sec.3.3.2. In the former case, aspect prints out all values including 0.0. This is convenient for  
1552 visual inspection, debugging, and smaller LUTs. Consider as an example only one HITRAN-  
1553 2020 record for O<sub>2</sub> from Sec.4.2-4.3, default MODTRAN's amount of the gas in atmosphere, US  
1554 1976 profile, 4 user defined levels  $z = 0, 2, 4, 8$  (km), and 6 user's  $v = 13000 + [0.80 : 0.01 :$   
1555  $0.85]$  ( $cm^{-1}$ ). The output file with optical thickness in ASCII format is

```
1556 # nu, zkm = 0.000 2.000 4.000 8.000
1557 0 13000.8000 3.077005e-02 1.877401e-02 1.106013e-02 3.841381e-03
1558 1 13000.8100 3.533850e-02 2.287806e-02 1.461589e-02 6.374547e-03
1559 2 13000.8200 3.425169e-02 2.232654e-02 1.442593e-02 6.519878e-03
1560 3 13000.8300 2.782967e-02 1.723955e-02 1.043387e-02 3.993817e-03
1561 4 13000.8400 2.084901e-02 1.196508e-02 6.532608e-03 1.837301e-03
1562 5 13000.8500 1.554367e-02 8.344352e-03 4.179478e-03 9.014089e-04
```

1563 These numbers are convenient for validation of integration over height because they correspond  
1564 to a single HITRAN record.

1565 In the case of binary output file, aspect checks the highest value (lowest level) against a  
1566 threshold, `tau_min`, defined in `const_param.h` (at present, `tau_min` = `1.0e-4` which  
1567 corresponds to the vertical one-way monochromatic transmittance of ~0.9999). If the highest  
1568 thickness does not exceed the threshold, the whole wavenumber is not saved to the binary file.  
1569 The check whether to save or skip **`tau_abs`** [nzkm] is made for each user's `v`. For that reason,  
1570 **`tau_abs`** [nzkm], does not depend on `inu` and is small even for a dense user's grid of heights  
1571 `zkm` [nzkm].

## 1572 [6.5 Practical units for water vapor](#)

1573 MODTRAN defines profiles for the particles number concentration in *ppmv*. In practice,  
1574 however, different units are commonly used for some molecules: *cm* (or sometimes *mm*) of  
1575 precipitable liquid water for water vapor (WV), and Dobson units (DU) for O<sub>3</sub>. In this part we  
1576 convert the atmospheric columnar amounts of WV from *ppmv* to *cm* of precipitated (liquid)  
1577 water.

1578 The atmosphere-centimeters shown in Table 7 for MODTRAN's US 1976 atmosphere  
1579 corresponds to aspect's  $h = 1766.42$  (cm). It the height of a column of the water vapor (ideal

1580 gas) at the normal conditions. When the vapor is condensed into the liquid water, the number of  
1581 molecules does not change, but the mass density does. Ratios of the mass densities and columns  
1582 of water in two physical states are the same:

1583 
$$h_{LW} = h_{wv} \frac{\rho_{LW}}{\rho_{wv}}$$
 (33)

1584 In Eq.(33), the subscript LW means “Liquid Water” and  $\rho_{LW} = 1.0$  ( $g/cm^3$ ) is the liquid water  
1585 mass density. The water vapor mass density is calculated via scaling the molar mass of the  $H_2O$   
1586 molecule  $\mu_{H_2O} = 18.01528$  ( $g/mole$ ) by the number of moles. The latter is computed as the ratio of  
1587 the Loschmidt number  $N_L = 2.6867811 \cdot 10^{19}$  ( $molec/cm^3$ ) and the Avogadro number  $N_A =$   
1588  $6.02214129 \cdot 10^{23}$  ( $molec/mole$ )

1589 
$$\rho_{wv} = \mu_{H_2O} \frac{N_L}{N_A}.$$
 (34)

1590 Eqs.(33) and (34) result in  $\approx 1.42$  ( $cm$ ) of liquid water for the MODTRAN’s Standard US1976  
1591 atmosphere. Recall, aspect expects the LW amount as input for  $H_2O$ .

1592 [6.6 Aspect validation](#)

1593 [6.6.1 Literature references](#)

1594 As for the gas cell, we recommend starting with a visual comparison of the spectral dependencies  
1595 calculated using aspect vs. figures published in literature. This helps catch misunderstandings  
1596 of units, which manifest as wrong order of magnitude. The existence and location of the spectral  
1597 line peaks (or drops in atmospheric transmittance) help verify the proper reading and  
1598 understanding of the HITRAN database. In Table 9, we combine some references to published  
1599 images that can be used for validation of separate molecules and the whole atmosphere. The list  
1600 is sporadic, non-exhaustive, and contains references to papers and books that we found while  
1601 working on this paper.

1602

1603 **Table 9:** References to published benchmark images that can be used to test codes like aspect. The  
1604 bottom row “total” refers to results for all gases mixed in atmosphere.

#	Mol.	Ref.	$\approx \Delta\nu$ ( $cm^{-1}$ )	$\approx \Delta\lambda$ ( $\mu m$ )	Brief description
---	------	------	-----------------------------------	-------------------------------------	-------------------

		Gao et al., 1993: Fig.2		0.4 - 2.5	Atmospheric water vapor transmittance spectrum, at 10 (nm) resolution, using LOWTRAN7 (Kneizys et al., 1988)
1	H <sub>2</sub> O	Goody & Yung, 1995: p.68, p.71	630 – 710 (p.71)	1 - 13 (p.68)	Low-resolution atmospheric absorption spectrum; high-resolution transmission near 14.9 ( $\mu\text{m}$ ) at 0 (km) and SZA = 30° and terrestrial concentration $\times 0.03$
		Petty, 2006: p.179		0.3 - 50	Zenith transmittance of a midlatitude summertime atmosphere.
		Thorpe et al., 2013: Fig.1		0.5 - 2.5 2.0 - 2.5	Transmittance spectra generated using MODTRAN v.5.3 for a sensor located at 8.9 (km) altitude.
		Yang et al., 2013: Fig.1		0.6 – 0.8	Atmospheric columnar water vapor absorption transmittance calculated using LBLRTM.
		Ibrahim et al., 2018: Fig.1		0.3 – 1.1	Columnar atmospheric transmittance for 3.3 (cm) of water vapor
		Coakley & Yang, 2014: p.157	800 - 900		Total atmospheric water vapor transmission for the 1976 US Standard Atmosphere. The water vapor continuum was not included “ <i>in order to better show the line structure</i> ”.
		Gordon, 2019: p.328		0.4 – 1.0 0.4 – 2.5	Water vapor transmittance in the US Standard Atmosphere at 20 (cm <sup>-1</sup> ) resolution (p.327)
		Mobley, 2022: Fig. 15.15	300 - 1000		Transmittance by a moist tropical atmosphere at 1 (nm) resolution.
		Docter et al., 2023: Fig. 2		0.6 – 2.35	Atmospheric transmittance.
		Gordon et al., 2022: Fig.3	9000 - 19000		Terrestrial atmospheric transmittance for HITRAN 2020 and 2016.
2	CO <sub>2</sub>	Gao et al., 1993: Fig.2		0.4 – 2.5	Atmospheric carbon dioxide transmittance spectrum, at 10 (nm) resolution, using LOWTRAN7 (Kneizys et al., 1988)

		<i>Goody &amp; Yung, 1995: p.68, p.71</i>	786 – 796 (p.71)	1.5 – 13 (p.68)	Low-resolution atmospheric absorption spectrum; high-resolution transmission near 12.64 ( $\mu\text{m}$ ) at 15 (km) and SZA = 30° and terrestrial concentration $\times 10$ .
		<i>Bohren &amp; Clothiaux, 2006: Fig.2.22</i>	746 - 758 756.5 - 758.0 1074 - 1086 1082.0-1082.75		Absorptivity along a vertical path for a Mid-latitude Summer atmosphere and 4 different concentrations of carbon dioxide; note non-zero values for 0 (ppm) of CO <sub>2</sub> .
		<i>Petty, 2006: p.179</i>		0.3 - 50	Zenith transmittance of a midlatitude summertime atmosphere.
		<i>Docter et al., 2023: Fig. 2</i>		0.6 – 2.35	Atmospheric transmittance.
3	O <sub>3</sub>	<i>Gao et al., 1993: Fig.3</i>		0.4 – 2.5	Atmospheric ozone transmittance spectrum, at 10 (nm) resolution, using LOWTRAN7 (Kneizys et al., 1988)
		<i>Goody &amp; Yung, 1995: pp. 68 &amp; 72</i>	1039 – 1041 (p.72)	3.5 – 15.5 (p.68)	Low-resolution atmospheric absorption spectrum; high-resolution transmission near 9.61 ( $\mu\text{m}$ ) at 30 (km) and SZA = 30°.
		<i>Petty, 2006: p.179</i>		0.3 - 50	Zenith transmittance of a midlatitude summertime atmosphere.
		<i>Ibrahim et al., 2018: Fig.1</i>		0.3 – 1.1	Columnar atmospheric transmittance for 277 DU of ozone
		<i>Gordon, 2019: p.329</i>		0.4 – 0.8	Ozone transmittance in the US Standard Atmosphere.
		<i>Mobley, 2022: Fig. 15.16</i>	300 - 1000		Vertical atmospheric transmittance for 200, 350, and 500 DU. Strong absorption in the Blue-UV band, not available from HITRAN's LBL database, is visible.
4	N <sub>2</sub> O	<i>Gao et al., 1993: Fig.3</i>		0.4 – 2.5	Atmospheric nitrous oxide transmittance spectrum, at 10 (nm) resolution, using LOWTRAN7 (Kneizys et al., 1988)

		<i>Goody &amp; Yung, 1995: p.68, p.70, p.96</i>	1245 - 1325 (p.70) 1160.0 – 1160.6 (p.96)	2 – 9.5 (p.68)	Low-resolution atmospheric absorption spectrum (p.68); high-resolution transmission near 7.78 ( $\mu\text{m}$ ) at 15 (km) and SZA = 30° (p.70); ultra-high resolution transmission for “physical conditions very different from those occurring in Earth’s atmosphere” (also useful for gas cell validation).
		<i>Petty, 2006: p.179</i>		0.3 - 50	Zenith transmittance of a midlatitude summertime atmosphere.
		<i>Coakley &amp; Yang, 2014: p.153</i>	1120 - 1220		$\text{N}_2\text{O}$ transmissivity near 8.6 ( $\mu\text{m}$ ) for 1976 US Standard Atmosphere, HITRAN 2008, at ground level for SZA = 0°.
5	CO	<i>Gao et al., 1993: Fig.3</i>		0.4 – 2.5	Atmospheric carbon monoxide transmittance spectrum, at 10 (nm) resolution, using LOWTRAN7 (Kneizys et al., 1988)
		<i>Goody &amp; Yung, 1995: p.68, p.70</i>	2102 - 2182 (p.70)	2 – 6 (p.68)	Low-resolution atmospheric absorption spectrum; high-resolution transmission near 4.67 ( $\mu\text{m}$ ) at 10 (km) and SZA = 30°.
		<i>Petty, 2006: p.179</i>		0.3 - 50	Zenith transmittance of a midlatitude summertime atmosphere.
6	$\text{CH}_4$	<i>Gao et al., 1993: Fig.3</i>		0.4 – 2.5	Atmospheric methane transmittance spectrum, at 10 (nm) resolution, using LOWTRAN7 (Kneizys et al., 1988)
		<i>Goody &amp; Yung, 1995: p.68, p.69</i>	2874 – 2946 2904 - 2908	1.5 – 8.5 (p.68)	Low-resolution atmospheric absorption spectrum (p.68); and medium and high-resolution transmission spectra near 3.44 ( $\mu\text{m}$ ) at 10 (km) above the ground for SZA = 30° (p.69)
		<i>Petty, 2006: p.179</i>		0.3 - 50	Zenith transmittance of a midlatitude summertime atmosphere.
		<i>Thorpe et al., 2013: Fig.1</i>		0.5 - 2.5 2.0 - 2.5	Transmittance spectra generated using MODTRAN v.5.3 for a sensor located at 8.9 (km) altitude.
		<i>Docter et al., 2023: Fig. 2</i>		0.6 – 2.35	Atmospheric transmittance.

		<i>Gao et al., 1993: Fig.3</i>		0.4 – 2.5	Atmospheric oxygen transmittance spectrum, at 10 ( $nm$ ) resolution, using LOWTRAN7 (Kneizys et al., 1988)
		<i>Goody &amp; Yung, 1995: p.196</i>	842 - 7922		IR atmospheric band of molecular oxygen near 1.27 ( $\mu m$ ) based on AFGL data at 0 ( $km$ ) and SZA = 30°.
		<i>Pfeilsticker et al., 1998: Fig. 2</i>		0.768 – 0.772 (A-band)	Direct Sun observations of the atmospheric O <sub>2</sub> A-band at different solar zenith angles.
7	O <sub>2</sub>	<i>Stam et al., 2000: Figs.1, 2(a), &amp; 3</i>		0.755 - 0.775 0.765 - 0.766	Fig.1: Molecular scattering and absorption columnar optical thickness based on HITRAN-92 for the A-band.  Fig.2(a): Like Fig.1 but for a narrow band $\Delta\lambda = 1$ ( $nm$ ) resolves peaks from the isotope minorities.  Fig.3: Like Fig.2(a) but for absorption cross-section as a function for 0 ( $km$ ) and 30 ( $km$ ) with specified temperature and pressure (also useful for gas cell validation).
		<i>Petty, 2006: p.179</i>		0.3 - 50	Zenith transmittance of a midlatitude summertime atmosphere.
		<i>Nowlan et al., 2007: Figs.1, 3</i>		0.690 – 0.692 0.680 – 0.700 0.755 – 0.780	A- and B-bands cross-sections (Figs. 1 & 3) and transmittances (Fig.1 only) in atmosphere at 0, 30 (A-band only), and 50 ( $km$ ); temperature and pressure are specified (also useful for gas cell validation).
		<i>Natraj et al., 2007: Fig.1</i>	12,995 - 13,020		Atmospheric columnar optical depth calculated using HITRAN 2000; corresponding Rayleigh optical depth is also shown.
		<i>Gordon et al., 2011: Figs. 2 &amp; 4</i>	15,050 - 15,930 14,496 - 14,504		Oxygen B- and $\gamma$ -bands: atmospheric transmittance.

		<i>Yang et al., 2013: Figs.1 &amp; 2(ab)</i>		0.6 - 0.8	Oxygen transmittance in the A- and B -bands (Fig.1). Figs. 2(a) and 2(b) show details for the A- and B-bands, respectively.
		<i>Ibrahim et al., 2018: Fig.1</i>		0.3 – 1.1	Columnar transmittance for tropical atmosphere.
		<i>Mobley, 2022: Fig. 15.15</i>	300 - 1000		Atmospheric columnar transmittance at 1 ( $nm$ ) resolution.
10	$\text{NO}_2$	<i>Ibrahim et al., 2018: Fig.1</i>		0.3 – 1.1	Columnar transmittance for tropical atmosphere
		<i>Gordon, 2019: p.328</i>		0.35 – 0.90	Columnar transmittance for the US Standard Atmosphere.
		<i>Mobley, 2022: Fig. 15.17</i>	300 - 1000		Vertical atmospheric for low, typical, and high concentrations of $\text{NO}_2$ .
-	Total	<i>Goody &amp; Yung, 1995: p.4</i>		0.1 - 100	Atmospheric absorption at ground level and at 11 ( $km$ )
		<i>Petty, 2006: p.179</i>		0.3 - 50	Zenith transmittance of a midlatitude summertime atmosphere.
		<i>Bohren &amp; Clothiaux, 2006: Fig.2.13</i>		0.1 ( $\mu\text{m}$ ) – 10 ( $\text{cm}$ )	Atmospheric transmissivity along a vertical path in a very broad band. There are 6 panels, each panel is one wavelength decade - hence the top covered limit: 10 <b>centimeters</b> . Ozone absorption, not included in our HITRAN-based LBL calculations, is visible in the 0.1 ( $\mu\text{m}$ ) – 1 ( $\mu\text{m}$ ) panel.
		<i>Thompson et al., 2015: Fig.1</i>		0.4 – 2.4	Atmospheric transmittance due to atmospheric gases.
		<i>Ibrahim et al., 2018: Fig.1</i>		0.3 – 1.1	Tropical atmosphere transmittance for 3.3 ( $cm$ ) of $\text{H}_2\text{O}$ , 277 DU of $\text{O}_3$ , $\text{O}_2$ , and $\text{NO}_2$ combined.
		<i>Gordon, 2019: p.329</i>		0.4 – 1.0 0.4 – 2.5	Columnar transmittance for the US Standard Atmosphere.

		<i>Chen et al., 2021: Fig.2(a)</i>		0.25 - 2.50	Atmospheric transmittance in the Solar reflectance band. Note, the ozone absorption at wavelength shorter than 700 ( <i>nm</i> ) is not included in HITRAN, hence, in our paper as well.
--	--	--	--	-------------	--

1605

1606 Once the user has verified the order of magnitude, it is time for accurate numerical comparison  
 1607 vs. tools mentioned in the Introduction. With this paper, we distribute our numbers for the  
 1608 oxygen A-band and methane optical thickness integrated from TOA to several levels in the  
 1609 atmosphere (see Sec. 3.2.2).

#### 1610 6.6.2 Numerical example for PACE OCI

1611 In this section we plot the HITRAN (without continuum) and band-integrated spectral  
 1612 dependences of the one-way transmittances of light from the overhead Sun by atmospheric water  
 1613 vapor in the PACE-OCI instrument bands and tabulate corresponding absorption optical depths  
 1614 as given by Eqs. (25) and (26), respectively. The spectral dependence of absorption optical  
 1615 thickness was calculated using US 1976 standard atmospheric profile (Sec.6.1), and HITRAN-  
 1616 2020, for the wavenumber ranging from 4000 ( $cm^{-1}$ ) to 40000 ( $cm^{-1}$ ) with equidistant step  $\Delta\nu =$   
 1617  $0.01 (cm^{-1})$ . In the wavelength domain, this interval spans from 250 (*nm*) to 2500 (*nm*) with a  
 1618 step  $\Delta\lambda$  increasing monotonically from  $\approx 6 \cdot 10^{-5} (nm)$  in the UV to  $\approx 6 \cdot 10^{-3} (nm)$  in the SWIR.

1619 The OCI relative spectral response functions (RSRs) were measured in laboratory, tabulated in  
 1620 netCDF file and available from the NASA GSFC Ocean Color website<sup>49</sup>. The netCDF file  
 1621 contains RSRs in three groups: ‘blue’ with 119 bands with centers located from  $\sim 314 (nm)$  to  
 1622  $\sim 605 (nm)$ , ‘red’ with 163 bands with centers located from  $\sim 600 (nm)$  to  $\sim 894 (nm)$ , and  
 1623 ‘SWIR’ with 9 band centers located from  $\sim 939 (nm)$  to  $\sim 2258 (nm)$ . For simplicity, here we  
 1624 indicate only integer part of values in the netCDF’s variable ‘center\_wavelength’, note  
 1625 the sign  $\sim$ . Also note that “blue” and “red” bands partially overlap at 600-605 (*nm*). The “blue”  
 1626 and “red” groups yield hyperspectral radiometry with 5 (*nm*) resolution bandwidth, spectral steps  
 1627 2.5 (*nm*) for most bands and 1.25 (*nm*) for some bands. Poor radiometric accuracy was reported  
 1628 for bands below 340 (*nm*), but we include these bands in our demonstration anyway. All RSRs

<sup>49</sup> <https://oceancolor.gsfc.nasa.gov/images/data/PACE OCI L1B LUT RSR baseline 1.1.1.nc>

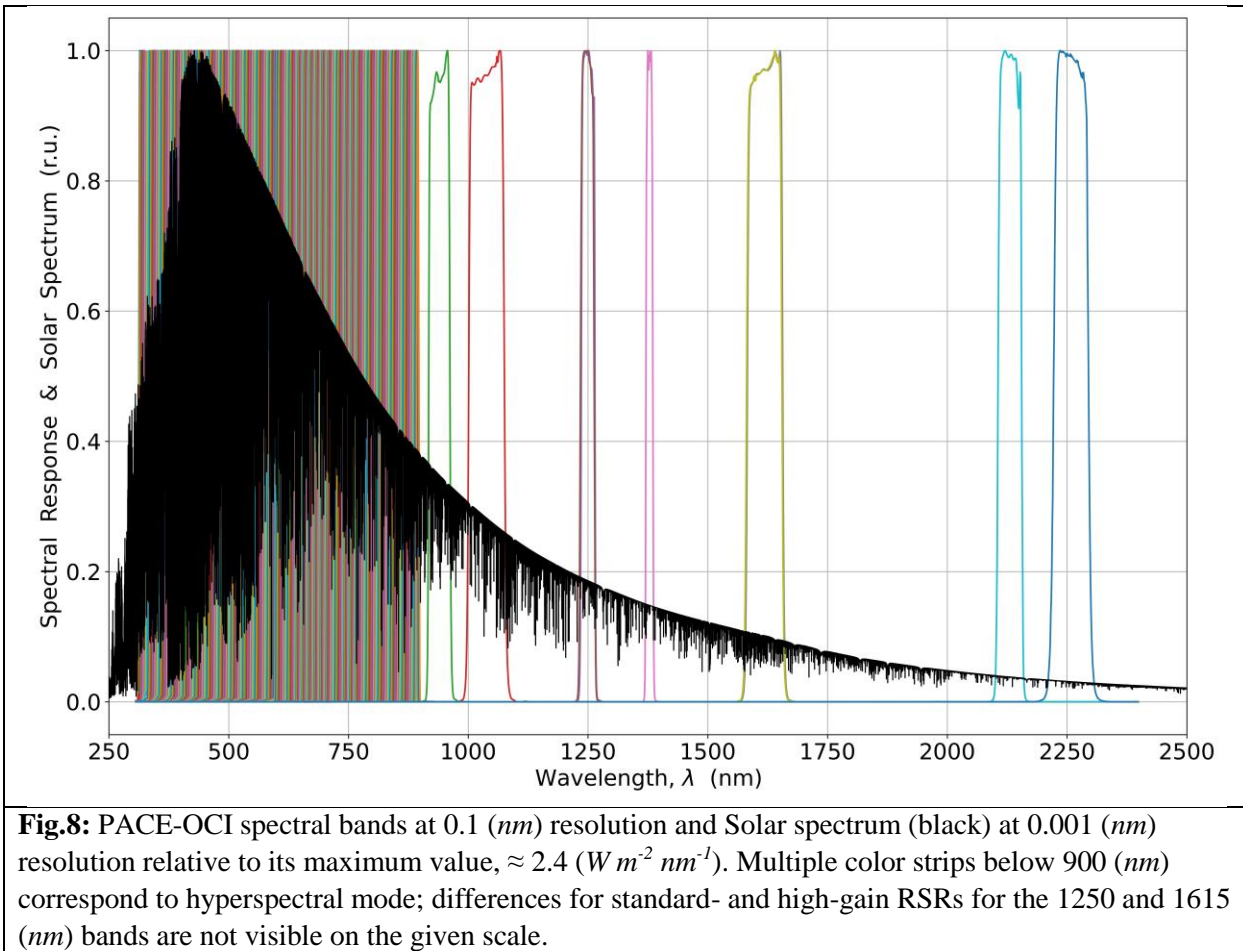
1629 are defined on the same grid of 20926 equidistant points of wavelength beginning at 306 ( $nm$ )  
1630 with 0.1 ( $nm$ ) step. RSRs for 2 sides of the OCI scanning mirror are close, so we take an average  
1631 of the two. In the SWIR group, each of the 1250 ( $nm$ ) and 1615 ( $nm$ ) have standard- and high-  
1632 gain options. We make calculations for both. **Fig.8** shows the OCI bands.

1633 In addition to RSRs, Fig.8 shows the Solar spectral irradiance relevant to its maximum value,  
1634  $\approx 2.4 (W m^{-2} nm^{-1})$ . For that we use a new solar irradiance reference spectrum recently published  
1635 in (Coddington et al, 2023). The solar spectrum is available online<sup>50</sup> for the wavelength spectral  
1636 range from 202 ( $nm$ ) to 2730 ( $nm$ ) with native (unconvolved) spectral resolution 0.001 ( $nm$ ) as  
1637 reported in `hybrid_reference_spectrum_c2022-11-30_with_unc.nc` file, which  
1638 we use in our calculations. **Fig.9** shows signal at TOA: the Solar spectrum is convolved with  
1639 RSRs.

1640 Due to the solar irradiance spectrum and RSRs are defined in the wavelength domain, we  
1641 integrate Eqs. (25) and (26) over  $\lambda$ . It means, however, that we must convert the HITRAN  
1642 absorption optical thickness from wavenumbers to wavelengths and then interpolate from one  
1643 wavelength grid into another. **Fig.10** shows that the constant step  $\Delta v = 0.01 (cm^{-1})$  for the  
1644 HITRAN calculations corresponds step  $\Delta \lambda$  (y-axis) not exceeding 0.001 ( $nm$ ) for  $\lambda < 1000 (nm)$  –  
1645 x-axis. Hence, we will interpolate the Sun, the hyperspectral RSRs, and the 940 ( $nm$ ) SWIR RSR  
1646 from their wavelength grid into that of HITRAN. And vice versa, we interpolate the rest SWIR  
1647 RSRs and the HITRAN atmospheric absorption into the Solar wavelength grid because it is  
1648 denser in that spectral region.

---

<sup>50</sup> [https://lasp.colorado.edu/lisird/data/tsis1\\_hsrsp1nm](https://lasp.colorado.edu/lisird/data/tsis1_hsrsp1nm)

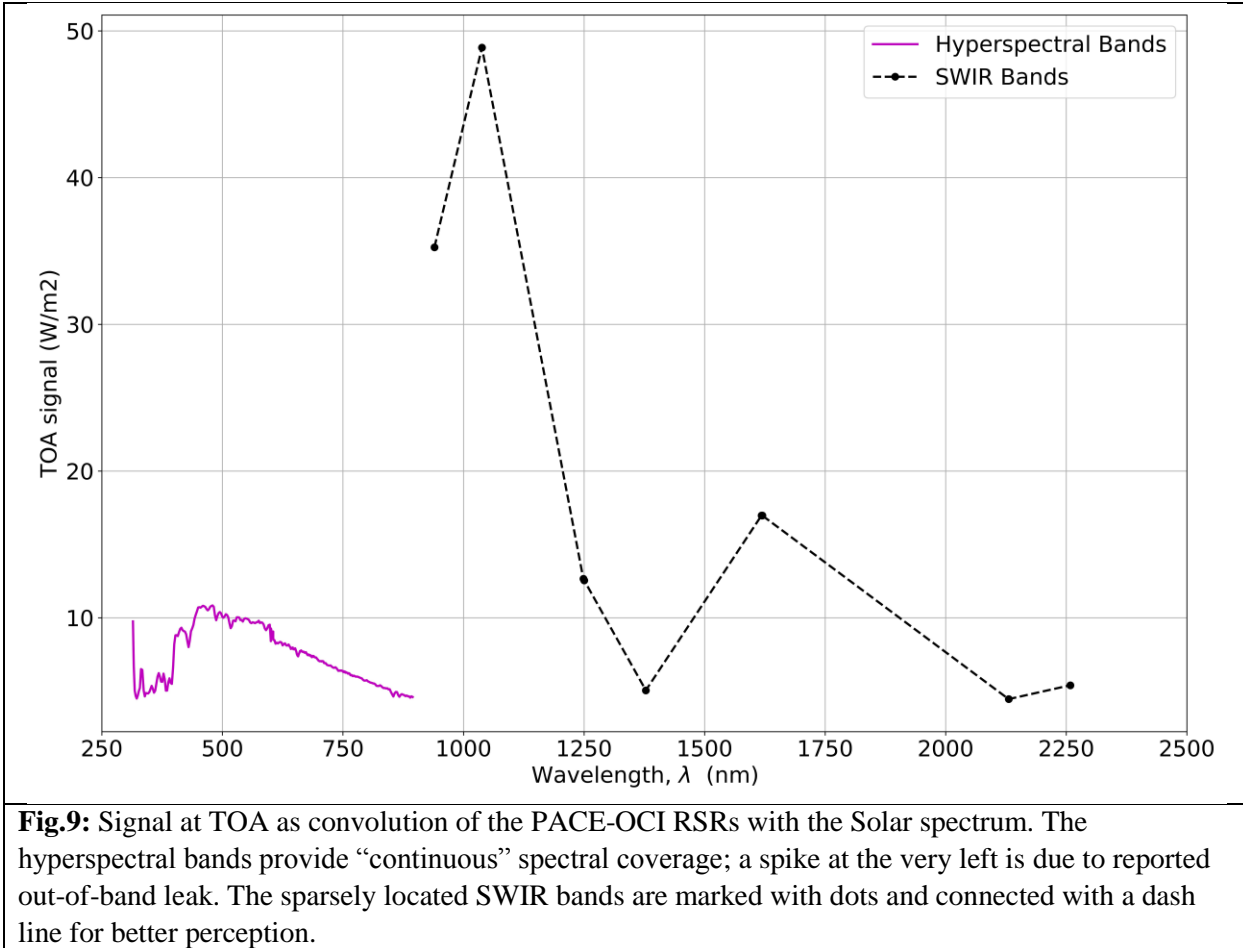


1649

1650 The thick black and thin red lines in Fig.10 correspond to analytical,  $\Delta\lambda \sim \frac{\Delta\nu}{v(\lambda)^2}$ , and finite

1651 difference,  $\Delta\lambda \sim \frac{1}{v} - \frac{1}{v+\Delta\nu}$ , calculations (note, sign is dropped in both).

1652



1653

1654 **Fig.11** shows our graphical results for transmittance at two altitudes, 0 and 8 (km), while a txt  
 1655 file `./benchmarks/Section6p6p2_PACE-OCI_tau_H2O.txt` contains  
 1656 corresponding optical depths for 0, 2, 4, and 8 (km). Columns of the file, left to right, contain  
 1657 band index (unit offset, from 1 to 291 – total number of bands), group number (1 – Blue, 2 –  
 1658 Red, 3 - SWIR), band center in (nm) rounded to two digits after decimal point, and optical  
 1659 thickness at the named altitudes. Recall, the optical thickness is defined from TOA to the given  
 1660 altitude.

1661

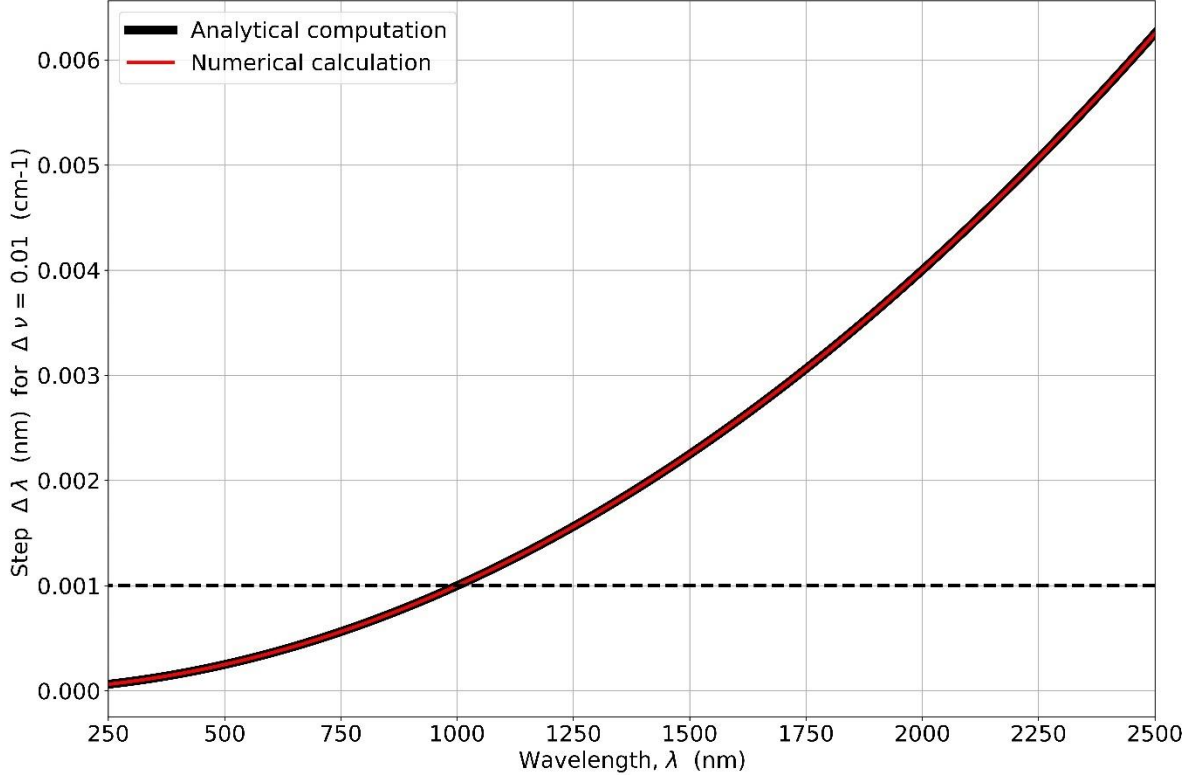


**Fig.10:** Wavelength dependence of size of step  $\Delta\lambda$  (nm) in the wavelength domain for a fixed step  $\Delta\nu = 0.01$  ( $\text{cm}^{-1}$ ) in the wavenumber domain. The figure shows that for the wavelength smaller than 1000 (nm),  $\Delta\nu = 0.01$  ( $\text{cm}^{-1}$ ) corresponds to  $\Delta\lambda < 0.001$  (nm) (horizontal dash line – full resolution of the solar reference spectrum). Two curves correspond to analytical and finite difference relationship between  $\Delta\lambda$  and  $\Delta\nu$ .

1662

1663 An example of the txt file looks like this:

```

1664 # iband, igroup, band center, tau(0km), tau(2km), tau(4km), tau(8km)
1665 116 1 598.26 1.05303e-02 4.18042e-03 1.40864e-03 9.29059e-05
1666 120 2 600.54 4.84732e-03 1.86964e-03 6.13570e-04 3.83326e-05
1667 117 1 600.88 4.31182e-03 1.64476e-03 5.32264e-04 3.24489e-05
1668 121 2 602.92 1.59311e-03 5.94251e-04 1.88954e-04 1.11415e-05
1669 118 1 603.30 1.34245e-03 4.93044e-04 1.53632e-04 8.73815e-06
1670 122 2 605.46 4.50808e-04 1.71362e-04 5.61512e-05 3.54368e-06

```

1671 Note that we sorted the band center wavelengths (3<sup>rd</sup> column) in ascending order which slightly  
 1672 changed the order of the bands (1<sup>st</sup> column) and the group index (2<sup>nd</sup> column) at the  
 1673 wavelengths where “Blue” and “Red” groups overlap.

1674

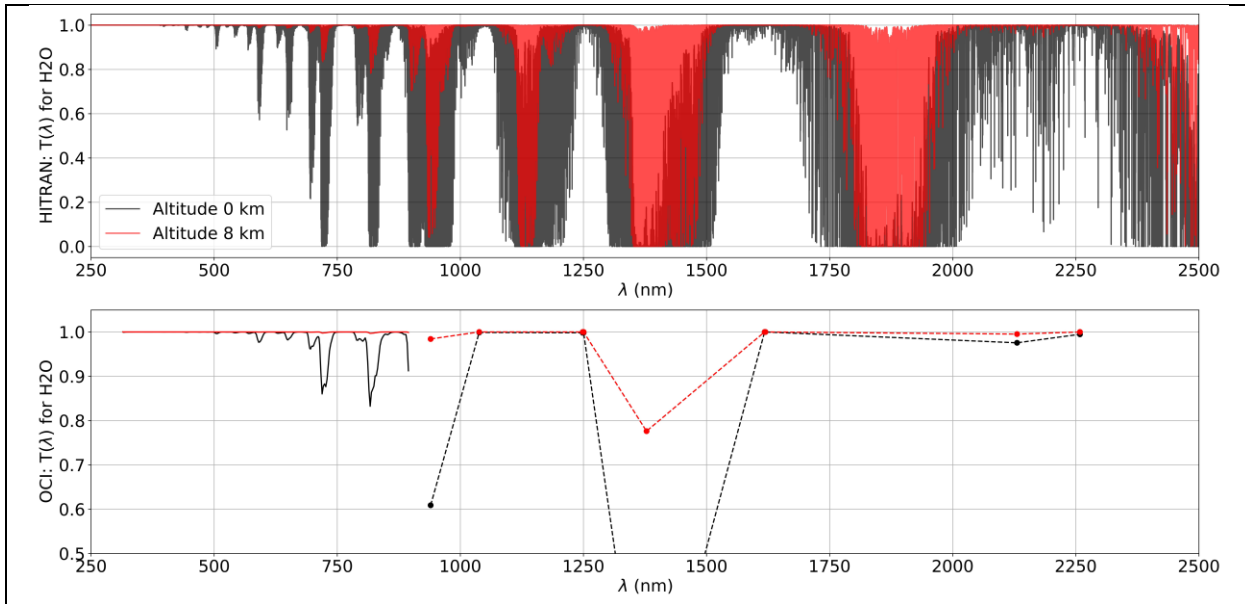


**Fig.11:** Top image: wavelength dependence of HITRAN-2020 transmittance by water vapor in US 1976 Standard atmosphere at  $\Delta v = 0.01 (cm^{-1})$  in the wavenumber domain at two altitudes, 0 (km) and 8 (km), marked in black and red, respectively. Bottom image: wavelength dependence of the same but convolved with OCI RSRs. The OCI band centers were used on the  $x$ -axis. For this reason, results for the SWIR bands are noted with dots and connected with dash lines to simplify visual perception. Bands in the Blue-Red region are sufficiently dense. At 1378 (nm), the transmittance of the total atmospheric column is zero.

1677 Developers of RT codes, including that for atmospheric spectroscopy, as well as users may use  
 1678 the plots and numbers reported here as a reference. We intend to compare these results with  
 1679 continuum absorption optical thickness in our subsequent paper, which will also discuss the  
 1680 continuum-code development process.

## 1681 7. Conclusion

1682 Following our published “A practical guide to writing a radiative transfer code”, this paper  
 1683 explains the development of a code for line-by-line trace gas absorption in Earth atmosphere  
 1684 within the solar reflectance band, 250-2500 (nm). We focus on the code, as opposed to  
 1685 theoretical background or practical applications, thoroughly discussed elsewhere. We start by  
 1686 reading the HITRAN database and simulate absorption by a single spectral line. Then we  
 1687 consider absorption by many lines in a gas cell at a given temperature and pressure. Finally,

1688 using the MODTRAN profiles, we simulate atmospheric absorption at user-defined altitudes.  
1689 This sequence deals with one problem at a time: reading and understanding HITRAN,  
1690 calculation of absorption for fixed thermodynamic conditions in a gas cell (code `gcell`), and  
1691 lastly dealing with atmospheric profiles in the code `aspect`. In terms of the code text, `gcell`  
1692 and `aspect` largely overlap.

1693 Unlike the mentioned “guide to writing a radiative transfer code”, which shows an entire scalar  
1694 plane-parallel RT code, the current paper explains only key parts of each program. All the source  
1695 codes and test data are available from the journal website and from our GitHub repository<sup>51</sup>. The  
1696 sources are carefully commented. In this paper, we pay particular attention to unit testing and  
1697 provide numerical and graphical material for debugging. We believe this detailed explanation  
1698 leads to a thorough understanding of our software. This, in its turn, should simplify the  
1699 completion of the basic tasks (e.g., the replacement for the current HITRAN database with a  
1700 newer version, or vice versa, reproducing results with an older version), moderate modification  
1701 of the code (acceleration of the *Humlíček* convolution algorithm; updating TIPS; adding a new  
1702 molecule or profile; account for the wavenumber shift due to refractive index of air, which  
1703 changes with height, as opposed to the HITRAN's line positions in vacuum), and fundamental  
1704 changes (eventual replacement of the Voigt line shape with the speed-dependent Voigt, or other  
1705 “beyond Voigt” models of line shape). The mentioned changes become necessary when one  
1706 faces the everlasting question: “is this effect important in my case?”. And even if numerical  
1707 simulation proves that no changes are required so far, our approach assures confident  
1708 exploitation of the code over time and smooth transition of knowledge between generations of  
1709 atmospheric scientists.

1710 Both our “practical guide”-papers differ from most scientific papers because they do not present  
1711 new information but rather act as an instructive resource to present necessary but disparate  
1712 materials that are not often discussed together in a practically convenient form of “get to coding  
1713 quickly”. Repeating our “RT guide”, we say here that a real understanding of how software  
1714 applications of a general type of work is, in most cases, truly only attainable by developing your

---

<sup>51</sup> [https://github.com/korkins/aspect\\_gcell](https://github.com/korkins/aspect_gcell)

1715 own. We encourage the reader to use our presented open-source scripts as an example to aid their  
1716 understanding and a basis to develop tools for their own needs, and not merely as a shortcut.

1717 Naturally, this paper and code have many limitations. We have restricted ourselves to absorption  
1718 in spectral lines under conditions typical for the Earth environment – the area of our expertise.  
1719 We take the line parameters from only one database – HITRAN. The main part of the HITRAN  
1720 database simulates the line shape using convolution of the Doppler and Lorentzian contours – the  
1721 Voigt profile. We mentioned above that we didn't go “beyond Voigt”: e.g., the speed  
1722 dependence (affecting the Doppler contour) and line mixing effects (affecting the Lorentzian  
1723 contour) are not considered. We have hard-coded atmospheric profiles from MODTRAN.  
1724 Therefore, our program is not ready for profile retrieval. Most importantly, we do not consider  
1725 spectrally smooth absorption, like water vapor or ozone continuum. Hence, our tools cannot be  
1726 used for ozone correction or in the microwave. We skip collision induced absorption (CIA),  
1727 which seems important for cloud top height retrieval in the oxygen A-band. The number of gas  
1728 species is limited to only the first few from a long HITRAN list.

1729 Each limitation comes for a reason. Due to different theoretical backgrounds and scaling of the  
1730 LBL and continuum-type absorption, e.g., for variations of temperature and pressure, it makes  
1731 little sense to combine LBL and continuum in one program. Parameters for CIA are still not  
1732 included in the “main” HITRAN database but come as separate ones. Same for non-Voigt line  
1733 shapes. In order to partially close the gap in capabilities, we provide a broad list of literature  
1734 references, 185 items, including some from the XIX-th century to give a historical perspective.  
1735 Separate sections of our papers are devoted to the effects that we have dropped and to multiple  
1736 tools for atmospheric spectroscopy that have been developed – many as open source, some with  
1737 tutorial goal in developers' mind. We encourage the reader to study literature focusing on their  
1738 spectral band, as well as the light source (e.g., Sun vs. laser) and figure out what effects are  
1739 important, and what are not so. One common reason for all the limitations was to balance the  
1740 simplicity of our codes with their practical value.

1741 As to the limitations on the list of molecules, we believe our explanation of the source code  
1742 bundled with theoretical background will help potential users to build-in and test any molecule  
1743 from the HITRAN list quickly yet confidently. Our belief is based on the feedback to our  
1744 proposal “The paper-and-code bundle as a new paradigm supporting the TOPS initiative in Earth

1745 Science” (NASA ROSES-22 program element F.15 High Priority Open-Source Science:  
1746 NNH22ZDA001N-HPOSS). Although we received no funding from the program, the  
1747 “selectable” status and overall positive review encouraged us to find extra time and finish this  
1748 work, as proposed, but on a volunteer basis.

## 1749 Acknowledgements

1750 The authors are grateful to Laurence Rothman, Iouli Gordon (Harvard, USA) and the broader  
1751 HITRAN team for the years of work developing and maintaining the data base and associated  
1752 resources. Sergey Korkin and Alexei Lyapustin thank Larry Gordley, Tom Marshall, and the  
1753 GATS Inc. team (USA) for sharing numerical results discussed in Sec. 5.3.2 “Methane band at  
1754 2.3 ( $\mu\text{m}$ )”. Andrew M. Sayer thanks Keith Shine and Jon Elsey (University of Reading, UK) for  
1755 useful discussions which aided our understanding of the history and conventions of line shape  
1756 models, and Luca Lelli (DLR, Germany) for independent verification of some numerical results  
1757 from his implementation of absorption line code. Sergey Korkin, Andrew M. Sayer, and Amir  
1758 Ibrahim are thankful to Bo-Cai Gao (Naval Research Laboratory, USA) for help with  
1759 understanding of the nature of “minor” lines in the oxygen absorption (see arrows in Fig.4a;  
1760 private communication, May 2020).

1761 Sergey Korkin thanks the Richard M. Goody Award Selection Committee for their decision,  
1762 anonymous colleagues for their nomination, and numerous colleagues collaboration with whom  
1763 resulted in the 2016 Award.

## 1764 Authors contribution

1765 SK: original draft and development of codes `gcell` and `aspect`; AMS: critical revision and  
1766 editing of the original draft, numerical validation of intermediate results in `gcell`; AI:  
1767 development of HAPI-based Python code for atmospheric absorption spectroscopy and  
1768 validation of `aspect` results; AL: development of the original SHARM-IPC package, which  
1769 LBL part we have refactored and updated in the current paper; funding acquisition for SK. All:  
1770 review and editing of the manuscript.

1771 **Funding information**

1772 This work received no target funding (see Conclusion: last paragraph). However, the work of S.  
1773 Korkin was partially supported by NASA Atmosphere Observing System (AOS) mission; the  
1774 work of A. Lyapustin and S. Korkin was partially supported by NASA VIIRS, DSCOVR, and  
1775 PACE programs via respective ROSES proposals (PI: A. Lyapustin); the work of A. M. Sayer  
1776 and A. Ibrahim was partially supported by NASA PACE Project Science.

1777 **References**

1778 See separate file.

## References<sup>1</sup>

1. Abrarov S. M. and Quine B. M., "Sampling by incomplete cosine expansion of the sinc function: Application to the Voigt/complex error function", *Applied Mathematics and Computation*, **258**, pp. 425-435, 2015. doi: <https://doi.org/10.1016/j.amc.2015.01.072>
2. Adorf C.S., Ramasubramani V., Anderson J. A., and Glotzer S.C., "How to Professionally Develop Reusable Scientific Software—And When Not To", *Computing in Science & Engineering*, **21** (2), pp. 66-79, 2019. doi: <https://doi.org/10.1109/MCSE.2018.2882355>
3. Amato U., Masiello G., Serio C., and Viggiano M., "The  $\sigma$ -IASI code for the calculation of infrared atmospheric radiance and its derivatives", *Environmental Modelling & Software*, **17** (7), pp. 651–667, **2002**. doi: [https://doi.org/10.1016/S1364-8152\(02\)00027-0](https://doi.org/10.1016/S1364-8152(02)00027-0)
4. Armstrong B.H., "Spectrum line profiles: The Voigt function," *Journal of Quantitative Spectroscopy and Radiative Transfer*, **7** (1), pp. 61-88, 1967. doi: [https://doi.org/10.1016/0022-4073\(67\)90057-X](https://doi.org/10.1016/0022-4073(67)90057-X)
5. Arrhenius S., "On the influence of carbonic acid in the air upon the temperature of the ground", *Philosophical Magazine and Journal of Science*, **41** (251), pp. 237-276, 1896. doi: <https://doi.org/10.1080/14786449608620846>
6. Arrhenius S., "On the influence of carbonic acid in the air upon the temperature of the Earth," *Publications of the Astronomical Society of the Pacific*, **9** (54), pp. 14-24, 1897. <https://www.jstor.org/stable/40670917>
7. Bailey J. and Kedziora-Chudczer L., "Modelling the spectra of planets, brown dwarfs and stars using vstar", *Monthly Notices of the Royal Astronomical Society*, **419** (3), pp. 1913-1929, 2012. doi: <https://doi.org/10.1111/j.1365-2966.2011.19845.x>
8. Baldridge A.M., Hook S.J., Grove C.I., and Rivera G., "The ASTER spectral library version 2.0", *Remote Sensing of Environment*, **113** (4), pp. 711-715, 2009. doi: <https://doi.org/10.1016/j.rse.2008.11.007>
9. Berk A., Conforti P., Kennett R., Perkins T., Hawes F., and van den Bosch J., "MODTRAN® 6: A major upgrade of the MODTRAN® radiative transfer code", *6th Workshop on Hyperspectral Image and Signal Processing: Evolution in Remote Sensing*, pp. 1-4, 2014. doi: <https://doi.org/10.1109/WHISPERS.2014.8077573>
10. Berk A. and Hawes F., "Validation of MODTRAN®6 and its line-by-line algorithm," *Journal of Quantitative Spectroscopy and Radiative Transfer*, **203**, pp. 542-556, 2017. doi: <https://doi.org/10.1016/j.jqsrt.2017.03.004>
11. Berk A., J. van den Bosch J., Hawes F., Perkins T., Conforti P. F., Acharya P.K., Anderson G.P., and Kennett R.G., *MODTRAN 6.0 User's Manual*. Kirtland AFB, NM: Air Force Research Laboratory, 2019.  
link: [https://wiki.harvard.edu/confluence/download/attachments/301915384/MODTRAN 6 User's Manual.pdf](https://wiki.harvard.edu/confluence/download/attachments/301915384/MODTRAN%206%20User's%20Manual.pdf)

<sup>1</sup> We refer to papers with 10+ authors by name of the first author and "Coauthors".

12. Bernath P. F., Steffen J., Crouse J., Boone C.D., Sixteen-year trends in atmospheric trace gases from orbit, *Journal of Quantitative Spectroscopy and Radiative Transfer*, 253, 107178, 2020. doi: <https://doi.org/10.1016/j.jqsrt.2020.107178>
13. Bertaux J.L., Lallement R., Ferron S., Boonne C., and Bodichon R., “TAPAS, a web-based service of atmospheric transmission computation for astronomy”, *Astronomy & Astrophysics*, **564**, A46, 2014. doi: <https://doi.org/10.1051/0004-6361/201322383>
14. Binkley D., Davis M., Lawrie D., and Morrell C., "To camelcase or under\_score", IEEE 17th International Conference on Program Comprehension, Vancouver, BC, Canada, pp. 158-167, 2009. doi: <https://doi.org/10.1109/ICPC.2009.5090039>
15. Bogumil K. and Coauthors, “Measurements of molecular absorption spectra with the SCIAMACHY pre-flight model: instrument characterization and reference data for atmospheric remote-sensing in the 230–2380 nm region”, *Journal of Photochemistry and Photobiology A: Chemistry*, **157** (2–3), pp.167-184, 2003.  
doi: [https://doi.org/10.1016/S1010-6030\(03\)00062-5](https://doi.org/10.1016/S1010-6030(03)00062-5)
16. Bohren C. F., and Clothier E. E., *Fundamentals of Atmospheric Radiation: An Introduction with 400 Problems*, Wiley, 2006.  
doi: <https://onlinelibrary.wiley.com/doi/book/10.1002/9783527618620>
17. Boone C.D., Walker K.A., and Bernath P.F., “Speed-dependent Voigt profile for water vapor in infrared remote sensing applications”, *Journal of Quantitative Spectroscopy and Radiative Transfer*, **105** (3), pp. 525–532, 2007. doi: <https://doi.org/10.1016/j.jqsrt.2006.11.015>
18. Boone C.D., Walker K.A., and Bernath P.F., “An efficient analytical approach for calculating line mixing in atmospheric remote sensing applications”, *Journal of Quantitative Spectroscopy and Radiative Transfer*, **112** (6), pp. 980–989, 2011.  
doi: <https://doi.org/10.1016/j.jqsrt.2010.11.013>
19. Bourassa A.E., Degenstein D.A., and Llewellyn E.J., “SASKTRAN: A spherical geometry radiative transfer code for efficient estimation of limb scattered sunlight”, *Journal of Quantitative Spectroscopy and Radiative Transfer*, **109** (1), pp. 52-73, 2008.  
doi: <https://doi.org/10.1016/j.jqsrt.2007.07.007>
20. Böhlke J. K., de Laeter J. R., De Bièvre P., Hidaka H., Peiser H. S., Rosman K. J. R., and Taylor P. D. P., “Isotopic Compositions of the Elements, 2001”, *Journal of Physical and Chemical Reference Data*, **34** (1), pp. 57 - 67, 2005. doi: <https://doi.org/10.1063/1.1836764>
21. Buehler S.A., Mendrok J., Eriksson P., Perrin A., Larsson R., and Lemke O., “ARTS, the Atmospheric Radiative Transfer Simulator – version 2.2, the planetary toolbox edition”, *Geoscientific Model Development*, **11** (4), pp. 1537-1556, 2018.  
doi: <https://doi.org/10.5194/gmd-11-1537-2018>
22. Burch D.E., “Continuum absorption by H<sub>2</sub>O”, AFGL Technical Report, 1982.  
link: <https://apps.dtic.mil/sti/citations/ADA112264>
23. Carissimo A., De Feis I., and Serio C., “The physical retrieval methodology for IASI: the δ-IASI code”, *Environmental Modelling & Software*, **20** (9), pp. 1111-1126, 2005.  
doi: <https://doi.org/10.1016/j.envsoft.2004.07.003>

24. Chance K. and Kurucz R.L., “An improved high-resolution solar reference spectrum for earth's atmosphere measurements in the ultraviolet, visible, and near infrared”, *Journal of Quantitative Spectroscopy and Radiative Transfer*, **111** (9), pp.1289-1295, 2010.  
doi: <https://doi.org/10.1016/j.jqsrt.2010.01.036>
25. Chapman I.M., Naylor D., Gom B.G., Querel R.R., and Davis-Imhof P., “BTRAM : An Interactive Atmospheric Radiative Transfer Model” in *The 30th Canadian Symposium on Remote Sensing*, pp. 22–25, 2010. link: <https://blueskyspectroscopy.com/>
26. Chen W., Ren T., and Zhao C., “A machine learning based model for gray gas emissivity and absorptivity of H<sub>2</sub>O-CO<sub>2</sub>-CO-N<sub>2</sub> mixtures”, *Journal of Quantitative Spectroscopy and Radiative Transfer*, **312**: 108798, 2024. doi: <https://doi.org/10.1016/j.jqsrt.2023.108798>
27. Chen X. and Coauthors, “First retrieval of absorbing aerosol height over dark target using TROPOMI oxygen B band: Algorithm development and application for surface particulate matter estimates”, *Remote Sensing of Environment*, **265**, 112674, 2021.  
doi: <https://doi.org/10.1016/j.rse.2021.112674>
28. Clough S.A., Kneizys F.X., Rothman L.S., and Gallery W.O., “Atmospheric Spectral Transmittance And Radiance: FASCOD1B”, *Proceedings of SPIE*, **277**, pp. 152–166, 1981.  
doi: <https://doi.org/10.1117/12.931914>
29. Clough S.A., Kneizys F.X., and Davies R.W., “Line shape and the water vapor continuum,” *Atmospheric Research*, **23** (3-4), pp. 229–241, 1989.  
doi: [https://doi.org/10.1016/0169-8095\(89\)90020-3](https://doi.org/10.1016/0169-8095(89)90020-3)
30. Clough S.A., Shephard M.W., Mlawer E.J., Delamere J.S., Iacono M.J., Cady-Pereira K., Boukabara S., and Brown P.D., “Atmospheric radiative transfer modeling: A summary of the AER codes”, *Journal of Quantitative Spectroscopy and Radiative Transfer*, **91** (2), pp. 233–244, 2005. doi: <https://doi.org/10.1016/j.jqsrt.2004.05.058>
31. Coakley J., and Yang P., *Atmospheric Radiation: A Primer with Illustrative Solutions*, Wiley Series in Atmospheric Radiation and Remote Sensing (Ed. A. Kokhanovsky), 2014.  
link: N/A.
32. Coddington O. M., Richard E. C., Harber D., Pilewskie P., Woods T. N., Chance K., Liu X., and Sun K., “The TSIS-1 Hybrid Solar Reference Spectrum”, *Geophysical Research Letters*, **48**, e2020GL091709, 2023. doi: <https://doi.org/10.1029/2020GL091709>
33. Collange S., Daumas M., and Defour D., “Line-by-line spectroscopic simulations on graphics processing units”, *Computer Physics Communications*, **178** (2), pp. 135–143, 2008.  
doi: <https://doi.org/10.1016/j.cpc.2007.08.013>
34. Cornette W.M., Acharya P.K., and Anderson G.P., “Using the MOSART code for atmospheric correction”, *Proceedings of IGARSS '94 - 1994 IEEE International Geoscience and Remote Sensing Symposium*, pp. 215–219, 1994.  
doi: <https://doi.org/10.1109/IGARSS.1994.399084>
35. De Biévre P., Gallet M., Holden N. E., and Barnes I. L., “Isotopic abundances and atomic weights of the elements”, *Journal of Physical and Chemical Reference Data*, **13**, pp. 809 - 891, 1984. doi: <https://doi.org/10.1063/1.555720>

36. Delahaye T. and Coauthors, "The 2020 edition of the GEISA spectroscopic database", *Journal of Molecular Spectroscopy*, **380**, 111510, 2021.  
doi: <https://doi.org/10.1016/j.jms.2021.111510>
37. Dicke R.H., "The effect of collisions upon the Doppler width of spectral lines", *Physical Review*, **89** (2), pp.472-473, 1953. doi: <https://link.aps.org/doi/10.1103/PhysRev.89.472>
38. Diner D. J. and Coauthors, "The Airborne Multiangle SpectroPolarimetric Imager (AirMSPI): a new tool for aerosol and cloud remote sensing", *Atmospheric Measurement Techniques*, **6**, pp. 2007–2025, 2013. doi: <https://doi.org/10.5194/amt-6-2007-2013>
39. Docter N., Preusker R., Filipitsch F., Kritten L., Schmidt F., and Fischer, J., "Aerosol optical depth retrieval from the EarthCARE Multi-Spectral Imager: the M-AOT product", *Atmospheric Measurement Techniques*, **16**, pp. 3437–3457, 2023.  
doi: <https://doi.org/10.5194/amt-16-3437-2023>
40. Domysławska J., Wójtewicz S., Masłowski P., Cygan A., Bielska K., Trawiński R.S., Ciuryło R., and Lisak D., "A new approach to spectral line shapes of the weak oxygen transitions for atmospheric applications", *Journal of Quantitative Spectroscopy and Radiative Transfer*, **169**, pp.111-121, 2016. doi: <https://doi.org/10.1016/j.jqsrt.2015.10.019>
41. Dudhia A., "The Reference Forward Model (RFM)," *Journal of Quantitative Spectroscopy and Radiative Transfer*, **186**, pp. 243–253, 2017.  
doi: <https://doi.org/10.1016/j.jqsrt.2016.06.018>
42. Dubey A., "Good Practices for High-Quality Scientific Computing", *Computing in Science & Engineering*, **24** (6), pp. 72-76, 2022.  
doi: <https://doi.ieeecomputersociety.org/10.1109/MCSE.2023.3259259>
43. Easterbrook S.M. and Johns T.C., "Engineering the Software for Understanding Climate Change", *Computing in Science & Engineering*, **11** (6), pp. 65-74, 2009.  
doi: <https://doi.org/10.1109/MCSE.2009.193>
44. Edwards D.P., "GENLN2: A General Line-by-line Atmospheric Transmittance and Radiance Model. Version 3.0 Description and Users Guide", University Corporation for Atmospheric Research (UCAR) Technical Report, No. NCAR/TN-367+STR, 1992.  
doi: <http://dx.doi.org/10.5065/D6W37T86>
45. Efremenko D., and Kokhanovsky A., *Foundations of Atmospheric Remote Sensing*, Springer, 2021. doi: <https://doi.org/10.1007/978-3-030-66745-0>
46. Elsasser W.M., *Heat transfer by infrared radiation in the atmosphere*, Harvard University Press, Cambridge, 108 pp., 1942. link: <https://archive.org/details/ElsasserFull1942>
47. Emde C. and Coauthors, "The libRadtran software package for radiative transfer calculations (version 2.0.1)", *Geoscientific Model Development*, **9** (5), pp. 1647-1672, 2016.  
doi: <https://doi.org/10.5194/gmd-9-1647-2016>
48. Fels S.B., "Simple strategies for inclusion of Voigt effects in infrared cooling rate calculations", *Applied Optics*, **18** (15), pp. 2634 - 2637, 1979.  
doi: <https://doi.org/10.1364/AO.18.002634>

49. Foote E., “Circumstances Affecting the Heat of the Sun’s Rays”, *American Journal of Art and Science*, 22 (66), pp. 383–384, 1856.  
link: [https://en.wikipedia.org/wiki/Eunice\\_Foote](https://en.wikipedia.org/wiki/Eunice_Foote) (see Section “Scientific Career”)
50. Galatry L., “Simultaneous Effect of Doppler and Foreign Gas Broadening on Spectral Lines”, *Physical Review*, 122 (4), pp. 1218–1223, 1961.  
doi: <https://doi.org/10.1103/PhysRev.122.1218>
51. Gamache R.R. and Coauthors, “Total internal partition sums for 166 isotopologues of 51 molecules important in planetary atmospheres: Application to HITRAN2016 and beyond,” *Journal of Quantitative Spectroscopy and Radiative Transfer*, 203, pp. 70–87, 2017.  
doi: <https://doi.org/10.1016/j.jqsrt.2017.03.045>
52. Gamache R.R., Vispoel B., Rey M., Nikitin A., Tyuterev V., Egorov O., Gordon I.E., and Boudon V., “Total internal partition sums for the HITRAN2020 database”, *Journal of Quantitative Spectroscopy and Radiative Transfer*, 271, 107713, 2021.  
doi: <https://doi.org/10.1016/j.jqsrt.2021.107713>
53. Gao B.-C., Heidebrecht K.B., and Goetz A.F.H., “Derivation of scaled surface reflectances from AVIRIS data”, *Remote Sensing of Environment*, 44 (2-3), pp. 165–178, 1993.  
doi: [https://doi.org/10.1016/0034-4257\(93\)90014-O](https://doi.org/10.1016/0034-4257(93)90014-O)
54. Goldenstein C.S., Miller V.A., Spearin R.M., and Strand C.L., “SpectraPlot.com: Integrated spectroscopic modeling of atomic and molecular gases,” *Journal of Quantitative Spectroscopy and Radiative Transfer*, 200, pp. 249–257, 2017.  
doi: <https://doi.org/10.1016/j.jqsrt.2017.06.007>
55. Goody R.M., and Yung Y.L., *Atmospheric Radiation. Theoretical Basis*. Oxford University Press, 2<sup>nd</sup> Edition, 1989. link: N/A.
56. Gordley L.L., Marshall B.T., and Chu D.A., “Linepak: Algorithms for modeling spectral transmittance and radiance”, *Journal of Quantitative Spectroscopy and Radiative Transfer*, 52 (5), pp. 563–580, 1994. doi: [https://doi.org/10.1016/0022-4073\(94\)90025-6](https://doi.org/10.1016/0022-4073(94)90025-6)
57. Gordon H. R., *Physical Principles of Ocean Color Remote Sensing*, University of Miami, 2019. doi: <https://doi.org/10.33596/ppoocrs-19>
58. Gordon I.E., Rothman L.S., and Toon G. C., “Revision of spectral parameters for the B- and  $\gamma$ -bands of oxygen and their validation against atmospheric spectra”, *Journal of Quantitative Spectroscopy and Radiative Transfer*, 112 (14), pp. 2310–2322, 2011, doi: 10.1016/j.jqsrt.2011.05.007.
59. Gordon I.E., Potterbusch M.R., Bouquin D., Erdmann C.C., Wilzewski J.S., and Rothman L. S., “Are your spectroscopic data being used?”, *Journal of Molecular Spectroscopy*, 327, pp. 232–238, 2016. doi: <https://doi.org/10.1016/j.jms.2016.03.011>
60. Gordon I.E. and Coauthors, “The HITRAN2016 molecular spectroscopic database,” *Journal of Quantitative Spectroscopy and Radiative Transfer*, 203, pp. 3–69, 2017.  
doi: <https://doi.org/10.1016/j.jqsrt.2017.06.038>
61. Gottschling P., *Discovering Modern C++. An Intensive Course for Scientists, Engineers, and Programmers*, 2<sup>nd</sup> Edition, Addison-Wesley Professional, 576 pp. 2021. link: N/A.

62. Greenblatt G. D., Orlando J. J., Burkholder J. B., and Ravishankara A. R., "Absorption measurements of oxygen between 330 and 1140 nm", *Journal of Geophysical Research*, **95**(D11), pp.18577 – 18582, 1990. doi: <https://doi.org/10.1029/JD095iD11p18577>
63. Havemann S., Thelen J.C., Taylor J.P., and Harlow R.C., "The Havemann-Taylor Fast Radiative Transfer Code (HT-FRTC): A multipurpose code based on principal components", *Journal of Quantitative Spectroscopy and Radiative Transfer*, **220**, pp. 180–192, 2018. doi: <https://doi.org/10.1016/j.jqsrt.2018.09.008>
64. He W., Wu K., Feng Y., Fu D., Chen Z., and Li F., "The Radiative Transfer Characteristics of the O<sub>2</sub> Infrared Atmospheric Band in Limb-Viewing Geometry", *Remote Sensing*, **11**(22): 2702, 2019. doi: <https://doi.org/10.3390/rs11222702>
65. Hearn A.G., "The Absorption of Ozone in the Ultra-violet and Visible Regions of the Spectrum", *Proceedings of the Physical Society*, **78** (5), pp. 932-940, 1961. link: <https://iopscience.iop.org/article/10.1088/0370-1328/78/5/340>
66. Heaton D. and Carver J.C., "Claims about the use of software engineering practices in science: A systematic literature review", *Information and Software Technology*, **67**, pp. 207-219, 2015. doi: <https://doi.org/10.1016/j.infsof.2015.07.011>
67. Hinsen K., "Dealing With Software Collapse", *Computing in Science & Engineering*, **21** (3), pp.104-108, 2019. doi: <https://doi.org/10.1109/MCSE.2019.2900945>
68. Hollis M.D.J., Tessenyi M., and Tinetti G., "Tau: A 1D radiative transfer code for transmission spectroscopy of extrasolar planet atmospheres", *Computer Physics Communications*, **184** (10), pp. 2351–2361, 2013. doi: <https://doi.org/10.1016/j.cpc.2013.05.011>
69. Hollis M.D.J., Tessenyi M., and Tinetti G., "TAU: A 1D radiative transfer code for transmission spectroscopy of extrasolar planet atmospheres", *Computer Physics Communications*, **185** (2), p. 695, 2014. doi: <https://doi.org/10.1016/j.cpc.2013.05.011>
70. Hill C., Gordon I.E., Rothman L.S., and Tennyson J., "A new relational database structure and online interface for the HITRAN database", *Journal of Quantitative Spectroscopy and Radiative Transfer*, **130**, pp. 51–61, 2013. doi: <https://doi.org/10.1016/j.jqsrt.2013.04.027>
71. Hill C., Gordon I.E., Kochanov R.V., Barrett L., Wilzewski J.S., and Rothman L.S., "HITRANonline: An online interface and the flexible representation of spectroscopic data in the HITRAN database," *Journal of Quantitative Spectroscopy and Radiative Transfer*, **177**, pp. 4-14, 2016. doi: <https://doi.org/10.1016/j.jqsrt.2015.12.012>
72. Humlíček J., "Optimized computation of the Voigt and complex probability functions," *Journal of Quantitative Spectroscopy and Radiative Transfer*, **27** (4), pp. 437-444, 1982. doi: [https://doi.org/10.1016/0022-4073\(82\)90078-4](https://doi.org/10.1016/0022-4073(82)90078-4)
73. Ibrahim A., Franz B., Ahmad Z., Healy R., Knobelispiesse K., Gao B-C, Proctor C, and Zhai P.-W., "Atmospheric correction for hyperspectral ocean color retrieval with application to the Hyperspectral Imager for the Coastal Ocean (HICO)", *Remote Sensing of Environment*, **204**, pp.60-75, 2018. doi: <https://doi.org/10.1016/j.rse.2017.10.041>

74. Iwabuchi H. and Okamura R., "Multispectral Monte Carlo radiative transfer simulation by the maximum cross-section method", *Journal of Quantitative Spectroscopy and Radiative Transfer*, **193**, pp. 40-46, 2017. doi: <https://doi.org/10.1016/j.jqsrt.2017.01.025>
75. Kanewala U. and Bieman J.M., "Testing scientific software: A systematic literature review", *Information and Software Technology*, **56** (10), pp. 1219-1232, 2014. doi: <https://doi.org/10.1016/j.infsof.2014.05.006>
76. Kendall R., Fisher D., Henderson D., Carver J., Mark A., Post D., Rhoades Jr. C.E., and Squires S., "Development of a Weather Forecasting Code: A Case Study", *IEEE Software*, **25** (4), pp. 59-65, 2008. doi: <https://doi.org/10.1109/MS.2008.86>
77. Karlovets E.V., Mondelain D., Tashkun S.A., and Campargue A., "The absorption spectrum of nitrous oxide between 7250 and 7653 cm<sup>-1</sup>", *Journal of Quantitative Spectroscopy and Radiative Transfer*, **301**, 108511, 2023. doi: <https://doi.org/10.1016/j.jqsrt.2023.108511>
78. Karman T., Koenis M. A. J., Banerjee A., Parker D. H., Gordon I. E., van der Avoird A., van der Zande W. J., and Groenenboom G. C., "O<sub>2</sub>–O<sub>2</sub> and O<sub>2</sub>–N<sub>2</sub> collision-induced absorption mechanisms unravelled", *Nature Chemistry*, **10** (5), pp. 549-554, 2018. doi: <https://doi.org/10.1038/s41557-018-0015-x>
79. Karman T., and Coauthors, "Update of the HITRAN collision-induced absorption section", *Icarus*, **328**, pp.160-175, 2019. doi: <https://doi.org/10.1016/j.icarus.2019.02.034>
80. Key J.R. and Schweiger A.J., "Tools for atmospheric radiative transfer: STREAMER and FLUXNET", *Computers & Geosciences*, **24** (5), pp. 443-451, 1998. doi: [https://doi.org/10.1016/S0098-3004\(97\)00130-1](https://doi.org/10.1016/S0098-3004(97)00130-1)
81. Kistenev Yu.V., Skiba V.E., Prischepa V.V., Vrazhnov D.A., and Borisov A.V., "Super-resolution reconstruction of noisy gas-mixture absorption spectra using deep learning", *Journal of Quantitative Spectroscopy and Radiative Transfer*, 289: 108278, 2022. doi: <https://doi.org/10.1016/j.jqsrt.2022.108278>
82. Kneizys F.X., Shettle E.P., Abreu L.W., Chetwynd J.H., Anderson G.P., Gallery W.O., Selby J.E.A., and Clough S.A., "Users Guide to LOWTRAN 7", Hanscom AFB, MA: Air Force Geophysics Laboratory, 1988. link: <https://apps.dtic.mil/sti/citations/ADA206773>
83. Kneizys F. X. and Coauthors, *The MODTRAN 2/3 Report and LOWTRAN 7 Model*, North Andover, MA, 1996. link: <https://web.gps.caltech.edu/~vijay/pdf/modrept.pdf>
84. Kochanov R.V., Gordon I.E., Rothman L.S., Weislo P., Hill C., and Wilzewski J.S., "HITRAN Application Programming Interface (HAPI): A comprehensive approach to working with spectroscopic data", *Journal of Quantitative Spectroscopy and Radiative Transfer*, **177**, pp. 15-30, 2016. doi: <https://doi.org/10.1016/j.jqsrt.2016.03.005>
85. Kochanov R. V., and Coauthors, "Infrared absorption cross-sections in HITRAN2016 and beyond: Expansion for climate, environment, and atmospheric applications", *Journal of Quantitative Spectroscopy and Radiative Transfer*, **230**, pp. 172-221, 2019. doi: <https://doi.org/10.1016/j.jqsrt.2019.04.001>
86. Korkin S., Sayer A.M., Ibrahim A., and Lyapustin A., "A practical guide to writing a radiative transfer code", *Computer Physics Communications*, **271**, 108198, 2022. doi: <https://doi.org/10.1016/j.cpc.2021.108198>

87. Kuntz M., "A new implementation of the Humlíček algorithm for the calculation of the Voigt profile function", *Journal of Quantitative Spectroscopy and Radiative Transfer*, **57** (60), pp. 819-824, 1997. doi: [https://doi.org/10.1016/S0022-4073\(96\)00162-8](https://doi.org/10.1016/S0022-4073(96)00162-8)
88. Kurucz R.L., "Synthetic infrared spectra", *Infrared Solar Physics*, IAU Symp. **154**, edited by D.M. Rabin and J.T. Jefferies, Kluwer, Acad., Norwell Massachusetts, 1992.  
link: <https://adsabs.harvard.edu/full/1994IAUS..154..523K>
89. Kurucz R.L., "The solar irradiance by computation", (unpublished) 1997.  
link: <http://kurucz.harvard.edu/sun/irradiance/solarirr.tab>
90. Laraia A.L., Gamache R.R., Lamouroux J., Gordon I.E., and Rothman L.S., "Total internal partition sums to support planetary remote sensing", *Icarus*, **215** (1), pp. 391-400, 2011.  
doi: <https://doi.org/10.1016/j.icarus.2011.06.004>
91. Laszlo I., Stamnes K., Wiscombe W., and Tsay S.-C., "The Discrete Ordinate Algorithm, DISORT for Radiative Transfer," in *Light Scattering Reviews*, Springer., A. A. Kokhanovsky, Ed. Berlin, 2016, pp. 3–65. doi: [https://doi.org/10.1007/978-3-662-49538-4\\_1](https://doi.org/10.1007/978-3-662-49538-4_1)
92. LeVeque R.J., Mitchell I.M., and Stodden V., "Reproducible research for scientific computing: Tools and strategies for changing the culture", *Computing in Science & Engineering*, **14** (4), pp. 13-17, 2012. doi: <https://doi.org/10.1109/MCSE.2012.38>
93. Liou K. N., *An Introduction to Atmospheric Radiation* (2<sup>nd</sup> Ed.), Academic Press, 2002.  
link: <https://shop.elsevier.com/books/an-introduction-to-atmospheric-radiation/liou/978-0-12-451451-5>
94. Liu X., Yang Q., Li H., Jin Z., Wu W., Kizer S., Zhou D.K., and Yang P., "Development of a fast and accurate PCRTM radiative transfer model in the solar spectral region", *Applied Optics*, **55** (29), pp. 8236-8247, 2016. doi: <https://doi.org/10.1364/AO.55.008236>
95. Lyapustin A.I., "Interpolation and Profile Correction (IPC) Method for Shortwave Radiative Transfer in Spectral Intervals of Gaseous Absorption," *Journal of the Atmospheric Sciences*, **60** (6), pp. 865–871, 2003.  
doi: [https://doi.org/10.1175/1520-0469\(2003\)060%3C0865:IAPCIM%3E2.0.CO;2](https://doi.org/10.1175/1520-0469(2003)060%3C0865:IAPCIM%3E2.0.CO;2)
96. Lyapustin A., Muldashev T., and Wang Y., "Code SHARM: fast and accurate radiative transfer over spatially variable anisotropic surfaces," in *Light Scattering Reviews 5. Single light scattering and radiative transfer* (A. Kokhanovsky, Ed.), Chichester, UK: Springer, 2010, pp. 205–247. doi: [https://doi.org/10.1007/978-3-642-10336-0\\_6](https://doi.org/10.1007/978-3-642-10336-0_6)
97. Luther F. M., Ellingson R. G., Fouquart Y., Fels S., Scott N. A., and Wiscombe W. J., "Intercomparison of Radiation Codes in Climate Models (ICRCCM): Longwave Clear-Sky Results – A Workshop Summary", *Bulletin of the American Meteorological Society*, **69**, pp. 40 – 48, 1988. doi: <https://doi.org/10.1175/1520-0477-69.1.40>
98. McClatchey R.A., Benedict W.S., Clough S.A., Burch D.E., Calfee R.F., Fox K., Rothman L.S., and Garing J.S., "AFCRL Atmospheric Absorption Line Parameters Compilation", Air Force Cambridge Research Laboratories, Bedford MA, 1973.  
link: [https://modis-images.gsfc.nasa.gov/JavaHAWKS/AFCRL\\_AALPC.pdf](https://modis-images.gsfc.nasa.gov/JavaHAWKS/AFCRL_AALPC.pdf)
99. McLean A. B., Mitchell C. E. J., and Swanston D. M., "Implementation of an efficient analytical approximation to the Voigt function for photoemission lineshape analysis",

*Journal of Electron Spectroscopy and Related Phenomena*, **69** (2), pp. 125–132, 1994.  
doi: [https://doi.org/10.1016/0368-2048\(94\)02189-7](https://doi.org/10.1016/0368-2048(94)02189-7)

100. Mlawer E.J., Taubman S.J., Brown P.D., Iacono M.J., and Clough S.A., “Radiative transfer for inhomogeneous atmospheres: RRTM, a validated correlated- $k$  model for the longwave,” *Journal of Geophysical Research: Atmospheres*, **102** (D14), pp. 16663–16682, 1997.  
doi: <https://doi.org/10.1029/97JD00237>
101. Mlawer E.J., Payne V.H., Moncet J.L., Delamere J.S., Alvarado M.J., and Tobin D.C., “Development and recent evaluation of the MT-CKD model of continuum absorption”, *Philosophical Transactions of the Royal Society A*, **370**, pp. 2520–2556, 2012.  
doi: <https://doi.org/10.1098/rsta.2011.0295>
102. Mlawer E.J., Cady-Pereira K.E., Mascio J., and Gordon I.E., “The inclusion of the MT\_CKD water vapor continuum model in the HITRAN molecular spectroscopic database”, *Journal of Quantitative Spectroscopy and Radiative Transfer*, **306**, 108645, 2023.  
doi: <https://doi.org/10.1029/97JD00237>
103. Mobley C. D. (Editor), *The Oceanic Optics Book*, International Ocean Colour Coordinating Group (IOCCG), Dartmouth, NS, Canada, 924 pp., 2022.  
doi: <http://dx.doi.org/10.25607/OPB-1710>
104. Mohankumar N. and Sen S., “On the very accurate evaluation of the Voigt functions,” *Journal of Quantitative Spectroscopy and Radiative Transfer*, **224**, pp. 192–196, 2019.  
doi: <https://doi.org/10.1016/j.jqsrt.2018.11.022>
105. Müller H.S.P., Schlöder F., Stutzki J., and Winnewisser G., “The Cologne Database for Molecular Spectroscopy, CDMS: a useful tool for astronomers and spectroscopists”, *Journal of Molecular Structure*, **742** (1-3), pp. 215–227, 2005.  
doi: <https://doi.org/10.1016/j.molstruc.2005.01.027>
106. Natraj V., Spurr R. J. D., Boesch H., Jiang Y., and Yung Y. L., “Evaluation of errors from neglecting polarization in the forward modeling of O<sub>2</sub> A band measurements from space, with relevance to CO<sub>2</sub> column retrieval from polarization-sensitive instruments”, *Journal of Quantitative Spectroscopy and Radiative Transfer*, **103** (2), pp. 245–259, 2007,  
doi: 10.1016/j.jqsrt.2006.02.073.
107. Ngo N. H., Lisak D., Tran H., and Hartmann J. M., “An isolated line-shape model to go beyond the Voigt profile in spectroscopic databases and radiative transfer codes”, *Journal of Quantitative Spectroscopy and Radiative Transfer*, **129**, pp. 89–100, 2013.  
doi: <https://doi.org/10.1016/j.jqsrt.2013.05.034>
108. Ngo N. H., Lisak D., Tran H., and Hartmann J. M., “Erratum to ‘An isolated line-shape model to go beyond the Voigt profile in spectroscopic databases and radiative transfer codes’ [J. Quant. Spectrosc. Radiat. Transf. 129 (2013) 89–100]”, *Journal of Quantitative Spectroscopy and Radiative Transfer*, **134**, p. 105, 2014.  
doi: <http://dx.doi.org/10.1016/j.jqsrt.2013.10.016>
109. Nordebo S., “Uniform error bounds for fast calculation of approximate Voigt profiles” *Journal of Quantitative Spectroscopy and Radiative Transfer*, **270**, 107715, 2021.  
doi: <https://doi.org/10.1016/j.jqsrt.2021.107715>

110. Nowlan C. R., McElroy C. T., and Drummond J. R., “Measurements of the O<sub>2</sub>A - and B-bands for determining temperature and pressure profiles from ACE-MAESTRO: Forward model and retrieval algorithm”, *Journal of Quantitative Spectroscopy and Radiative Transfer*, **108** (3), pp. 371–388, 2007. doi: <https://doi.org/10.1016/j.jqsrt.2007.06.006>
111. Oliveira S., and Stewart D., *Writing Scientific Software: A Guide to Good Style*, Cambridge University Press, New York, 303 pp., 2006.
112. Orphal J., and Coauthors, “Absorption cross-sections of ozone in the ultraviolet and visible spectral regions: Status report 2015”, *Journal of Molecular Spectroscopy*, **327**, pp. 105-121, 2016. doi: <http://dx.doi.org/10.1016/j.jms.2016.07.007>
113. Pannier E. and Laux C.O., “RADIS: A nonequilibrium line-by-line radiative code for CO<sub>2</sub> and HITRAN-like database species”, *Journal of Quantitative Spectroscopy and Radiative Transfer*, **222–223**, pp. 12–25, 2019.  
doi: <https://doi.org/10.1016/j.jqsrt.2018.09.027>
114. Payne V.H. and Coauthors, “Absorption coefficient (ABSCO) tables for the Orbiting Carbon Observatories: Version 5.1”, *Journal of Quantitative Spectroscopy and Radiative Transfer*, **255**, 2020. doi: <https://doi.org/10.1016/j.jqsrt.2020.107217>
115. Petty G. W., *A First Course in Atmospheric Radiation* (2<sup>nd</sup> ed.), Sundog Publishing, Madison, Wisconsin, 2006. Link: N/A.
116. Pfeilsticker K., Erle F., Funk O., Veitel H., and Platt U., “First geometrical pathlengths probability density function derivation of the skylight from spectroscopically highly resolving oxygen A-band observations: 1. Measurement technique, atmospheric observations and model calculations”, *Journal of Geophysical Research: Atmospheres*, **103** (D10), pp. 11483–11504, 1998. doi: <https://doi.org/10.1029/98JD00725>
117. Pickett H.M., Poynter R.L., Cohen E.A., Delitsky M.L., Pearson J.C., and Muller H.S.P., “Submillimeter, millimeter, and microwave spectral line catalog”, *Journal of Quantitative Spectroscopy and Radiative Transfer*, **60** (5), pp. 883–890, 1998.  
doi: [https://doi.org/10.1016/S0022-4073\(98\)00091-0](https://doi.org/10.1016/S0022-4073(98)00091-0)
118. Pincus R. and Coauthors, “Benchmark calculations of radiative forcing by greenhouse gases”, *Journal of Geophysical Research*, **125**: e2020JD033483, 2020.  
doi: <https://doi.org/10.1029/2020JD033483>
119. Pipitone J. and Easterbrook S., “Assessing climate model software quality: a defect density analysis of three models”, *Geoscientific Model Development*, **5**, 1009–1022, 2012.  
doi: <https://doi.org/10.5194/gmd-5-1009-2012>
120. Pliutau D. and Roslyakov K., “Bytran - |- spectral calculations for portable devices using the HITRAN database”, *Earth Science Informatics*, **10**, pp. 395–404, 2017.  
doi: <https://doi.org/10.1007/s12145-017-0288-4>
121. Pouillet C., “Memoir on the solar heat, on the radiating and absorbing powers of atmospheric air, and on the temperature of space”, in *Scientific Memoirs, Selected from the Transactions of Foreign Academies of Science and Learned Societies, and from Foreign Journals* (Taylor R., Editor), London, England: Richard and John E. Taylor, pp.44-90, 1846.  
link: [https://en.wikipedia.org/wiki/Claude\\_Pouillet](https://en.wikipedia.org/wiki/Claude_Pouillet) (see Ref. 6: English translation for pdf)

122. Predoi-Cross A., Hambrook K., Keller R., Povey C., Schofield I., HurtmansD., Over H., and Mellau G. Ch., “Spectroscopic lineshape study of the self-perturbed oxygen A-band”, *Journal of Molecular Spectroscopy*, **248** (2), pp. 85–110, 2008.  
doi: <https://doi.org/10.1016/j.jms.2007.11.007>
123. Press W.H., Teukolsky S.A., Vettering W.T., and Flannery B.P , *Numerical Recipes in C: the Art of Scientific Computing*, Cambridge University Press, New York, 1992.  
link: link: <https://numerical.recipes/>
124. Press W.H., Teukolsky S.A., Vettering W.T., and Flannery B.P , *Numerical Recipes. The Art of Scientific Computing*, Cambridge University Press, New York, 2007.  
link: <https://numerical.recipes/>
125. Prischepa V.V., Skiba V.E., Vrazhnov D.A., Kistenev Yu. V., “Gas mixtures IR absorption spectra decomposition using a deep neural network”, *Journal of Quantitative Spectroscopy and Radiative Transfer*, **301**: 108521, 2023.  
doi: <https://doi.org/10.1016/j.jqsrt.2023.108521>
126. Puthukkudy A., Martins J. V., Remer L. A., Xu X., Dubovik O., Litvinov P., McBride B., Burton S., and Barbosa H. M. J., “Retrieval of aerosol properties from Airborne Hyper-Angular Rainbow Polarimeter (AirHARP) observations during ACEPOL 2017”, *Atmospheric Measurement Techniques*, **13**, 5207–5236, 2020.  
doi: <https://doi.org/10.5194/amt-13-5207-2020>
127. Rautian S. G., and Sobel'man I. I., “The effect of collisions on the Doppler broadening of spectral lines”, *Soviet Physics Uspekhi*, **9** (5), pp.701-716, 1967.  
doi: <https://dx.doi.org/10.1070/PU1967v009n05ABEH003212>
128. Richard C., and Coauthors, “New section of the HITRAN database: Collision-induced absorption (CIA)”, *Journal of Quantitative Spectroscopy and Radiative Transfer*, **113** (11), pp. 1276-1285, 2012. doi: <https://doi.org/10.1016/j.jqsrt.2011.11.004>
129. Rothman L.S., “Update of the AFGL atmospheric absorption line parameters compilation”, *Applied Optics*, **17** (22), pp. 3517–3518, 1978. doi: <https://doi.org/10.1364/AO.17.003517>
130. Rothman L.S. and Coauthors, “The HITRAN database: 1986 edition”, *Applied Optics*, **26** (19), pp. 4058–4097, 1987. doi: <https://doi.org/10.1364/AO.26.004058>
131. Rothman L.S. and Coauthors, “The HITRAN molecular spectroscopic database and HAWKS (HITRAN atmospheric workstation): 1996 edition”, *Journal of Quantitative Spectroscopy and Radiative Transfer*, **60** (5), pp. 665-710, 1998.  
doi: [https://doi.org/10.1016/S0022-4073\(98\)00078-8](https://doi.org/10.1016/S0022-4073(98)00078-8)
132. Rothman L.S. and Coauthors, “The HITRAN molecular spectroscopic database: edition of 2000 including updates through 2001”, *Journal of Quantitative Spectroscopy and Radiative Transfer*, **82** (1-4), pp. 5–44, 2003.  
doi: [https://doi.org/10.1016/S0022-4073\(03\)00146-8](https://doi.org/10.1016/S0022-4073(03)00146-8)
133. Rothman L.S. and Coauthors, “The HITRAN 2004 molecular spectroscopic database”, *Journal of Quantitative Spectroscopy and Radiative Transfer*, **96** (2), pp. 139–204, 2005.  
doi: <https://doi.org/10.1016/j.jqsrt.2004.10.008>

134. Rothman L.S., Jacquinet-Husson N., Boulet C., and Perrin A. M., "History and future of the molecular spectroscopic databases", *Comptes Rendus Physique*, **6**(8), pp.897-907, 2005. doi: <https://doi.org/10.1016/j.crhy.2005.09.001>
135. Rothman L.S. and Coauthors, "The HITRAN 2008 molecular spectroscopic database," *Journal of Quantitative Spectroscopy and Radiative Transfer*, **110** (9–10), pp. 533–572, 2009. doi: <https://doi.org/10.1016/j.jqsrt.2009.02.013>
136. Rothman L.S., "The evolution and impact of the HITRAN molecular spectroscopic database", *Journal of Quantitative Spectroscopy and Radiative Transfer*, **111** (11), pp. 1565–1567, 2010. doi: <https://doi.org/10.1016/j.jqsrt.2010.01.027>
137. Rothman L.S., and Coauthors, "The HITRAN2012 molecular spectroscopic database", *Journal of Quantitative Spectroscopy and Radiative Transfer*, **130**, pp. 4-50. doi: <http://dx.doi.org/10.1016/j.jqsrt.2013.07.002>
138. Rothman L.S., "History of the HITRAN Database", *Nature Reviews Physics*, **3** (5), pp. 302–304, 2021. doi: <https://doi.org/10.1038/s42254-021-00309-2>
139. Rozanov V.V., Rozanov A.V., Kokhanovsky A.A., and Burrows J.P., "Radiative transfer through terrestrial atmosphere and ocean : Software package SCIATRAN," *Journal of Quantitative Spectroscopy and Radiative Transfer*, **133**, pp. 13–71, 2014 doi: <https://doi.org/10.1016/j.jqsrt.2013.07.004>
140. Ruyten W., "Comment on 'A new implementation of the Humlíček algorithm for the calculation of the Voigt profile function' by M. Kuntz [JQSRT 57(6) (1997) 819–824]", *Journal of Quantitative Spectroscopy and Radiative Transfer*, **86** (2), pp. 231-233, 2004. doi: <https://doi.org/10.1016/j.jqsrt.2003.12.027>
141. Sanders R. and Kelly D., "Dealing with Risk in Scientific Software Development", *IEEE Software*, **25** (4), pp. 21-28, 2008. doi: <https://doi.org/10.1109/MS.2008.84>
142. Sayer A.M., Lelli L., Cairns B., van Diedenhoven B., Ibrahim A., Knobelspiesse K.D., Korkin S., and Werdell P.J., "The CHROMA cloud-top pressure retrieval algorithm for the Plankton, Aerosol, Cloud, ocean Ecosystem (PACE) satellite mission", *Atmospheric Measurement Techniques*, **16** (4), pp.969-996, 2023. doi: <https://doi.org/10.5194/amt-16-969-2023>
143. Saunders R., Matricardi M., and Brunel P., "An improved fast radiative transfer model for assimilation of satellite radiance observations", *Quarterly Journal of Royal Meteorological Society*, **125** (556), pp. 1407-1425, 1999. doi: <https://doi.org/10.1002/qj.1999.49712555615>
144. Segal J. and Morris C., "Developing Scientific Software", *IEEE Software*, **25** (4), pp. 18-20, 2008. doi: <https://doi.ieeecomputersociety.org/10.1109/MS.2008.85>
145. Schreier F., "The Voigt and complex error function: A comparison of computational methods", *Journal of Quantitative Spectroscopy and Radiative Transfer*, **48** (5), pp. 743-762, 1992. doi: [https://doi.org/10.1016/0022-4073\(92\)90139-U](https://doi.org/10.1016/0022-4073(92)90139-U)
146. Schreier F. and Schimpf B., "A New Efficient Line-By-Line Code for High Resolution Atmospheric Radiation Computations incl. Derivatives", IRS 2000: Current Problems in

- Atmospheric Radiation, A. Deepak Publishing, pp.381-385, 2001.  
link: <https://www.gbv.de/dms/goettingen/333853989.pdf>
147. Schreier F. and Böttger U., “MIRART, a line-by-line code for infrared atmospheric radiation computations incl. derivatives”, *Atmospheric and Oceanic Optics*, **16** (3), pp. 262–268, 2003. link: <https://ao.iao.ru/en/content/vol.16-2003/iss.03>
148. Schreier F., Gimeno García S., Hedelt P., Hess M., Mendrok J., Vasquez M., and Xu J., “GARLIC - A general purpose atmospheric radiative transfer line-by-line infrared-microwave code: Implementation and evaluation”, *Journal of Quantitative Spectroscopy and Radiative Transfer*, **137**, pp. 29–50, 2014. doi: <https://doi.org/10.1016/j.jqsrt.2013.11.018>
149. Schreier F., “Computational aspects of speed-dependent Voigt profiles”, *Journal of Quantitative Spectroscopy and Radiative Transfer*, **187**, pp. 44–53, 2017.  
doi: <https://doi.org/10.1016/j.jqsrt.2016.08.009>
150. Schreier F., “The Voigt and complex error function: Humlíček’s rational approximation generalized”, *Monthly Notices of the Royal Astronomical Society*, **479** (3), pp. 3068–3075, 2018(a). doi: <https://doi.org/10.1093/mnras/sty1680>
151. Schreier F., “Comments on the Voigt function implementation in the Astropy and SpectraPlot.com packages”, *Journal of Quantitative Spectroscopy and Radiative Transfer*, **213**, pp. 13–16, 2018(b). doi: <https://doi.org/10.1016/j.jqsrt.2018.03.019>
152. Schreier F., Gimeno García S., Hochstafel P., and Städter S., “Py4CAtS—PYthon for Computational ATmospheric Spectroscopy”, *Atmosphere*, **10** (5), 262, 2019.  
doi: <https://doi.org/10.3390/atmos10050262>
153. Schreier F. and Hochstafel P., “Computational aspects of speed-dependent Voigt and Rautian profiles”, *Journal of Quantitative Spectroscopy and Radiative Transfer*, **258**, 107385, 2021. doi: <https://doi.org/10.1016/j.jqsrt.2020.107385>
154. Scott N.A. and Chedin A., “A Fast Line-by-Line Method for Atmospheric Absorption Computations: The Automatized Atmospheric Absorption Atlas”, *Journal of Applied Meteorology and Climatology*, 20 (7), pp. 802–812, 1981.  
doi: [https://doi.org/10.1175/1520-0450\(1981\)020%3C0802:AFLBLM%3E2.0.CO;2](https://doi.org/10.1175/1520-0450(1981)020%3C0802:AFLBLM%3E2.0.CO;2)
155. Shine K. P., Ptashnik I.V., and Rädel G., “The water vapour continuum: brief history and recent developments”, *Surveys in Geophysics*, **33**, pp. 535 – 555, 2012.  
doi: <https://doi.org/10.1007/s10712-011-9170-y>
156. Smette A. and Coauthors, “Molecfit: A general tool for telluric absorption correction”, *Astronomy & Astrophysics*, **576**, A77, 2015.  
doi: <https://doi.org/10.1051/0004-6361/201423932>
157. Spänkuch D., “Effects of line shapes and line coupling on the atmospheric transmittance,” *Atmospheric Research*, **23**(3), pp. 323–344, 1989.  
doi: [https://doi.org/10.1016/0169-8095\(89\)90024-0](https://doi.org/10.1016/0169-8095(89)90024-0)
158. Stam D. M., de Haan J. F., Hovenier J. W., and Stammes P., “A fast method for simulating observations of polarized light emerging from the atmosphere applied to the oxygen-A band”, *Journal of Quantitative Spectroscopy and Radiative Transfer*, **64** (2), pp. 131–149, 2000. doi: [https://doi.org/10.1016/S0022-4073\(99\)00009-6](https://doi.org/10.1016/S0022-4073(99)00009-6)

159. Stamnes K., Tsay S.-C., Wiscombe W., and Jayaweera K., “Numerically stable algorithm for discrete-ordinate-method radiative transfer in multiple scattering and emitting layered media”, *Applied Optics*, **27** (12), pp. 2502–2509, 1988.  
doi: <https://doi.org/10.1364/AO.27.002502>
160. Stamnes K., Thomas G. E., and Stamnes J. J., *Radiative Transfer in the Atmosphere and Ocean* (2<sup>nd</sup> Ed.), Cambridge University Press, 2017.  
doi: <https://doi.org/10.1017/9781316148549>
161. Stiller G.P., von Clarmann T., Funke B., Glatthor N., Hase F., Höpfner M., and Linden A., “Sensitivity of trace gas abundances retrievals from infrared limb emission spectra to simplifying approximations in radiative transfer modelling”, *Journal of Quantitative Spectroscopy and Radiative Transfer*, **72** (3), pp. 249–280, 2001.  
doi: [https://doi.org/10.1016/S0022-4073\(01\)00123-6](https://doi.org/10.1016/S0022-4073(01)00123-6)
162. Storer T., “Bridging the Chasm: A Survey of Software Engineering Practice in Scientific Programming”, *ACM Computing Surveys*, 50(4), 47, pp.1-32, 2017.  
doi: <https://doi.org/10.1145/3084225>
163. Tennyson J. and Coauthors, “Recommended isolated-line profile for representing high-resolution spectroscopic transitions (IUPAC technical report)”, *Pure and Applied Chemistry*, **86** (12), pp. 1931–1943, 2014. doi: <https://doi.org/10.1515/pac-2014-0208>
164. Thompson D.R., Gao B.-C., Green R.O., Roberts D.A., Dennison P.E., and Lundein S.R., “Atmospheric correction for global mapping spectroscopy: ATREM advances for the HypsIRI preparatory campaign”, *Remote Sensing of Environment*, **167**, pp. 64–77, 2015.  
doi: <https://doi.org/10.1016/j.rse.2015.02.010>
165. Thorpe A. K., Roberts D.A., Bradley E.S., Funk C.C., Dennison P.E., and Leifer I., “High resolution mapping of methane emissions from marine and terrestrial sources using a Cluster-Tuned Matched Filter technique and imaging spectrometry”, *Remote Sensing of Environment*, **134**, pp. 305-318, 2013. doi: <https://doi.org/10.1016/j.rse.2013.03.018>
166. Tonkov M. V., Filippov N. N., Timofeyev Yu. M., and Polyakov A.V., “A simple model of the line mixing effect for atmospheric applications: Theoretical background and comparison with experimental profiles”, *Journal of Quantitative Spectroscopy and Radiative Transfer*, **56** (5), pp.783-795, 1996. doi: [https://doi.org/10.1016/S0022-4073\(96\)00113-6](https://doi.org/10.1016/S0022-4073(96)00113-6)
167. Tran H., Boulet C., and Hartmann J.-M., “Line mixing and collision-induced absorption by oxygen in the A band: Laboratory measurements, model, and tools for atmospheric spectra computations”, *Journal of Geophysical Research*, **111**, D15210, 2006.  
doi: <https://doi.org/10.1029/2005JD006869>
168. Tran H. and Hartmann J.-M., “An improved O<sub>2</sub> A band absorption model and its consequences for retrievals of photon paths and surface pressures”, *Journal of Geophysical Research*, **113**, D18104, 2008. doi: <https://doi.org/10.1029/2008JD010011>
169. Tran H., Ngo N.H., and Hartmann J.-M., “Efficient computation of some speed-dependent isolated line profiles”, *Journal of Quantitative Spectroscopy and Radiative Transfer*, **129**, pp. 199–203, 2013, doi: <https://doi.org/10.1016/j.jqsrt.2013.06.015>
170. Tran H., Ngo N.H., Hartmann J.-M., “Erratum to “Efficient computation of some speed-dependent isolated line profiles” [J. Quant. Spectrosc. Radiat. Transfer 129 (2013) 199–

- 203]”, *Journal of Quantitative Spectroscopy and Radiative Transfer*, **134**, p.104, 2014.  
doi: <https://doi.org/10.1016/j.jqsrt.2013.10.015>
171. Turner E., Rayer P., and Saunders R., “AMSLTRAN: A microwave transmittance code for satellite remote sensing”, *Journal of Quantitative Spectroscopy and Radiative Transfer*, **227**, pp. 117–129, 2019. doi: <https://doi.org/10.1016/j.jqsrt.2019.02.013>
172. Tyndall J., “Note on the transmission of radiant heat through gaseous bodies”, *Proceedings of the Royal Society of London*, **10**, pp. 37-39, 1860.  
doi: <https://doi.org/10.1098/rspl.1859.0017>
173. Urban J., Baron P., Lautié N., Schneider N., Dassas K., Ricaud P., and De La Noë J., “Moliere (v5): A versatile forward- and inversion model for the millimeter and sub-millimeter wavelength range,” *Journal of Quantitative Spectroscopy and Radiative Transfer*, **83** (3–4), pp. 529–554, 2004. doi: [https://doi.org/10.1016/S0022-4073\(03\)00104-3](https://doi.org/10.1016/S0022-4073(03)00104-3)
174. van de Hulst H.C. and Reesinck J. J. M., “Line Breadths and Voigt Profiles”, *The Astrophysical Journal*, **106**, pp. 121-127, 1947.  
link: <https://adsabs.harvard.edu/pdf/1947ApJ...106..121V>
175. Vangvichith M., Tran H., and Hartmann J.-M., “Line-mixing and collision induced absorption for O<sub>2</sub>–CO<sub>2</sub> mixtures in the oxygen A-band region”, *Journal of Quantitative Spectroscopy and Radiative Transfer*, **110** (18), pp.2212-2216, 2009.  
doi: <https://doi.org/10.1016/j.jqsrt.2009.06.002>
176. Villanueva G.L., Smith M.D., Protopapa S., Faggi S., and Mandell A.M., “Planetary Spectrum Generator: An accurate online radiative transfer suite for atmospheres, comets, small bodies and exoplanets”, *Journal of Quantitative Spectroscopy and Radiative Transfer*, **217**, pp. 86-104, 2018. doi: <https://doi.org/10.1016/j.jqsrt.2018.05.023>
177. Wcisło P. and Coauthors, “The first comprehensive dataset of beyond-Voigt line-shape parameters from ab initio quantum scattering calculations for the HITRAN database: He-perturbed H<sub>2</sub> case study”, *Journal of Quantitative Spectroscopy and Radiative Transfer*, **260**, 2021. doi: <https://doi.org/10.1016/j.jqsrt.2020.107477>
178. Wells R.J., “Rapid approximation to the Voigt/Faddeeva function and its derivatives”, *Journal of Quantitative Spectroscopy and Radiative Transfer*, **62** (1), pp. 29–48, 1999.  
doi: [https://doi.org/10.1016/S0022-4073\(97\)00231-8](https://doi.org/10.1016/S0022-4073(97)00231-8)
179. Werdell P. J., and Coauthors, “The Plankton, Aerosol, Cloud, Ocean Ecosystem Mission: Status, Science, Advances”, *Bulletin of the American Meteorological Society*, **100** (9), pp. 1775–1794, 2019. doi: <https://doi.org/10.1175/BAMS-D-18-0056.1>
180. Wilson G., and Coauthors, “Best practices for scientific computing”, *PLOS Biology*, **12** (1), e1001745, 2014. doi: <https://doi.org/10.1371/journal.pbio.1001745>
181. Xie Y., Sengupta M., and Dudhia J., “A Fast All-sky Radiation Model for Solar applications (FARMS): Algorithm and performance evaluation”, *Solar Energy*, **135**, pp. 435–445, 2016. doi: <https://doi.org/10.1016/j.solener.2016.06.003>
182. Yang Q., Liu X., Wu W., Kizer S., and Baize R. R., “Fast and accurate hybrid stream PCRTM-SOLAR radiative transfer model for reflected solar spectrum simulation in the

- cloudy atmosphere”, *Optics Express*, **24** (26), pp. A1514-A1527, 2016.  
doi: <https://doi.org/10.1364/OE.24.0A1514>
183. Yang Y., Marshak A., Mao J., Lyapustin A., and Herman J., “A method of retrieving cloud top height and cloud geometrical thickness with oxygen A and B bands for the Deep Space Climate Observatory (DSCOVR) mission: Radiative transfer simulations”, *Journal of Quantitative Spectroscopy and Radiative Transfer*, **122**, pp. 141–149, 2013.  
doi: <https://doi.org/10.1016/j.jqsrt.2012.09.017>
184. Zhou Y., Wang C., Ren T., and Zhao C., “A machine learning based full-spectrum correlated k-distribution model for nonhomogeneous gas-soot mixtures”, *Journal of Quantitative Spectroscopy and Radiative Transfer*, 268: 107628, 2021.  
doi: <https://doi.org/10.1016/j.jqsrt.2021.107628>
185. Zhu M., Zhang F., Li W., Wu Y, and Xu N., “The impact of various HITRAN molecular spectroscopic databases on infrared radiative transfer simulation”, *Journal of Quantitative Spectroscopy and Radiative Transfer*, 234, pp.55-63, 2019.  
doi: <https://doi.org/10.1016/j.jqsrt.2019.04.031>

## Declaration of Interest Statement

Authors of this manuscript declare no conflicts of interests.



Click here to access/download  
**Supplementary Material**  
01\_hitdb.par



Click here to access/download  
**Supplementary Material**  
02\_hitdb.par



Click here to access/download  
**Supplementary Material**  
03\_hitdb.par



Click here to access/download  
**Supplementary Material**  
04\_hitdb.par



Click here to access/download  
**Supplementary Material**  
05\_hitdb.par



Click here to access/download  
**Supplementary Material**  
06\_hitdb.par



Click here to access/download  
**Supplementary Material**  
07\_hitdb.par



Click here to access/download  
**Supplementary Material**  
07\_hitdb\_one\_line.par



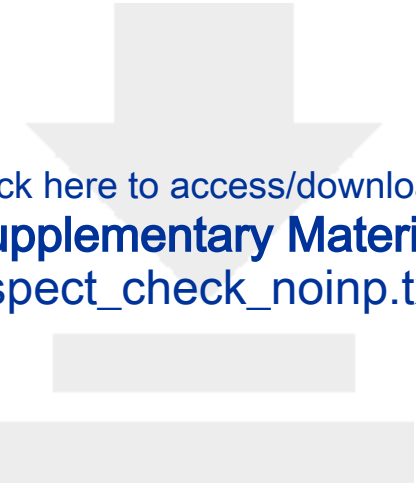
Click here to access/download  
**Supplementary Material**  
10\_hitdb.par



Click here to access/download  
**Supplementary Material**  
aspect.bld



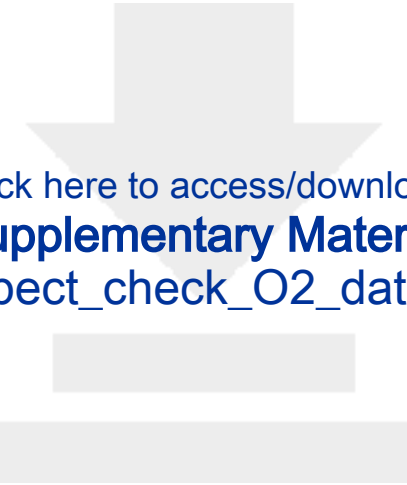
Click here to access/download  
**Supplementary Material**  
aspect\_check\_CH4.txt



Click here to access/download  
**Supplementary Material**  
aspect\_check\_noinp.txt



Click here to access/download  
**Supplementary Material**  
aspect\_check\_O2.bin



Click here to access/download  
**Supplementary Material**  
aspect\_check\_O2\_dat.txt



Click here to access/download  
**Supplementary Material**  
aspect\_check\_O2\_inu.bin



Click here to access/download  
**Supplementary Material**  
aspect-ao2.inp



Click here to access/download  
**Supplementary Material**  
aspect-ch4.inp



Click here to access/download  
**Supplementary Material**  
cmplx.cpp



Click here to access/download  
**Supplementary Material**  
cmplx.h



Click here to access/download  
**Supplementary Material**  
const\_param.h



Click here to access/download  
**Supplementary Material**  
count\_lines.cpp



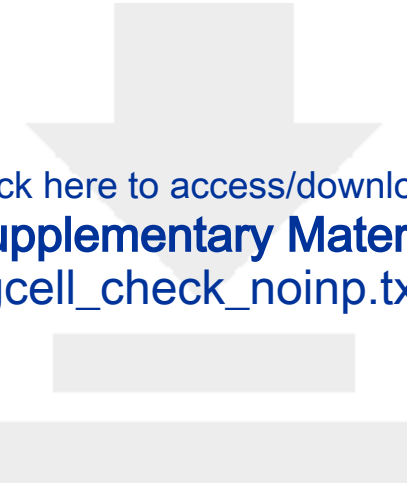
Click here to access/download  
**Supplementary Material**  
count\_lines100.cpp



Click here to access/download  
**Supplementary Material**  
gcell.bld



Click here to access/download  
**Supplementary Material**  
gcell\_check\_CH4.txt



Click here to access/download  
**Supplementary Material**  
gcell\_check\_noinp.txt



Click here to access/download  
**Supplementary Material**  
gcell\_check\_O2.txt



Click here to access/download  
**Supplementary Material**  
gcell-ao2.inp



Click here to access/download  
**Supplementary Material**  
gcell-ch4.inp



Click here to access/download  
**Supplementary Material**  
hisotops.cpp



Click here to access/download  
**Supplementary Material**  
hprofiles.h



Click here to access/download  
**Supplementary Material**  
humlicek.cpp



Click here to access/download  
**Supplementary Material**  
intparab.cpp



Click here to access/download  
**Supplementary Material**  
isotops.cpp



Click here to access/download  
**Supplementary Material**  
ix1ix2.cpp



Click here to access/download  
**Supplementary Material**  
kabs.cpp



Click here to access/download  
**Supplementary Material**  
link.txt



Click here to access/download  
**Supplementary Material**  
main\_aspect.cpp



Click here to access/download  
**Supplementary Material**  
main\_gcell.cpp



Click here to access/download  
**Supplementary Material**  
make\_directories.py



Click here to access/download  
**Supplementary Material**  
molparam.txt



Click here to access/download  
**Supplementary Material**  
paths.h



Click here to access/download  
**Supplementary Material**  
q1.txt



Click here to access/download  
**Supplementary Material**  
q10.txt



Click here to access/download  
**Supplementary Material**  
q11.txt



Click here to access/download  
**Supplementary Material**  
q12.txt



Click here to access/download  
**Supplementary Material**  
q120.txt



Click here to access/download  
**Supplementary Material**  
q121.txt



Click here to access/download  
**Supplementary Material**  
q122.txt



Click here to access/download  
**Supplementary Material**  
q129.txt



Click here to access/download  
**Supplementary Material**  
q13.txt



Click here to access/download  
**Supplementary Material**  
q14.txt



Click here to access/download  
**Supplementary Material**  
q15.txt



Click here to access/download  
**Supplementary Material**  
q16.txt



Click here to access/download  
**Supplementary Material**  
q17.txt



Click here to access/download  
**Supplementary Material**  
q18.txt



Click here to access/download  
**Supplementary Material**  
q19.txt



Click here to access/download  
**Supplementary Material**  
q2.txt



Click here to access/download  
**Supplementary Material**  
q20.txt



Click here to access/download  
**Supplementary Material**  
q21.txt



Click here to access/download  
**Supplementary Material**  
q22.txt



Click here to access/download  
**Supplementary Material**  
q23.txt



Click here to access/download  
**Supplementary Material**  
q24.txt



Click here to access/download  
**Supplementary Material**  
q25.txt



Click here to access/download  
**Supplementary Material**  
q26.txt



Click here to access/download  
**Supplementary Material**  
q27.txt



Click here to access/download  
**Supplementary Material**  
q28.txt



Click here to access/download  
**Supplementary Material**  
q29.txt



Click here to access/download  
**Supplementary Material**  
q3.txt



Click here to access/download  
**Supplementary Material**  
q30.txt



Click here to access/download  
**Supplementary Material**  
q31.txt



Click here to access/download  
**Supplementary Material**  
q32.txt



Click here to access/download  
**Supplementary Material**  
q33.txt



Click here to access/download  
**Supplementary Material**  
q34.txt



Click here to access/download  
**Supplementary Material**  
q35.txt



Click here to access/download  
**Supplementary Material**  
q36.txt



Click here to access/download  
**Supplementary Material**  
q37.txt



Click here to access/download  
**Supplementary Material**  
q38.txt



Click here to access/download  
**Supplementary Material**  
q4.txt



Click here to access/download  
**Supplementary Material**  
q44.txt



Click here to access/download  
**Supplementary Material**  
q5.txt



Click here to access/download  
**Supplementary Material**  
q6.txt



Click here to access/download  
**Supplementary Material**  
q7.txt



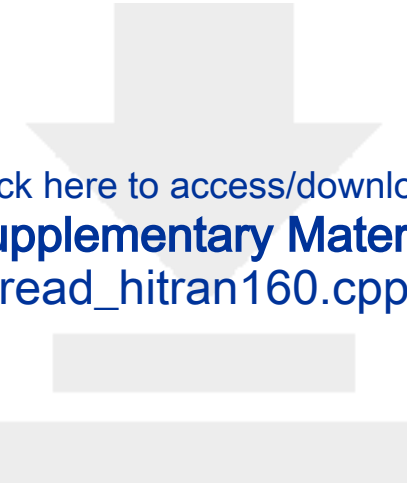
Click here to access/download  
**Supplementary Material**  
q8.txt



Click here to access/download  
**Supplementary Material**  
q9.txt



Click here to access/download  
**Supplementary Material**  
read\_hitran100.cpp



Click here to access/download  
**Supplementary Material**  
read\_hitran160.cpp



Click here to access/download  
**Supplementary Material**  
readme.txt



Click here to access/download  
**Supplementary Material**  
readme\_voigt.txt



Click here to access/download  
**Supplementary Material**  
Section5p3p1\_\_test\_gcell\_ao2.txt



Click here to access/download  
**Supplementary Material**  
Section5p3p2\_\_\_\_test\_gcell\_ch4.txt



Click here to access/download  
**Supplementary Material**  
Section6p6p2\_\_PACE-OCI\_tau\_H2O.txt



Click here to access/download  
**Supplementary Material**  
simpson.cpp



Click here to access/download  
**Supplementary Material**  
tauabs25.cpp